

PERMEABILITY OF INDIANA LIMESTONE: EXPERIMENTS AND THEORETICAL CONCEPTS FOR INTERPRETATION OF RESULTS

Paul A. Selvadurai
June 15, 2010



Department of Civil Engineering and Applied Mechanics
McGill University
Montréal, Quebec, Canada, H3A 2K6

A Thesis submitted to McGill University in partial
fulfillment of the requirements of the degree of
Master of Engineering

Copyright ©
2010 Paul A. Selvadurai

Abstract

This thesis describes the experimental configuration and theoretical and computational techniques used to estimate the surface permeability of Indiana Limestone. The experimental procedure involves the application of a uniform flow rate to an open central region of a sealed annular patch. The law governing fluid flow within the porous medium is described by Darcy's Law which relates the steady flow rate to the steady state pressure within the central region. Both theoretical and computational models can be used to determine the distribution of intrinsic surface permeability of the cuboidal Indiana Limestone sample measuring 508 mm. Using the surface data and an inverse analysis, the spatial permeability distribution within the sample is determined. The spatial distribution can then be used to estimate the *effective permeability* of the tested block. The effective permeabilities are also estimated using theoretical relationships found in the literature and the spatial values obtained from surface data and the inverse analysis.

Résumé

Cette thèse présente la configuration expérimentale ainsi que les techniques théoriques et numérique utilisées pour l'estimation de la perméabilité superficielle du Calcaire d'Indiana. La procédure expérimentale consiste en l'application d'un débit d'eau constant à la région centrale ouverte d'un 'patch' annulaire. Les lois qui définissent l'écoulement d'eau à travers des milieux poreux sont décrites par la loi de Darcy qui relie le débit constant d'un fluide à l'obtention d'une pression constante de ce fluide dans la région centrale. Les deux modèles (théorique et numérique) peuvent être utilisés pour déterminer la distribution de la perméabilité superficielle intrinsèque dans l'échantillon cubique de Calcaire d'Indiana qui mesure 508 mm de côté. Les données superficielles et l'analyse inverse sont utilisées pour déterminer la distribution spatiale de la perméabilité dans l'échantillon. Cette distribution spatiale permet l'estimation de la perméabilité effective de l'échantillon. La perméabilité effective est aussi estimée en appliquant les données spatiales obtenues avec les données superficielles et de l'analyse inverse dans des relations théoriques trouvées dans la littérature.

Acknowledgements

The author would firstly like to express an immense appreciation to his family and friends for all their support, time and patience while undertaking his Master's research at McGill University.

The author would like to express his great appreciation to Professor Yixin Shao, Associate Professor, Department of Civil Engineering and Applied Mechanics, McGill University, who's generosity, patience and kindness allowed the author to perform his Master's of Engineering program under his supervision. A special thanks to Professor Shao for encouraging me to consult with other faculty, especially Professor A. P. S. Selvadurai FRSC, William Scott Professor and James McGill Professor, Department of Civil Engineering and Applied Mechanics, whose insight, guidance and knowledge allowed me to complete many aspects of my chosen topic of research. The experimental facilities were funded by an NSERC Discovery Grant awarded to Professor Selvadurai and access to the Environmental Geomechanics Research Facilities is greatly appreciated. University support was also provided through a Provost Scholarship awarded to the author.

The author is indebted to the Technical Staff of the Department Civil Engineering and Applied Mechanics at McGill University, notably Mr. John Bartczak, Mr. Marek Pryzkorski, Mr. Damon Kiperchuk, Mr. Ronald Sheppard, Dr. Bill Cook and Mr. Jorge Sayat. Furthermore, a special thanks is due to his colleagues notably; Dr. Hani Ghiabi, Mr. Tuan Anh Luu, Dr. Wenjun Dong, Dr. Quifeng Yu, Mr. Adrian Glowacki, Mr. Antoine Letendre, Mr. Luc Jenner and Mr. Patrick Mattar for all their help and advice received during this research. The

author would like to thank Mrs. Sally Selvadurai for her editorial assistance.

Contents

Abstract	i
Résumé	ii
Acknowledgements	iii
Table of Contents	vii
List of Tables	viii
List of Figures	xii
Papers Resulting from Research	xiii
1 Introduction	1
2 Literature Review	6
2.1 Importance of Permeability	6
2.2 Historical Background	7
2.3 Steady-State Permeability Tests	7
2.4 Transient Permeability Measurements	14
2.5 <i>In situ</i> Permeability Testing	20
2.6 Designed Permeameters	22
3 Theoretical Background	26
3.1 General	26
3.2 One-dimensional Permeability Calculation	27

3.3	Surface Permeability Measurements	29
4	Indiana Limestone	32
4.1	Historical Background	32
4.2	Composition and Mechanical Properties	32
4.3	Previous Permeability Coefficients for Indiana Limestone	33
4.4	Sample Preparation and Manipulation	34
5	Experimental Facility	37
5.1	Overall Setup	37
5.1.1	Gum Rubber Gasket	37
5.1.2	General Components	37
5.1.3	The Permeameter	40
5.1.4	Liquid Chromatographic Pump	40
5.1.5	Data Acquisition	42
5.2	Technical Specifications of the Equipment and Components Used in this Research	42
6	Experimental Procedures	44
6.1	Sealing Procedure	44
6.2	Darcy Flow in the Support Volume	45
6.3	General Experimental Procedure	48
6.4	Influence of Boundary	50
6.5	Computational Modelling	54
6.5.1	Validation of the computational modelling	56

6.5.2	Computational Validation of a sub-region	60
6.6	Experimental Results and Interpretation	62
6.7	Kriging	64
6.8	Effective Permeability	69
6.8.1	Background	69
6.8.2	Application to the Experiment	72
6.8.3	Theoretical Estimates	73
6.8.4	Computational Study	75
7	Conclusions and Recommendations for Future Research	80
	Appendices	83
	Appendix A: Details of the Hydraulic Cylinder	83
	Appendix B: Details of the Reaction Frame	85
	Appendix C: Details of the Permeameter	90
	Appendix D: Sub-region permeability values	96
	Appendix E: Kolomogorov-Smirnov test for lognormal distribution . . .	97
	References	98

List of Tables

1	Physical properties of Indiana Limestone as recorded by ILIA (1998) and Glowacki (2007).	33
2	Reported permeability coefficients for Indiana limestone (after Mattar, 2009)	34
3	Typical input values for COMSOL TM validation.	56
4	Computational estimates of surface permeability on all six faces of a cuboidal sample of Indiana Limestone. [The Table gives the average value along with the corrections to estimate the maximum (+) and minimum (-) values]	64
5	Input values for modelling a heterogeneous cuboidal sample of Indiana Limestone in COMSOL TM	77
6	A summary of the relationships used to estimate the effective permeability of the Indiana Limestone block [$\times 10^{-15}$ m ²].	80

List of Figures

1	Schematic view of the processes involved with carbon sequestraion in deep geological repositories.	4
2	A modified Hoek-Franklin triaxial cell. The modifications allow the cell to be used for permeability testing of cylindrical rock samples (25.4 mm diameter by 34.1 mm length). (Daw, 1971)	9
3	A cross-section of the triaxial cell used for the testing of cylindrical cores (100 mm diameter by 200 mm length). (after Glowacki, 2007)	11
4	A cross-section of the radial steady-state permeability testing apparatus with Indiana limestone sample (central cavity diameter = 25.4 mm, sample diameter = 100 mm and sample length = 200 mm). (after Mattar, 2009)	13
5	Steady state radial permeability tests for a large cuboid block of Berea sandstone. (after Selvadurai and Selvadurai, 2007)	15
6	The flow net applicable to the sector domain of a cuboidal sample of Berea Sandstone (plan view). (after Selvadurai and Selvadurai, 2007)	15
7	The confined sample arrangement used in transient pulse decay test. (after Brace et al., 1968)	19
8	Single (a) and double (b) packer test for determining <i>in situ</i> hydraulic conductivity. Observation wells not shown. (after Franklin and Dusseault, 1989)	22

9	Influence of the geometry of the sealing patch of the permeameter on the intake shape factor G_o [The solid line indicates the result obtained from equation (10)] (after Selvadurai and Selvadurai, 2010)	25
10	Cuboidal Indiana limestone sample (508 mm) with ‘block grab’ mechanism.	35
11	Process of lifting Indiana limestone sample using ‘block grab’ mechanism.	36
12	Two natural gum rubber gaskets (40 Shore A durometer).	38
13	The general arrangement of the laboratory-scale surface permeability test and the details of the test set up.	39
14	Details of the permeameter.	41
15	Determining the appropriate sealing load.	46
16	Steady-state pressures versus flow rate using a constant sealing pressure.	49
17	Plan view of the test locations (nine in total) on one surface of the cuboidal sample.	50
18	Method for centrally locating the sample with respect to the coordinate system of the reaction frame.	51
19	Sketch of the flow geometry for an unconfined core plug sample. (after Goggin et al., 1988)	52
20	Plot of geometrical factor (G_o) curves showing the effect of the core sample length. (after Goggin et al., 1988)	53
21	Plot of geometrical factor (G_o) curves showing the effect of the core sample radius. (after Goggin et al., 1988)	53

22	Plan view of estimated ‘plug’ sample for a corner location on cuboidal Indiana limestone sample (plug in dashed line).	54
23	Plan view of estimated ‘plug’ sample for an edge location on cuboidal Indiana limestone sample (plug in dashed line).	55
24	Computational modelling boundary conditions for validation of potential steady-state fluid flow problem.	58
25	Finite element discretizations of the flow domain	58
26	Annular sealing patch validation model (where a and $b = 12.7$ mm and 50.8 mm, respectively).	59
27	Computational modelling for fluid flow associated with the permeameter located either along the edge or at the corner of the cuboidal specimen	60
28	Modelling of flow in a sub-cube of the cuboidal region.	62
29	Sample data for steady state pressure attainment during constant flow, permeameter test (Face 1, position D).	63
30	Locations of surface permeability with respect to Table 4. Locations are also marked on Indiana limestone sample.	65
31	Preliminary distributions of permeability corresponding to the test data shown in Table 4.	66
32	Initial data points (from Table 1) sampled by EasyKrig V3.0 . . .	67
33	The exponential-Bessel theoretical semi-variogram (red) based on experimental semi-variogram (black).	68

34	Distributions of permeability within the Indiana Limestone block as estimated by kriging the experimental data obtained from surface permeability measurements	70
35	A sub-structured unit of the cuboidal sample of Indiana Limestone with permeabilities derived from the kriging procedure. Red is high permeability (maximum $149.54 \times 10^{-15} \text{ m}^2$) and blue is low permeability (minimum $25.18 \times 10^{-15} \text{ m}^2$).	76
36	A sub-structured unit of the cuboidal sample of Indiana Limestone with the directions of testing denoted as 1,2 and 3.	78
37	Stream tube patterns along three orthogonal directions	79

Papers Resulting from Research

References

Selvadurai, P. A. and Selvadurai, A. P. S. (2009), On the surface permeability of Indiana Limestone, *in* ‘Proceedings of the 3rd CANUS Rock Mechanics Symposium,(M.Diederichs and G. Grasselli, eds), May 2009’, Toronto, Ontario, 237-238.

Selvadurai, A. P. S. and Selvadurai, P. A. (2010), ‘Surface permeability tests: Experiments and modelling for estimating effective permeability’, *Proceedings of the Royal Society: Proceedings A* **Under Review**, RSPA–2009–0475.R2.

1 Introduction

Fluid flow through geomaterials is a key factor in the field of environmental geosciences and geomechanics. The parameter used to describe the phenomena of fluid flow through a porous material, caused by hydraulic gradients, is referred to as the permeability. Permeability is a key property in many fields of geosciences, such as hydrology, groundwater flow, petroleum sciences and geotechnical engineering. Many problems in hydrology, including contaminant transport require a clear knowledge of the permeability of the porous materials involved. With respect to the relatively new field of environmental geomechanics, carbon dioxide sequestration, nuclear waste disposal and deep injection of hazardous wastes (Laughton et al. 1986; Chapman and McKinley 1987; Gnirk, 1993; Apps and Tsang, 1996; Selvadurai and Nguyen, 1997; Selvadurai, 2006), require accurate estimates of the permeability of the geologic media encountered. Permeability is described as the ability of fluids to flow through the pore space of low and medium permeability rocks. Permeability (K) describes the ability of the porous medium to transmit fluids through its accessible pore space, independent of the permeating fluid. It has units of $(length)^2$. The conventional hydraulic conductivity (k) depends on the pore fluid and the porous medium, with $k = K \cdot \gamma_w / \mu$, where γ_w is the unit weight of the fluid and μ its dynamic viscosity. Permeability of geomaterials and particularly rocks can vary in range 10^{-12} to 10^{-21} m². In fields such as hydrology, this property is considered to be sessile, contrary to geomechanical problems where the stress states induced by large *in situ* overburden can influence the permeability (Selvadurai and Glowacki, 2008). In all fields discussed above,

the accuracy of permeability measurements becomes even more crucial when computational models are used to predict flow and transport processes in long-term strategies for geo-environmental remediation. For example, timelines for carbon dioxide sequestration in sedimentary formations and deep geological disposal of heat-emitting nuclear waste, have been estimated at 100,000 to 10,000 years respectively; a geologically small timeframe but one that presents many problems from an engineering stand point.

Permeability is a primary characteristic in the geoscience discipline and many scientists and engineers have attempted to determine this property accurately. As a basic property of a porous medium, it is relatively easy to define but particularly difficult to measure accurately. One reason is that the permeability of rocks can be scale-dependant; it varies from the crustal scale 0.5 to 5 km, to the borehole scale 30 to 300 m and finally to the laboratory scale 5 to 50 cm. Natural inhomogeneities can be derived from a number of factors including stratifications, fractures, fissures, damage zones, voids and vugs. These natural and man made processes can drastically changes the permeability when examined at successive scales. The scale that is chosen for experimentation can influence the outcome of the permeability. This research attempts to develop an experimental laboratory procedure that can measure the '*effective permeability*' of a large cuboidal Indiana Limestone block of length 508 mm. The more accurate the estimation of permeability at a laboratory scale, the greater the reliability of extrapolation to a larger scale.

Indiana Limestone used in this research is a sedimentary rock with some visual evidence of natural stratification and the sample used is considered to be relatively

intact. Intact sedimentary rocks such as sandstones and saline limestones are candidate rocks for sequestration of carbon dioxide in supercritical form (Bachu and Adams, 2003) (Figure 1). They have natural properties that neutralize the gas and are found abundantly in nature. The intact permeability of the limestone is of particular interest since this will determine how the injected fluids can access the substantial pore volume where the majority of the chemical and hydrodynamic trapping takes place. It should be noted that if fractures and other defects are present in the host geologic medium, they will be sealed before any waste isolation activity can commence. Upon sealing, the primary mode of fluid transport through the porous geologic medium is through the pore space of the intact material.

Recent research concerning the topic of nuclear waste disposal relates to thermal effects on permeability of rocks (Summers et al., 1978; Morrow et al., 1981; Vitovtova and Shmonov, 1982; Zonov et al., 1989; Shmonov et al., 1994, 2003; Selvadurai et al., 2005). Highly radioactive wastes emit heat which can affect the pore structure of a geological material, which can in turn affect the permeability. Selvadurai et al. (2005) examine both isothermal permeability measurements and the influence of heating on the permeability of an igneous rock (Barre Granite). Many computational models have been developed to relate the hydro-mechanical and thermal-hydro-mechanical processes (Selvadurai and Armand, 2003) in order to assist predictions for long term remediation. Furthermore, the accuracy of these proposed simulation techniques are highly dependant on the accuracy with which permeability is prescribed in the calculations.

Fissures, fractures and cracks pose inherent problems when calculating the permeability of geological materials (Haimson, 1975; Zoback and Byerlee, 1975;

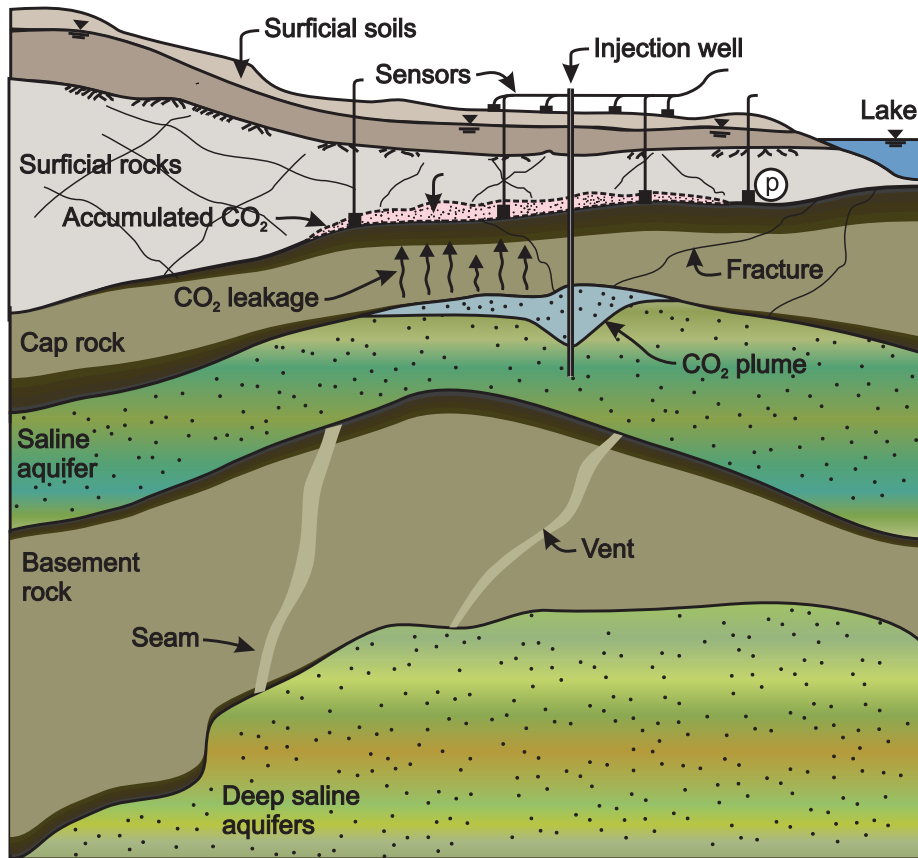


Figure 1: Schematic view of the processes involved with carbon sequestraion in deep geological repositories.

Selvadurai, 2008; Mattar, 2009). Mattar (2009) obtained an increase from 10^{-15} m² for the intact permeability of Indiana limestone to 10^{-11} m² for a fractured sample. Fractures increase the permeability and must be accounted for in all types of geo-scientific applications. Deep geological nuclear waste repositories must take this into consideration due to the ability of the fracture to transport harmful radionuclides over long distances and to pose a threat to human health and the environment. Most techniques for determining fractured rock permeability also require the knowledge of the intact permeability, reinforcing the need for new and accurate laboratory methods for measuring the latter.

The proposed research is a departure from the conventional use of rock cores to determine the permeability characteristics of a geologic medium. Permeability on large laboratory scale samples is essential to this research and such large block samples can be obtained from rock outcrops, tunnels and adits, and test pits used for other geological investigations. This thesis will provide an extensive report on the methods used to determine the ‘*effective permeability*’ of a large intact and homogeneous sample of Indiana Limestone. The advantage of determining the ‘*effective permeability*’ is that a larger support volume is tested in comparison to the conventional laboratory experiments conducted on core samples. Traditional laboratory experiments, intricately discussed in the literature review, commonly test cylindrical samples measuring 100 mm in diameter and 200 mm in length, correlating to a test volume approximately equivalent to 0.0015 m³. The ‘*effective permeability*’ methodology uses a cuboidal sample measuring 508 mm, which translates to a support volume of approximately 0.1311 m³. The volume being tested is therefore about 87 times greater than traditional laboratory permeability

tests and, justifiably, the results give a more accurate estimation of the overall intact permeability as required for complex, large scale, flow simulations.

2 Literature Review

2.1 Importance of Permeability

Permeability of an intact sample of Indiana limestone devoid of any fractures, fissures or visual solution channels (wormholes), should provide a good insight to the intact permeability. The technique of using surface permeability measurements to generate an overall estimate, and the possible orientation, of the permeability is a novel technique for a laboratory environment. This novel technique can only be applied when one fully understands the nature of permeability and the methods required to estimate this parameter. References to seminal work and current literature in this area can be found in the articles by Brace et al. (1968), Hsieh et al. (1981), Selvadurai and Carnaffan (1997), Suri et al. (1997), Butler Jr. (1998), Tokunaga and Kameya (2003), Selvadurai et al. (2005), Selvadurai and Selvadurai (2007), Selvadurai and Glowacki (2008) and Selvadurai (2007, 2009). We will give a brief overview of past experiments performed that attempted to quantify the permeability of geologic materials. To fully appreciate the methodologies proposed, it is important to discuss the procedures that have been used to estimate the permeability in the laboratory.

2.2 Historical Background

The flow of fluid through porous media was first examined in a scientific way by the French scientist Henry Philibert Gaspard Darcy (1803-1856), who was given the task of designing the water supply for the town of Dijon. He published his findings in the Memoir titled “Les Fontaines Publiques de la Ville de Dijon” (Darcy, 1856). A falling head column experiment was the basis for Darcy’s fundamental Law. Initially developed to describe flow through sands, it was later discovered to be applicable to many geologic media including rock. Test methodologies have improved but the fundamental principles observed by Darcy remain; the flow velocity of a fluid permeating in a porous medium is related to the hydraulic gradient and the relationship is made specific through the introduction of the parameter, hydraulic conductivity.

2.3 Steady-State Permeability Tests

Much research has been conducted since Darcy’s initial observation of the flow through porous media. Permeability measurements can be performed using two main techniques; steady-state flow and transient flow experiments. The main difference between the two techniques is how the hydraulic gradient is applied. During steady-state tests a constant flow rate induces a hydraulic gradient resulting in Darcy flow through the pore space of the sample. In relation to rocks, Hoek and Franklin (1967) were the first to use the steady-state technique and their apparatus is shown in Figure 2. They used a modified tri-axial cell to test rock core samples measuring 25.4 mm diameter by 25.4 mm length. After ap-

plying a confining pressure of 70 MPa to a rubber membrane, which sealed the outside surface of the sample, they then applied a constant rate of water influx, in the axial direction; the steady-state pressure was measured and the permeability was determined using the relevant theoretical result. Daw (1971) confirmed the previous studies but performed additional tests to ensure that adequate sealing was present at the rubber-sample interface. This test ensured that the membrane was sealing correctly so that there was no flow at the surface-membrane interface, which would markedly increase the measured permeability. According to Daw (1971), to adequately seal the cylindrical surface of the rock sample, a sealing pressure 20% higher than the pressure generated by the fluid influx is necessary. The research conducted in the Environmental Geomechanics Laboratory at McGill University indicates that the pressure required to seal the sample should be much greater than the fluid pressure inducing flow and this pressure also depends on the hardness of the sealing rubber membrane and the surface texture of the rock sample.

Selvadurai and Glowacki (2008) provide an excellent overview of a modified tri-axial, steady-state, axial permeability experiment. They performed tests on Indiana limestone samples, measuring 100 mm in diameter and 200 mm in length, and confined by a rubber membrane. They applied a constant flow of de-ionized and de-aired water in the axial direction of the sample (Figure 3). Their research discusses the confining pressure needed to seal the sample with respect to the surface texture, but also discusses the importance of measuring the permeability of the system (i.e. sources of leaks in valves, connections, etc.), since this can induce experimental errors. Different types of experiments have been conducted using

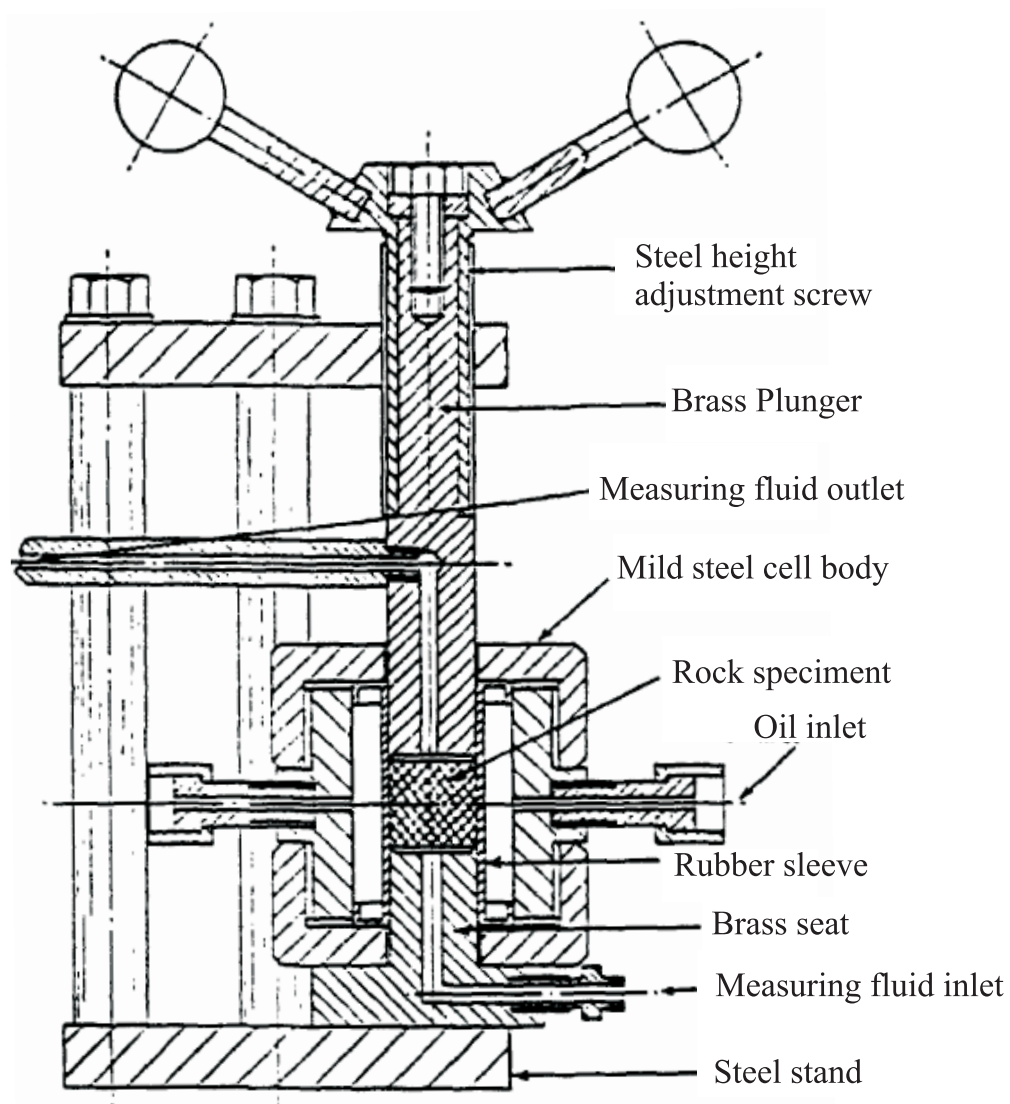


Figure 2: A modified Hoek-Franklin triaxial cell. The modifications allow the cell to be used for permeability testing of cylindrical rock samples (25.4 mm diameter by 34.1 mm length). (Daw, 1971)

the modified tri-axial apparatus; one such test investigates the effect of isotropic confining pressure on permeability (Knutson and Bohor, 1963; Daw, 1971; Brace, 1977; Trimmer et al., 1980; Vitovtova and Shmonov, 1982; Heiland, 2003; and Selvadurai and Glowacki, 2008). The most recent of these studies shows the results from quasi-static cyclical loading of the confining pressure, which give rise to a hysteresis in the measured permeability, possibly due to irreversible void reduction caused by changes to the porous fabric. Selvadurai and Glowacki (2008) observed a change in the permeability when Indiana Limestone was subjected to confining pressures up to 60 MPa; the permeability varied from $1.6 \times 10^{-14} \text{ m}^2$ at 5 MPa to $3.9 \times 10^{-14} \text{ m}^2$ at 60 MPa. The permeability evolution of geological media under confining stress is assumed to decrease with increased confining pressure. The theoretical relationship used to determine the axial permeability of rock samples, in the modified tri-axial setup, is

$$K = \frac{Q\mu L}{(\Delta P)A} \quad (1)$$

where K is the intrinsic permeability (m^2), Q is the constant influx of fluid (m^3/s), μ is the dynamic viscosity of the fluid ($\text{N}\cdot\text{s}/\text{m}^2$), L is the length of the sample (m), ΔP is the differential pressure caused by the influx of fluid (N/m^2) and A is the cross-sectional area of the sample (m^2).

Steady-state techniques are not limited to procedures that involve flow in the axial direction. Mattar (2009) performed radial steady-state tests on intact and fractured cylindrical samples of Indiana limestone, measuring 100 mm in diameter by 200 mm in length. Samples were cored then turned to the appropriated external

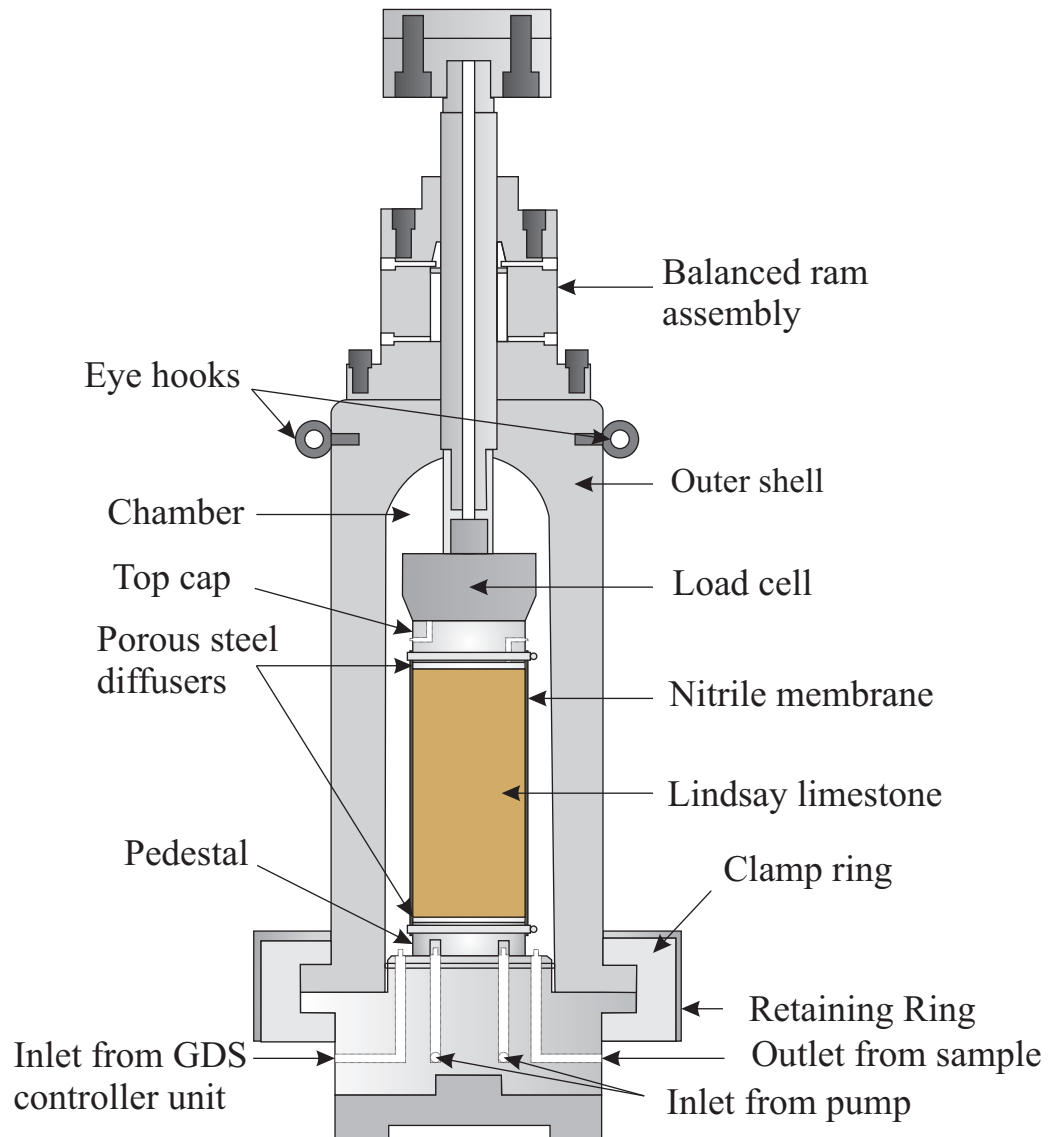


Figure 3: A cross-section of the triaxial cell used for the testing of cylindrical cores (100 mm diameter by 200 mm length). (after Glowacki, 2007)

diameter and a central cavity was drilled, then bored. The upper and lower plane ends of the cylindrical sample were sealed with epoxy. A constant flow rate was applied to the central cavity (Figure 4). The innovative preparation of the interior cavity (Mattar, 2009), reduced the amount of damage and clogging normally associated with the outward radial flow permeability tests on cylindrical samples with a central core. The analytical result governing the radial fluid flow through a porous cylindrical sample can be used to estimate the permeability: i.e.

$$K = \frac{Q\mu}{2\pi L(\Delta P)} \ln \left(\frac{b}{a} \right) \quad (2)$$

where K is the intrinsic permeability (m^2), Q is the constant flow rate (m^3/s), μ is the dynamic viscosity of the fluid ($\text{N}\cdot\text{s}/\text{m}^2$), L is the length of the sample (m), ΔP is the pressure differential (N/m^2) between the inside cavity and outside surface caused by the influx of fluid, a is the radius of the internal cavity (m) and b is the radius of the sample. The estimates for the permeability of Indiana Limestone given by Mattar (2009) are between $(0.9 \text{ and } 1.5) \times 10^{-15} \text{ m}^2$.

Selvadurai and Selvadurai (2007) performed radial steady-state permeability experiments on a cuboid block (450 mm) of Berea Sandstone. The experimental configuration that Mattar (2009) used follows from this study, where the upper and lower surface of the rock was sealed with epoxy and a borehole drilled at the center was used to initiate the steady flow (Figure 5). Using a liquid chromatographic pump (Shimadzu, model LC-3A), a constant flow rate was applied to the internal borehole. Computational methods, were used to analyse the two-dimensional flow from the central cavity and a flow net was generated. The permeability of the

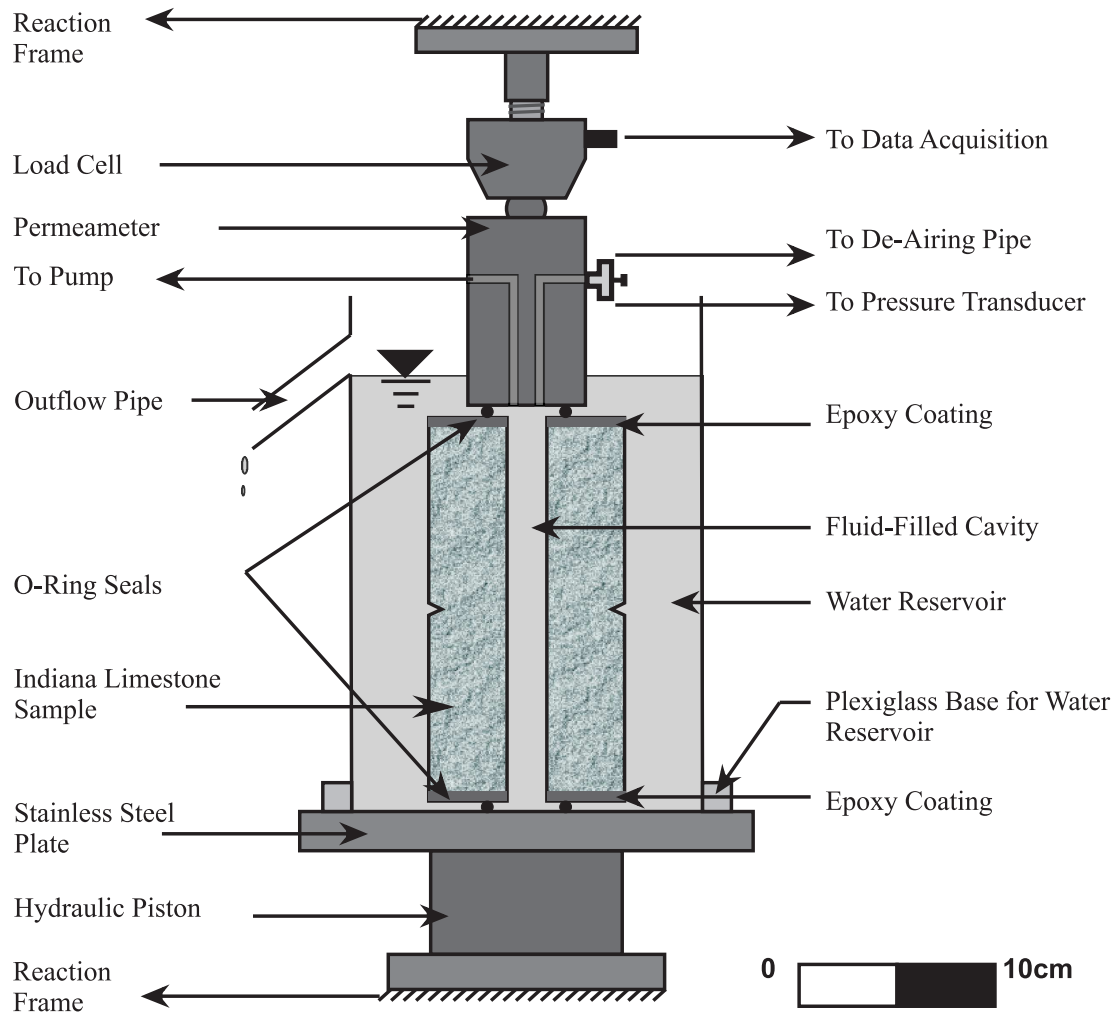


Figure 4: A cross-section of the radial steady-state permeability testing apparatus with Indiana limestone sample (central cavity diameter = 25.4 mm, sample diameter = 100 mm and sample length = 200 mm). (after Mattar, 2009)

Berea Sandstone was estimated using the result

$$K = \frac{Q\mu}{\gamma_w H_o(\Delta\Phi)} \left(\frac{N_d}{N_f} \right) \quad (3)$$

where K is the intrinsic permeability (m^2), Q is the constant flow rate induced at the cavity boundary (m^3/s); μ is the dynamic viscosity of the fluid ($\text{N}\cdot\text{s}/\text{m}^2$); γ_w is the unit weight of the percolating fluid (kN/m^3), H_o is the length of the internal cavity, $\Delta\Phi$ is the pressure differential between the interior cavity and exterior surface (m), and N_d and N_f are the number of computational potential drops and the total number of computational flow channels, respectively (for the flow net shown in Figure 6, $N_f = 104$; $N_d \cong 31$). The experimental estimate for the permeability of the intact Berea sandstone was approximately $3.46 \times 10^{-15} \text{ m}^2$. A further analytical result for estimation of the permeability of the near radial flow configuration is given by Harr (1962); i.e.

$$K = \frac{Q\mu}{\gamma_w H_o(\Delta\Phi)} \left(\frac{\ln(4b/\pi a)}{2\pi} \right) \quad (4)$$

where the same definitions from (3) apply but b is the distance from the center of cavity to the nearest edge (m) and a is the radius of the central cavity (m).

2.4 Transient Permeability Measurements

The use of steady-state techniques are appropriate experimental procedures for measuring permeabilities of rock samples provided steady flow rates can be induced without inducing any damage to the sample. The procedures have limitations: when the tested rock is ‘tight’, i.e. when permeability values are very low

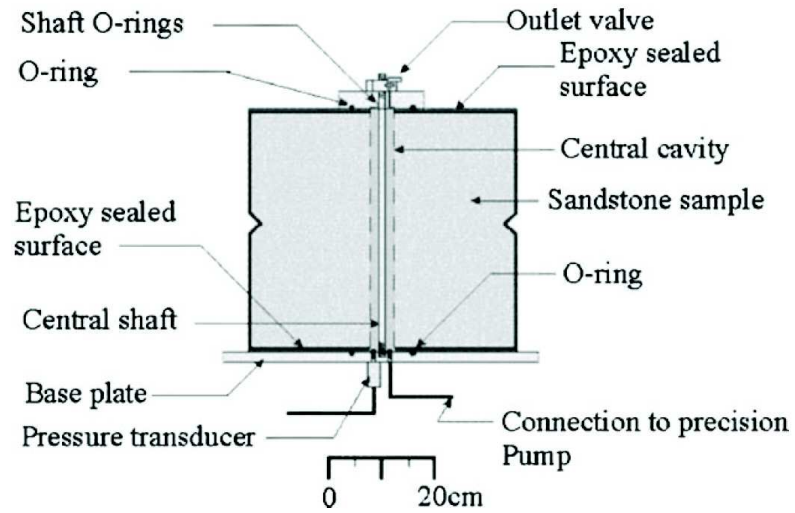


Figure 5: Steady state radial permeability tests for a large cuboid block of Berea sandstone. (after Selvadurai and Selvadurai, 2007)

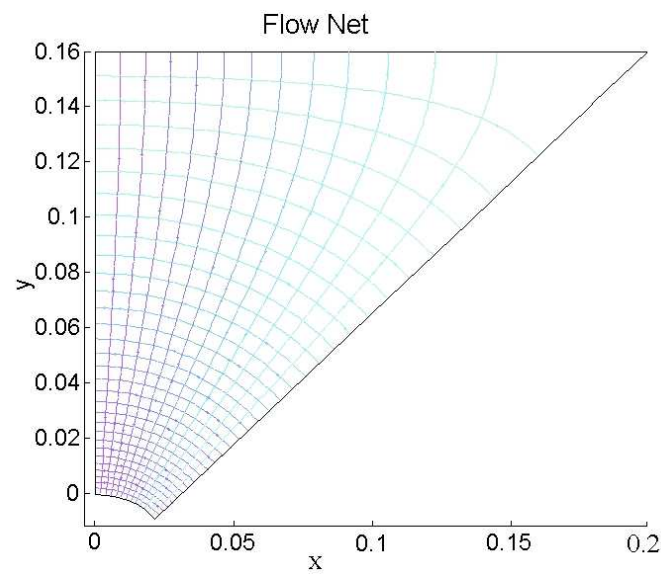


Figure 6: The flow net applicable to the sector domain of a cuboidal sample of Berea Sandstone (plan view). (after Selvadurai and Selvadurai, 2007)

($> 10^{-17} \text{ m}^2$), a number of problems arise that make the use of steady-state experiments unfeasible. Firstly, the equipment needed becomes more complex. The pumps, used to deliver a constant flow rate, need to achieve very low flow rates in order to obtain acceptable fluid pressures that will not induce damage in the rock or compromise the sealing. Secondly, the time that it takes for steady-state to be achieved at low flow rates in ‘tight’ rocks increases dramatically from those with higher permeabilities (i.e. $< 10^{-17} \text{ m}^2$). The duration of these experiments varies from days (‘loose’ rocks) to months (for ‘tight’ rocks) rendering it impractical for laboratory experimentation. To counteract this, researchers have attempted to change the percolating fluid from liquid (water) to gas (most commonly nitrogen, N_2). The dynamic viscosity of most gases at room temperature ($\approx 1.775 \times 10^{-5} \text{ N}\cdot\text{s}/\text{m}^2$) is 55 times less than that of water ($\approx 9.772 \times 10^{-4} \text{ N}\cdot\text{s}/\text{m}^2$), ultimately reducing the time needed to obtain steady-state conditions. Using gas, however, introduces an unknown factor known as the *Klinkenberg effect* (Ahmed et al., 1991). Unlike liquids, gases experiences higher velocities near the grain surface, referred to as gas slippage. This increased velocity allows more gas to permeate through the pore space than would with a fluid. A gas-slippage coefficient was developed by Klinkenberg (1941) to account for the this effect. The relationship between the gas and liquid permeabilities is experimentally derived. Due to the absence of a satisfactory analytical solution, it is preferable to use liquid-based permeability tests (Carnaffan, 1994). In summary, transient permeability tests prove to be highly useful when testing low permeability rocks.

Generally speaking, rocks which exhibit low permeabilities (i.e. 10^{-17} m^2 to 10^{-24} m^2) are very challenging to test using steady-state flow experiments (Sel-

vadurai et al., 2005). The most common transient permeability test is the pulse decay test. A one-dimensional experimental arrangement involves a confined sample connected to upstream and downstream reservoirs. Each reservoir is equipped with a pressure transducer, capable of on-line pressure measurements and a pressure supply source. An incremental pressure is applied to one reservoir and the pressure decay is monitored. Conversely, the pressure increase curve can be monitored in the opposite reservoir until the system reaches a new equilibrium state. The rate at which the pressure decays and increases allows for the calculation of the permeability. The problems encountered when using this method can be seen when we analyze the partial differential equation which governs the pressure distributions in a one-dimensional axial configuration (see e.g. Bear, 1972; Brace et al., 1977; Hsieh et al., 1981; Barenblatt et al., 1990; Philips, 1991; Selvadurai, 2000, 2002; Selvadurai, 2009; Selvadurai et al., 2010),

$$\frac{\partial^2 p}{\partial x^2} = \frac{S_s \mu}{K \gamma_w} \frac{\partial p}{\partial t}; \quad x \in (0, L_o) \quad (5)$$

where $p(x, t)$ is the fluid pressure (kPa), L_o is the extent of the domain, μ is the dynamic viscosity ($N \cdot s / m^2$), K is the permeability (m^2), γ_w is the unit weight of water (kN / m^3), S_s is the specific storage of the porous medium ($1/m$), composed of a solid material that is incompressible and defined by

$$S_s = \gamma_w (nC_w + C_{eff}) \quad (6)$$

In (6), n is the porosity, C_w and C_{eff} ($1/Pa$) are the compressibility of the pore fluid and the pore skeleton, respectively. The experimental and theoretical results

related to the pulse test are well documented (see e.g. Cooper et al., 1967; Brace et al., 1968; Wang and Hart, 1993; Hsieh et al., 1981; Rutquist, 1995; Butler Jr., 1998; Wu and Pruess, 2000; Liang et al., 2001; Selvadurai and Carnaffan, 1997; Selvadurai et al., 2005; Selvadurai, 2009). Without solving (5), we notice that in the one-dimensional pulse test, the decay curves depend on a number of mechanical and physical parameters related to both the porous medium and the permeating fluid. These parameters must be measured separately and errors in their estimations can result in errors in the estimation of the permeability. Brace et al. (1968) performed the first documented case of the pulse decay test (Figure 7). They tested Westerly granite cylinders measuring 25.2 mm in diameter and 16.1 mm in height. The cylinders were confined by pressures ranging from 10 MPa to 400 MPa, since they were attempting to determine the effect of confining stress on the permeability. The measured permeability ranged from $350 \times 10^{-21} \text{ m}^2$ to $4 \times 10^{-21} \text{ m}^2$, for confining pressures of 10 MPa and 400 MPa, respectively. As in the steady-state experiments, the incremental pulse pressures were maintained at around 20% of the sealing pressure, which was later confirmed by Bernabe et al. (1982) who performed pulse decay measurements on hot pressed calcite. Selvadurai and Carnaffan (1997) successfully measured the intact permeability of cement grout using the transient pulse decay method and determined the permeability to be around 10^{-21} to 10^{-22} m^2 . Furthermore, these tests are sensitive to temperature gradients, which was noted by Brace et al. (1968).

A variation of the transient pulse decay method involves the use of one single upstream reservoir. The governing equation (5), describing the pulse decay curve with time is the same as the two reservoir pulse decay, differing only in the

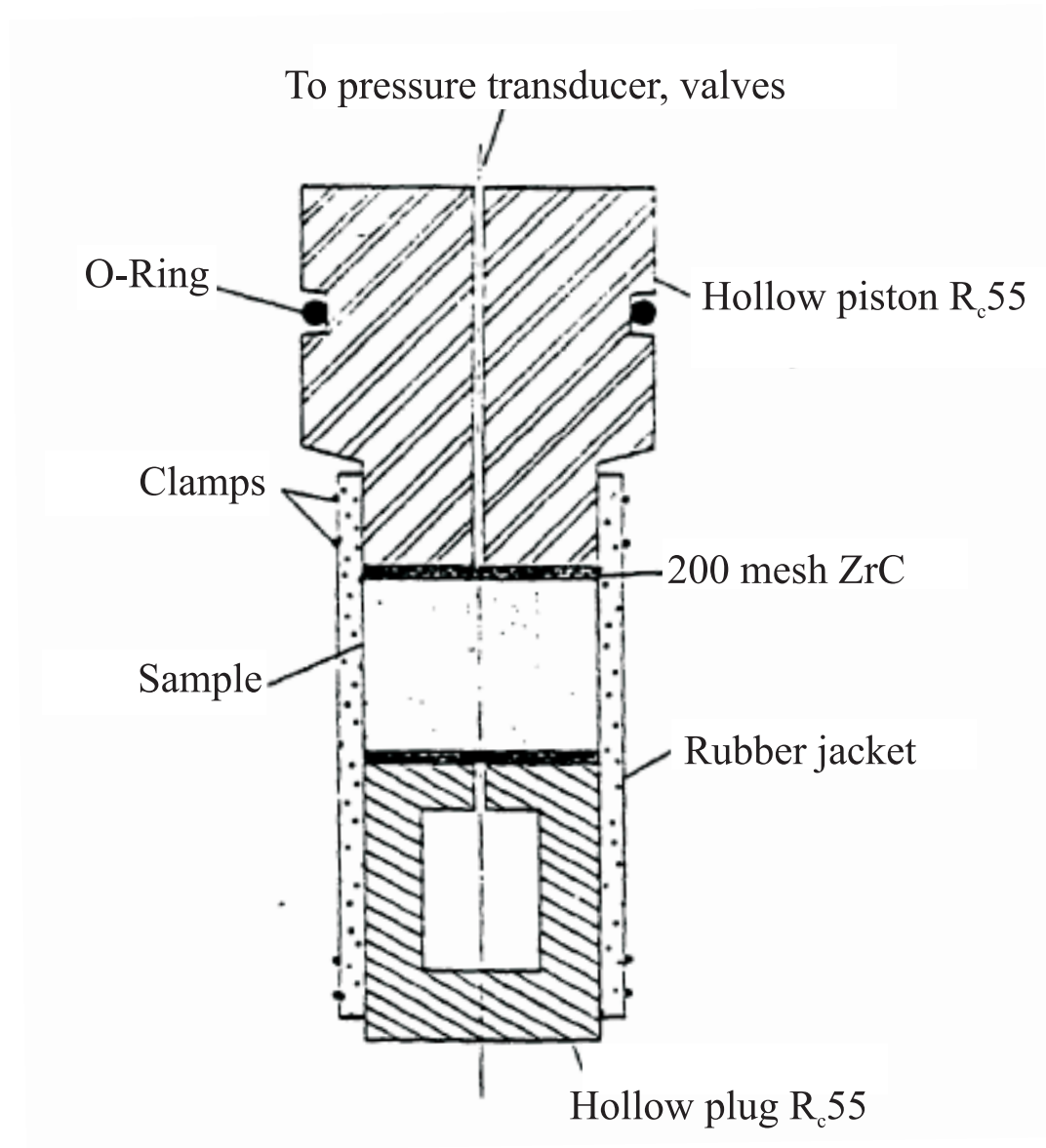


Figure 7: The confined sample arrangement used in transient pulse decay test. (after Brace et al., 1968)

boundary conditions. The boundary condition on the non-reservoir side is now considered to be null Dirichlet and the pressure impulse is only applied on the reservoir side. This variation on the transient pulse decay technique still involves a knowledge of all the mechanical and physical properties of the system to determine the permeability. Recent research by Selvadurai (2009), has pointed to another potential problem associated with the transients tests; internal pressure gradients that remain in the sample post-testing, which can influence the pulse decay curves. If the initial pressure within the sample is not allowed to reach atmospheric conditions, dramatic errors can occur in the pulse decay results. To alleviate this problem, Selvadurai (2009) recommends leaving the sample to 'relax', under atmospheric conditions, for the same amount of time as the the duration of pressure pulse applied.

2.5 *In situ* Permeability Testing

The most common form of *in situ* test is the 'packer test'. The test involves placing a submersible pump in an exploratory borehole, and sealing the specific region using inflatable bladders, known as 'packers'. The single packer test involves placing the pump at the bottom of the borehole and sealing the upper region of the borehole. The double packer test involves sealing the region above and below the pump (Figure 8). A constant flow rate is applied to the sample via the pump and the increase in the steady water level in an observatory well at a distance R from the test section is noted. The following relationship is used to calculate the hydraulic conductivity of the geologic material using a shape factor ($\ln(2R/D)$) to account for the size of the fluid flow domain (Franklin and Dusseault, 1989):

i.e.

$$k = \frac{Q}{2\pi l(H_1 - H_2)} \ln \left(\frac{2R}{D} \right) \quad (7)$$

where k is the hydraulic conductivity (m/s), Q is the constant flow rate (m³/s), l is the length of the test section (m), R is the distance from test hole to observation hole (m), D is the diameter of the drill hole (m), H_1 is total head in the test section (m) and H_2 is the total head in the observation section (m). The packer test is commonly used in conjunction with a network of boreholes. A properly defined network can provide the hydraulic conductivity in multiple directions in a single test.

Papadapoulous et al. (1973) used a modified slug test to calculate the transmissivity of aquifers. The test involves the instantaneous removal or input of a known quantity of water for a borehole, and observing the recovery time of the water level in the well with time. The expression, based on a solution that assumes a well of infinitesimal diameter (mathematical line source), can be written as

$$\frac{H}{H_o} = \frac{r_c^2}{4Tt} \quad (8)$$

where H_o is the instantaneous change in the well head (m), H is the head in the well at $t > 0$ (m), r_c is the radius of the well casing where the head change takes place (m), T is the transmissivity of the aquifer (m²/s) and t is the time since the instantaneous head change. The transmissivity of the aquifer is defined by $T = (D \cdot K \cdot \gamma_w / \mu)$, where D is the thickness of the aquifer (m); K is the permeability

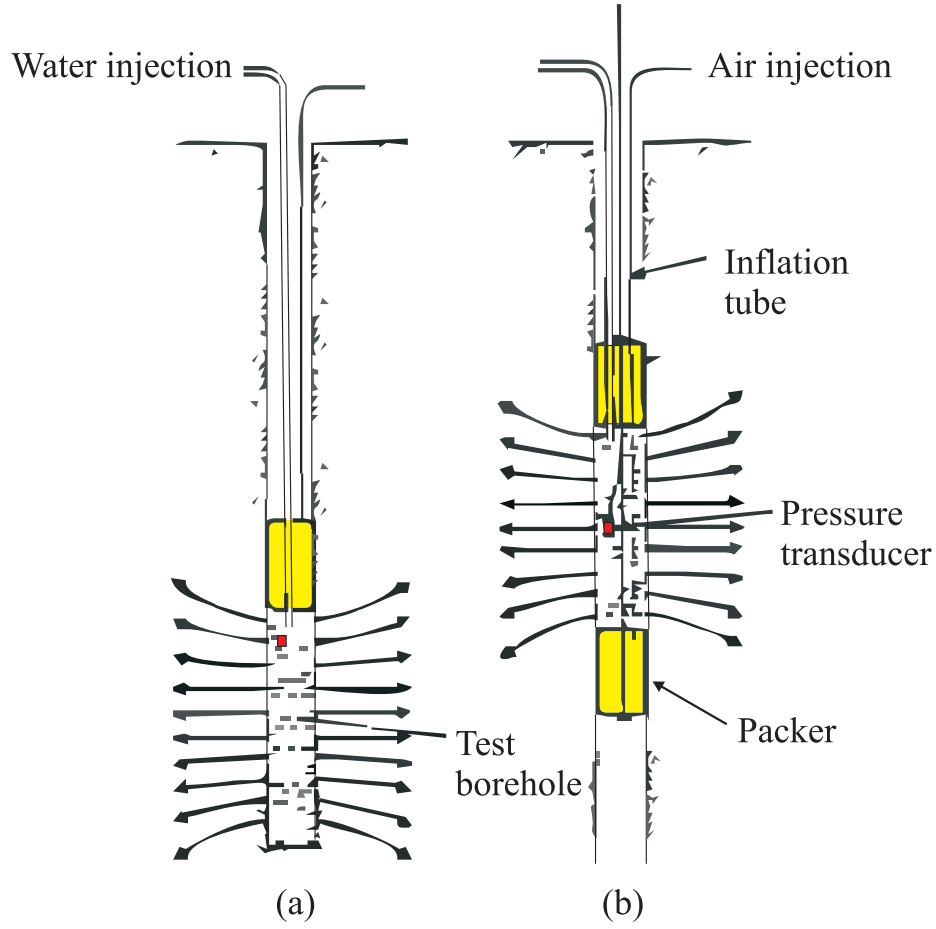


Figure 8: Single (a) and double (b) packer test for determining *in situ* hydraulic conductivity. Observation wells not shown. (after Franklin and Dusseault, 1989)

(m^2); γ_w is the unit weight of the water (kN/m^3) and μ is the dynamic viscosity of the fluid ($\text{N}\cdot\text{s}/\text{m}^2$).

2.6 Designed Permeameters

A gas permeameter is the most commonly used instrument both for laboratory and *in situ* environments (Bernabe, 1987; Jalbert and Dane, 2003; Chief et al.,

2006). Permeameters have been used extensively in the petroleum industry (Dykstra and Parsons, 1950; Eijpe and Weber, 1971) to determine spatial distributions of permeabilities in outcrops, rock cores and slabs. The gas permeameter is an efficient and light-weight device capable of measuring permeabilities quickly without inducing damage to the sample. A wide range of geological materials have been tested using gas permeameters such as Eolian Sandstones (Chandler et al., 1989), fluvial sandstones (Dreyer et al., 1990; Davis et al., 1993), carbonates (Kittridge et al., 1990) and volcanic tuffs (Fuller and Sharp Jr., 1992). Much of the research described in this thesis is drawn from these techniques and particularly the studies by Tidwell and Wilson (1997) who devised a permeameter for a similar experiment; steady state permeability tests conducted on a large cuboidal block. Tidwell and Wilson (1997) were more interested in determining the effect of the tip seal ratio (outer radius versus inner radius of annular seal) on the measurement of permeability and applications of surficial semi-variograms for data analysis.

The permeability test involves the application of a constant flow rate to the interior of an annular region maintaining sealed contact with the geomaterial; this is commonly referred to as a tip seal. The character of the flow field, and ultimately the support volume being tested, is defined by the dimensions of the tip seal. This flow region is a semi-toroid confocal with the pressurized central cavity. By applying a constant flow rate and measuring the steady state pressure inside the tip seal region, a mathematical expression, which depends on the dimensions of the annulus, can be used to compute the permeability. Goggin et al. (1988) determined the following mathematical expression for the permeability derived from the flow of fluid through the central cavity of a sealed annular patch on the

surface of a porous geo-material: i.e.

$$K = \frac{Q_1 P_1 \mu}{0.5 r_i G_o \left(\frac{r_o}{r_i} \right) [P_1^2 - P_o^2]} \quad (9)$$

where K is the permeability (m^2), Q_1 is the constant fluid influx (m^3/s), P_o is the atmospheric pressure (eg. kPa), P_1 is the fluid pressure at the inner region of the annulus (eg. kPa), μ is the dynamic viscosity of the percolating fluid ($\text{Pa}\cdot\text{s}$) and $G_o \left(\frac{r_o}{r_i} \right)$ is a non-dimensional shape factor that depends only on the inner to outer radii ratio for the annular region.

As stated previously, a geometric factor ($G_o \left(\frac{r_o}{r_i} \right)$) is indicative of the support volume or the volume of the porous material participating in the fluid flow. Permeameter studies performed by Goggin et al. (1988), Tartakosky (2002) and Selvadurai and Selvadurai (2010) are in excellent agreement about the shape factor function. Selvadurai and Selvadurai (2010) obtained the following approximate relationship for the function $G_o(c)$ by solving the system of triple integral equations governing the potential flow problem for the annulus: i.e.

$$G_o(c) = 4 \left\{ \begin{aligned} &1 + \left(\frac{4}{\pi^2} \right) c + \left(\frac{16}{\pi^4} \right) c^2 + \left(\frac{64}{\pi^6} + \frac{8}{9\pi^2} \right) c^3 + \left(\frac{64}{9\pi^4} + \frac{256}{\pi^8} \right) c^4 \\ &+ \left(\frac{92}{225\pi^2} + \frac{384}{9\pi^6} + \frac{1024}{\pi^{10}} \right) c^5 + \text{O}(c^6) \end{aligned} \right\} \quad (10)$$

where c is the ratio of r_o/r_i . This expansion is only applicable to a limited range of the values of c (accurate for values of r_o/r_i approximately 0.833). Figure 9 illustrates the variation in the shape factor $G_o(c)$ as a function of (r_o/r_i) obtained

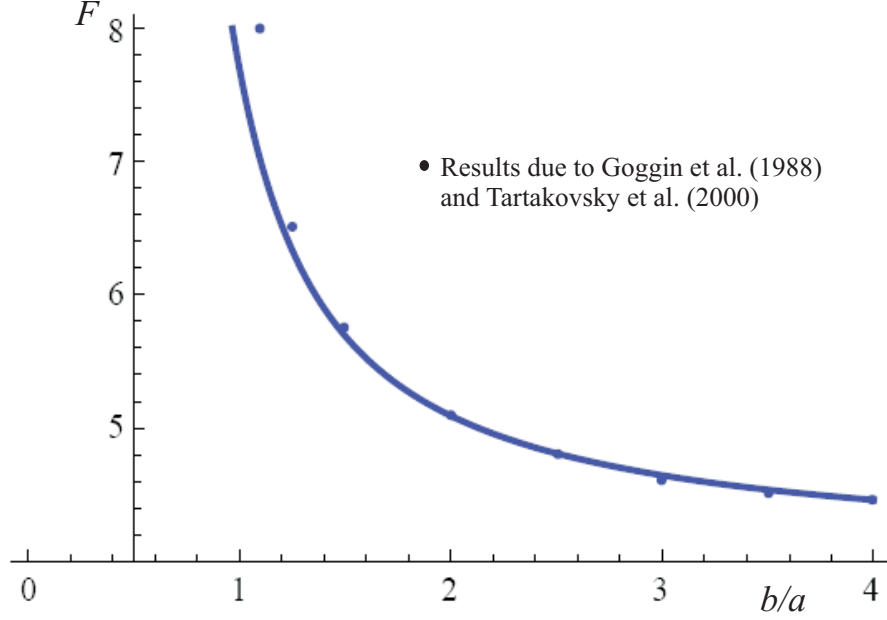


Figure 9: Influence of the geometry of the sealing patch of the permeameter on the intake shape factor G_o [The solid line indicates the result obtained from equation (10)] (after Selvadurai and Selvadurai, 2010)

from (10) and there is excellent agreement with results given by Goggin et al. (1988). In this research, the annular sealing region has r_o/r_i equal to 4; thus the value of $G_o(c)$ was determined to be approximately 4.456.

The objective of this thesis is to discuss the experimental procedures associated with the use of a designed permeameter, provide a mathematical treatment of special cases of the experimental configuration and describe the computational models used to interpret the data for general situations.

3 Theoretical Background

3.1 General

Fluid flow through saturated porous media was first documented by a French researcher, Darcy (1856), who proposed Darcy's Law. Darcy (1856) noticed that the position dependant potential $[\Phi(\mathbf{x})]$ is what moves fluid through a porous medium with a certain velocity $[\mathbf{v}(\mathbf{x})]$. Using the simplified Bernoulli potential (which includes only the datum head and the pressure head) he related this potential to the velocity of fluid in the medium:

$$\mathbf{v}(\mathbf{x}) \propto \nabla \Phi(\mathbf{x}) \quad (11)$$

Furthermore, Darcy considered the relationship where the velocity is directly proportional to the gradient of the potential. The proportionality related the velocity of fluid traveling through a porous medium to the potential acting on the porous medium. Equation (11), now becomes

$$\mathbf{v}(\mathbf{x}) = \frac{K}{\mu} \nabla \Phi(\mathbf{x}) \quad (12)$$

where K is the isotropic intrinsic permeability (m^2) and μ is the dynamic viscosity ($\text{Pa}\cdot\text{s}$). For an incompressible fluid moving through a non-deformable porous medium, the mass conservation equation simplifies to

$$\nabla \cdot \mathbf{v}(\mathbf{x}) = 0 \quad (13)$$

By combining equations (12) and (13) we obtain the governing equation for fluid

flow through a porous media,

$$\nabla^2 \Phi(\mathbf{x}) = 0 \quad (14)$$

which is the Laplace equation.

3.2 One-dimensional Permeability Calculation

Darcy's Law can also be presented in the following form which differs from (12). This next derivation should clarify any misconceptions associated with the nomenclature encountered in permeability measurements for one-dimensional conditions:

$$v = ki \quad (15)$$

where v is the velocity of percolating fluid (m/sec), k is the hydraulic conductivity (m/sec) and i is the hydraulic gradient (non-dimensional). In this report we are interested in the intrinsic permeability.

The intrinsic permeability is independent of the percolating fluid, whereas the hydraulic conductivity is fluid- and temperature-dependant. By definition, the hydraulic conductivity reflects the ability of the porous medium to transmit water. The intrinsic permeability can be related to the hydraulic conductivity in the following way (Bear, 1972)

$$K = \frac{\mu(T)}{\gamma_w} k \quad (16)$$

where γ_w is the density of the fluid (N/m³), $\mu(T)$ is the temperature dependent

fluid dynamic viscosity ($\text{N}\cdot\text{sec}/\text{m}^2$) and K is the intrinsic permeability (m^2). For isothermal conditions, the fluid dynamic viscosity is assumed to remain constant and equation (16) simplifies to

$$K = \frac{\mu}{\gamma_w} k \quad (17)$$

Using Bernoulli's definition of the potential of a fluid particle and assuming relatively low fluid velocities within the pore space of the medium Darcy's Law can be restated in the form

$$Q = kiA \quad (18)$$

where Q is the flow rate (m^3/sec), i is the hydraulic gradient (non-dimensional) and A is the cross-sectional area through which flow occurs (m^2).

Darcy's definition (Terzaghi and Peck, 1967) for a non-dimensional hydraulic gradient (i) is obtained by normalizing the difference in head between two locations, which drives fluid flow through the pore space, with respect to the length over which the difference occurs. The hydraulic gradient is given by

$$i = \frac{\phi_1 - \phi_2}{L} \quad (19)$$

where ϕ_n are the total heads (m) and L is the distance between pressure measurements. Combining equation (19) and (17) with equation (18) we obtain

$$Q = \frac{KA\gamma_w}{\mu L}(\Delta\phi) \quad (20)$$

and

$$K = \frac{Q\mu L}{\gamma_w A (\Delta\phi)} \quad (21)$$

Dimensional analysis allows us to determine the units of K

$$K = \frac{\left[\frac{m^3}{s}\right] \left[\frac{N \cdot s}{m^2}\right] \cdot m}{\left[\frac{N}{m^3}\right] \cdot m \cdot m^2} = m^2 \quad (22)$$

Equation (21) governs the flow of fluid through a porous medium for the one dimensional fluid flow problem. The surface permeability experiments discussed in this thesis consist of geometries where the fluid flow takes place under either two-dimensional axisymmetric states or three-dimensional states. The geometry of the flow paths will be discussed in a subsequent section of the thesis. For completeness, the modelling of the axisymmetric problem of fluid flow induced by the pressurizing of the central region of an annular sealing patch is presented.

3.3 Surface Permeability Measurements

When using a permeameter on the surface of a semi-infinite porous medium a flow occurs mainly in a region with a shape that can be described as a semi-toroid. The extent of this semi-toroidal region is directly related to the dimensions of the annular patch (Tartakovsky, 2000), used to seal the surface of the medium. Since the potential flow problem corresponding to (14) is axisymmetric, the appropriate form of Laplace's equation is given by

$$\nabla^2 \phi(r, z) = 0 \quad (23)$$

$$\left(\frac{\partial^2}{\partial r^2} + \frac{1}{r} \frac{\partial}{\partial r} + \frac{\partial^2}{\partial z^2} \right) \Phi(r, z) = 0 \quad (24)$$

Solutions of (24) applicable to semi-infinite domains can be obtained by using Hankel integral transforms techniques (Sneddon, 1966; Selvadurai, 2000) and the relevant solution for the semi-infinite domain $r \in (0, \infty)$ and $z \in (0, \infty)$ is given by

$$\Phi(r, z) = \int_0^\infty \varphi(\xi) e^{-\xi z} J_0(\xi r) d\xi \quad (25)$$

where $\varphi(\xi)$ is an arbitrary function and $J_0(\xi r)$ is the zeroth-order Bessel function of the first-kind. It may be ruled that the potential $\Phi(r, z)$ given by (25) satisfies the limiting conditions applicable to semi-infinite regions; i.e. $\Phi(r, z) \rightarrow 0$ as $r, z \rightarrow \infty$.

The flow through the porous medium initiated by a prescribed potential Φ_o in the central region of the sealed annulus gives rise to the following three-part mixed boundary value problem

$$\int_0^\infty \varphi(\xi) J_0(\xi r) d\xi = \Phi_o \quad ; \quad 0 \leq r \leq a \quad (26)$$

$$\int_0^\infty \xi \varphi(\xi) J_0(\xi r) d\xi = 0 \quad ; \quad a < r < b \quad (27)$$

$$\int_0^\infty \varphi(\xi) J_0(\xi r) d\xi = 0 \quad ; \quad b \leq r < \infty \quad (28)$$

Further development of the solution is given in Selvadurai and Selvadurai (2010) and the boundary conditions associated with the surface permeability test is given as,

$$Q = a \Phi_0 \left(\frac{K \gamma_w}{\mu} \right) G_o(c) \quad (29)$$

where Φ_0 is the head generated within the interior surface of the annular region (m) defined by the application of a constant flow rate Q (m³/sec), a is the interior radius of the annular region (m), K is the intrinsic permeability of the porous medium (m²), γ_w is the unit weight of the percolating fluid (N/m³), μ is the dynamic viscosity of the fluid (N·sec/m²) and $G_o(c)$ is the non-dimensional shape factor function given by (10). Rearranging equation (29) we obtain

$$K = \frac{Q\mu}{a\Phi_0\gamma_w G_o(c)} \quad (30)$$

Dimensional analysis gives:

$$K = \frac{\left[\frac{m^3}{s} \right] \left[\frac{N \cdot s}{m^2} \right]}{m \cdot m \cdot \left[\frac{N}{m^3} \right]} = m^2 \quad (31)$$

The theoretical solution for the semi-infinite, *axisymmetric* permeameter (31) will be used to validate the computational models developed later. The computational models account for the more complicated finite regions, which are difficult to model analytically.

4 Indiana Limestone

4.1 Historical Background

Indiana Limestone was primarily used as a construction material from the beginning of the 18th century (ILIA, 1998). Indiana limestone was highly regarded for its fire resistant properties. By the end of the 19th century, Indiana Limestone was the architectural material of choice in most governmental and private projects due to its appealing light-coloured appearance and structural properties.

4.2 Composition and Mechanical Properties

Indiana Limestone, also known as Salem Limestone, was formed in a shallow inland sea that dates back to the Mississippian geologic epoch (approximately 318.1-359.2 Ma). The rock is a calcite cemented grainstone formed from fossil fragments (mainly bryozoans, echinoderms, foraminifers, brachiopods and mollusks) and concentrically lamellar calcium carbonate particles named oolites (Churcher et al., 1991). With regards to its physical properties, Indiana limestone is excellent for conducting laboratory experiments of a fundamental nature, particularly because of its relatively homogenous composition. Indiana limestone can be categorized into three groups based on its colour; buff-coloured, grey-coloured and variegated colour. According to ILIA (1998), buff and grey samples exhibit different properties primarily due to their deposition and lithification. The lower grey limestone lies in the reducing zone below the present day water table. It has a substantially lower permeability than the buff-coloured limestone. The upper buff-coloured limestone has a markedly higher permeability and lies above the

Table 1: Physical properties of Indiana Limestone as recorded by ILIA (1998) and Glowacki (2007).

Property	Glowacki (2007)	ILIA (1998)
Modulus of Elasticity	24 GPa	2.27-37.2 GPa
Ultimate compressive strength	37.5 MPa	27.6 MPa (min)
Ultimate tensile strength	3.6 MPa	2.1 - 4.9 MPa
Specific Density	2.24	2.1 - 2.75
Poisson's ratio	0.14	N/A
Porosity	16.6 %	N/A
Modulus of rupture (dry)	N/A	4.8 MPa
Absorption	N/A	7.5 % (max)
Ultimate shear	N/A	6.2 - 12.4 MPa

present day water table. Indiana limestones that display variegated colourations are regarded as less homogenous than the other types. Table 1 shows a comparison of the mechanical properties noted by ILIA (1998) compared to those by Glowacki (2007) on a particular sample, identified as grey-coloured Indiana Limestone. A petrographic analysis of the three types of Indiana limestone (Churcher et al., 1991) reveals a composition made up predominantly of mineral calcite (99%) with a small amount of quartz (1%).

4.3 Previous Permeability Coefficients for Indiana Limestone

Mattar (2009) has provided a comprehensive summary for permeabilities recorded in the literature. The techniques provided in the literature were assumed to be conventional since the techniques used were not adequately discussed (Churcher et al., 1991; Suri et al., 1997; Bencsik and Ramanathan, 2001; Zeng and Grigg,

2006). Table 2 shows a comparison of techniques and the associated values of permeability.

Table 2: Reported permeability coefficients for Indiana limestone (after Mattar, 2009)

Permeability ($\times 10^{-15} \text{ m}^2$)	External Stress	Direction of Testing	Permeating Fluid	Reference
1.3 to 1.4	none	Radial	Nuto A10 oil	(Heystee and Roegiers, 1981)
4 to 57	Not mentioned	Not mentioned	Not Mentioned	(Churcher et al., 1991)
6	none	Axial	Oil	(Suri et al., 1997)
1.16 ± 0.02	none	Not mentioned	Not mentioned	(Bencsik and Ramanathan, 2001)
21.6	Hydrostatic pressure (2.75 MPa)	Axial	Nitrogen gas	(Zeng and Grigg, 2006)
5.7 to 8	Confining pressure (5 MPa)	Axial	De-aired water	(Selvadurai and Glowacki, 2007)
0.9 to 1.9	none	Axial	Filtered water	(Mattar, 2009)

4.4 Sample Preparation and Manipulation

Primcar Inc., a rock supplier located in Montreal, supplied a near cuboidal block of Indiana Limestone measuring 508 mm (Figure 10). The surfaces were cut using an industrial diamond saw platform, creating a surface texture consistent with that of FEPA grade P120 emery paper. During the cutting procedure the limestone block was constantly lubricated with water. It was noted that the cuts were rougher in certain areas, although the actual surface roughness characterization

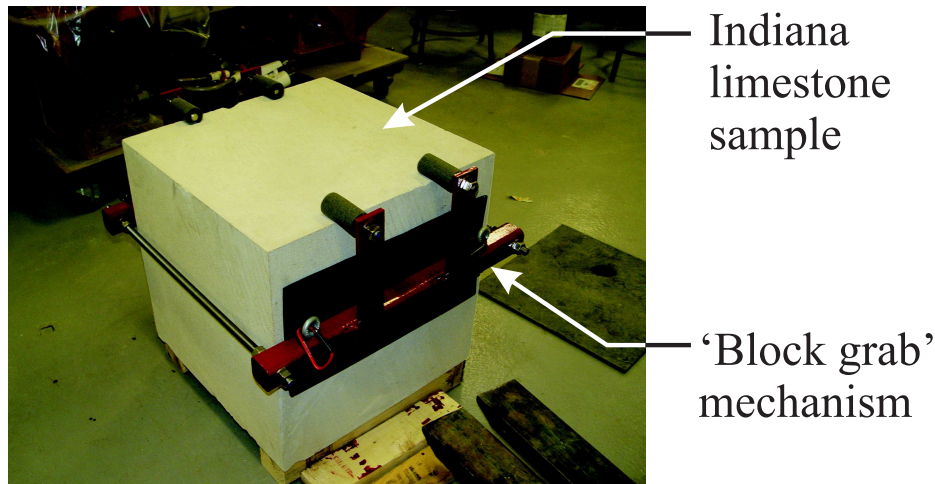


Figure 10: Cuboidal Indiana limestone sample (508 mm) with 'block grab' mechanism.

was not required for the current research investigation. Later, it was shown that the rough areas were indicative of locations with lower permeability, suggesting that it was more difficult to saw through those sections where the rock was denser. Furthermore, this leads us to believe that the sample being tested was variegated, which was also suggested by the slight differences in surface colour.

The block, which weighed approximately 300 kg, was difficult to handle manually. Consequently, a 'block grab' mechanism was fabricated. The mechanism consisted of two 24" tubular sections, with a square cross-section (2" x 2" x 1/4" thick) connected by 1/2" stainless steel threaded rods. Rubber sheets were placed between the samples surface and square sections and the threaded rods were tighten to a specific torque to provide a gripping mechanism. Eye hooks were placed on the steel sections and metal chains were used to lift the block (Figure 11). For safety reasons, the block was initially lifted 1" off the ground and left for a period of 2 days. A torque of 120 N·m was sufficient to lift the block

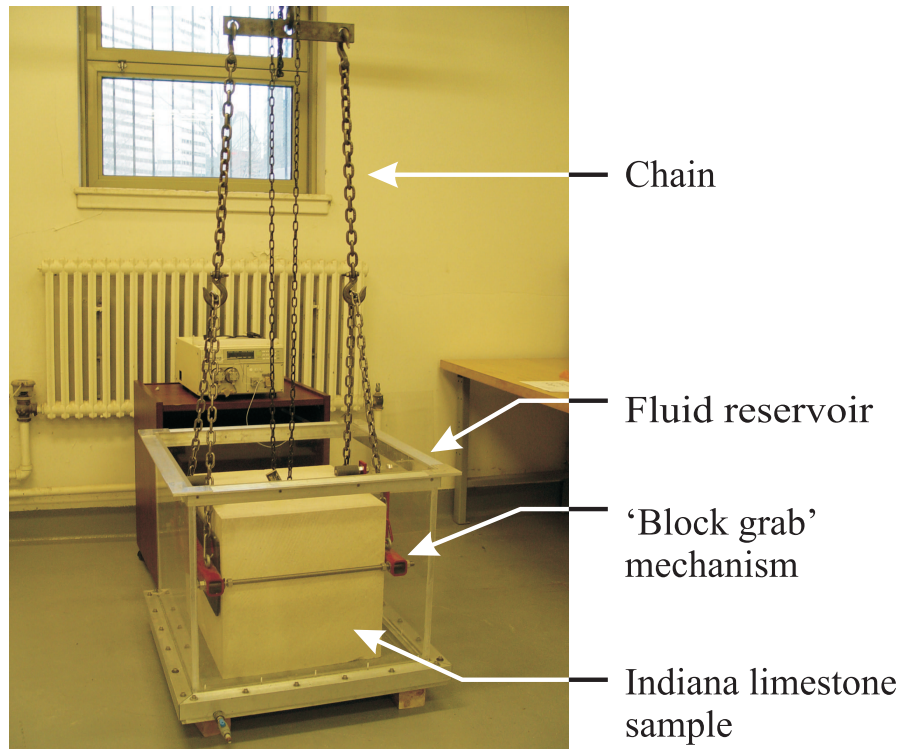


Figure 11: Process of lifting Indiana limestone sample using 'block grab' mechanism.

without damaging its porous skeleton at the contact regions. This produced an estimated pressure of 0.146 MPa over the clamping surface. The experiments performed by Selvadurai and Glowacki (2008), indicate that an external load of approximately 8-10 MPa is needed to cause irreversible deformations to the porous skeleton.

5 Experimental Facility

5.1 Overall Setup

5.1.1 Gum Rubber Gasket

In order to perform surface permeability tests, it was necessary to create a perfect hydraulic seal over an annular region in contact with the surface of the Indiana limestone sample. This hydraulic seal is essential for the accuracy of the experiment. A natural gum rubber gasket with a rubber hardness of 40 Shore A durometer (Figure 12), was pressed onto the surface of the limestone. When the rubber became compressed it closed the surface voids, creating stagnant pores directly underneath the rubber preventing flow at the interface. The thickness of the rubber gasket was 3.175 mm and the inner and outer radii were 12.7 mm and 50.8 mm, respectively. The ratio of the tip seal ($r_o/r_i=4$) determined the shape factor, (10), used in equation (30). During the computational modelling, the surface in contact with the gasket was assumed to be null Neumann. Separate tests that were conducted to ensure that no water flow was taking place at the gasket-limestone interface will be discussed in section 6.1.

5.1.2 General Components

Compressive stress required to provide sealing of the annular patch was applied using a hydraulic cylinder (Appendix A), actuated by a manually-operated hydraulic hand-jack. The cylinder provided an adequate load to effectively seal the annular region and maintained a constant load during the permeability experiments. The loads were measured using an Interface 1200 on-line load cell. A drop

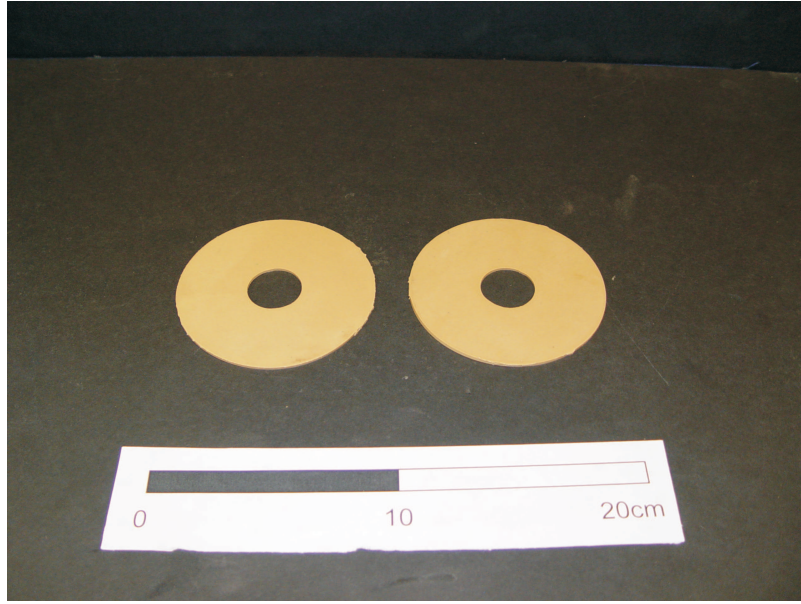


Figure 12: Two natural gum rubber gaskets (40 Shore A durometer).

of 3.2% of the load was recorded over the span of 12 hours and the duration of the longest experiment required 3 hours to reach steady-state conditions. The hydraulic cylinder was mounted to a stiff aluminum reaction frame, and the cuboidal Indiana Limestone sample being tested remained submerged in a water reservoir. The water reservoir in which the limestone block was immersed was maintained at room temperature ($\approx 22^{\circ}\text{C}$). The reaction frame (Appendix B) was fabricated using sectioned tubular (90mm x 90mm and 90mm x 180mm) Bosch Rexroth elements, reinforced by steel stiffeners, provided by Avrex Canada. The sectioned elements were fitted with grooves allowing the hydraulic cylinder to move with respect to the Indiana Limestone sample. The reasons for the frame mobility will be discussed in the experimental procedure (section 6.3). A schematic and actual view of the overall setup is shown in Figure 13.

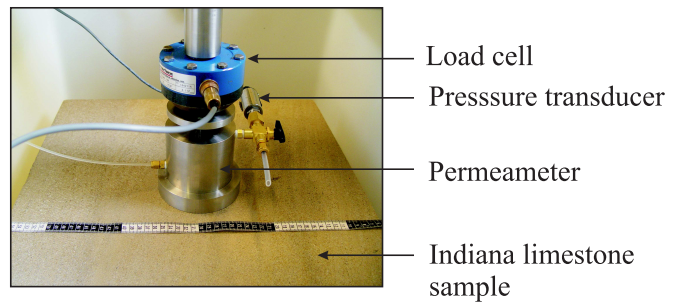
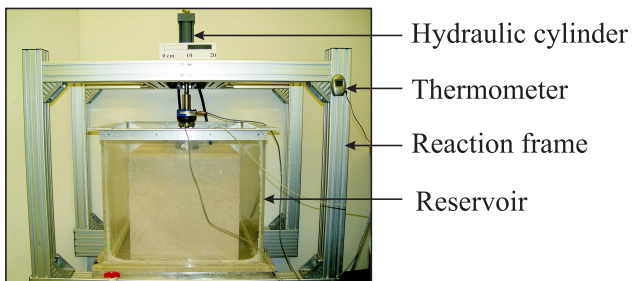
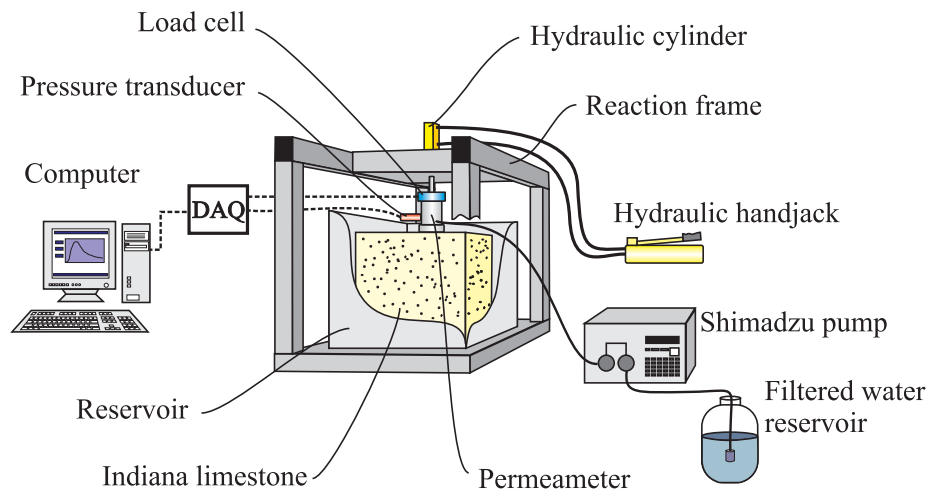


Figure 13: The general arrangement of the laboratory-scale surface permeability test and the details of the test set up.

5.1.3 The Permeameter

The permeameter (Figure 14), constructed of stainless steel, is considered to be the main component of the surface permeability test (Appendix C). This apparatus was used to transfer the load, through a self-aligning joint, from the hydraulic cylinder to the gum rubber gasket. As seen in Figure 14, the central region of the permeameter was hollow. This cavity was used to deliver a constant flow rate of filtered water to the central region of the annulus. The central cavity of the permeameter was equipped with a de-airing port and an online pressure transducer (DCT Instruments, model PZA 100 AC) to monitor the cavity pressure as it reached steady-state. The central cavity also housed an inside retaining ring, which was used to constrain the inner expansion of the rubber when the sealing load was applied. An outside retaining ring, which rested on the rock surface at the periphery of the permeameter, constrained the outward expansion of the gasket during its sealing compression. Due to the near incompressible attributes of rubber (Herrmann, 1965), we can confidently assume that the rubber formed an annular sealing section, where the boundaries (r_o and r_i) were correctly defined. This well defined boundary ensures that errors in the experiment definition are minimized compared to previous research using experimental permeameters (Tidwell and Wilson, 1997).

5.1.4 Liquid Chromatographic Pump

Water filtered to 1 μm was supplied to the central cavity at a constant flow rate, using a liquid chromatographic pump (Shimadzu LC-3A). The pump employs a

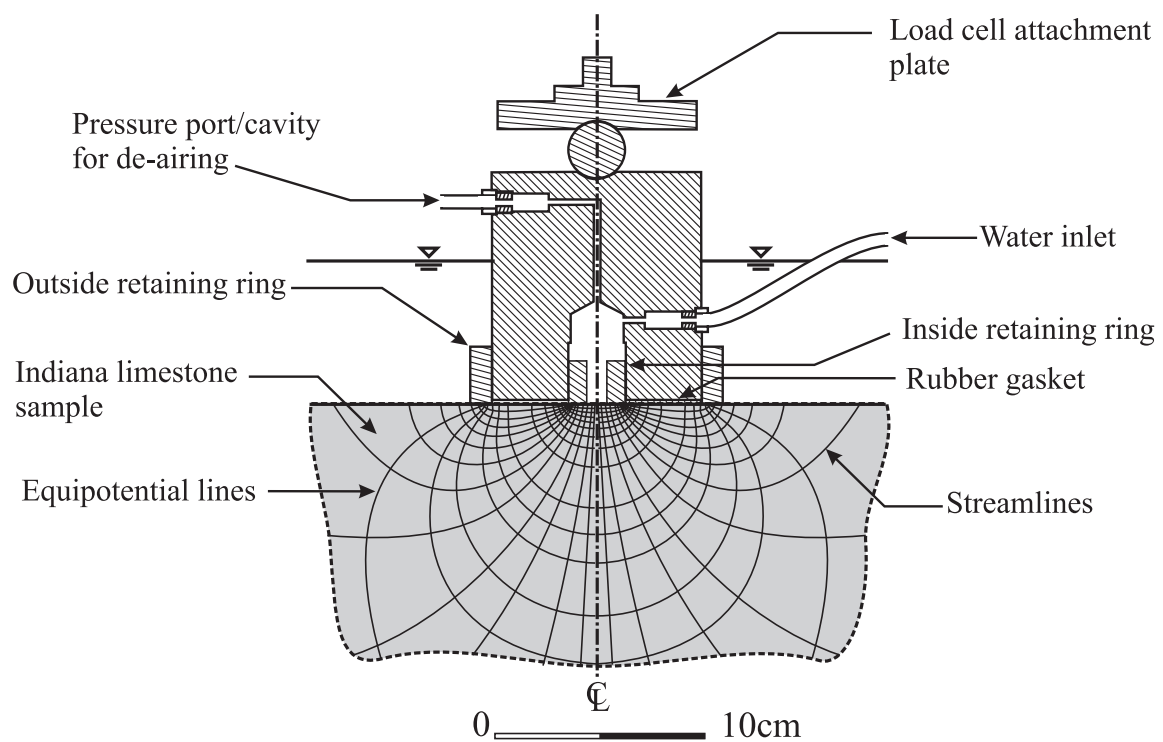


Figure 14: Details of the permeameter.

dual piston mechanism that can accurately deliver flow rates ranging from 0.1-150 ml/min. The pump was checked routinely with direct volume measurements to ensure the delivery of a correct flow rate. Calibration tests showed the flow rates were accurate to within 2% of the set value, as specified by the pump manufacturers. Isothermal conditions were monitored using a thermometer placed in the filtered water reservoir, recording prior to and after completion of each experiment.

5.1.5 Data Acquisition

A Techmatron data acquisition system was used to monitor both the online pressure transducer and the load cell. This system is equipped with isolated signal process control and signal conditioning modules. The results were converted and graphically produced using TracerDAQ pro software. A detailed record of the technical equipment used in the research work is outlined in the following section.

5.2 Technical Specifications of the Equipment and Components Used in this Research

1. Pump: LC-8A Shimadzu Liquid Chromatographic pump.
 - Double plunger, reciprocating pump delivering 250l per stroke per head.
 - Operating temperature: 10 to 35°C.
 - Accuracy in flow rate setting: $\pm 2\%$.
 - Flow rate stability: $\pm 0.5\%$.
 - Flow rates varied between 2 and 10 ml/min.

- Pressure range 0 - 30 MPa
2. Pressure transducer: DCT Instruments (PZA 100 AC)
- 0.05% accuracy.
 - 0-100 psi range.
 - Output 7.65mV/V
 - Excitation 10 V
3. Load Cell: Interface 1210, 10 kip (≈ 4545 kg).
- Hysteresis = $\pm 0.05\%$ FS
 - Nonlinearity = $\pm 0.05\%$ FS
 - Static error band = $\pm 0.05\%$ FS
 - Non repeatability = $\pm 0.01\%$ RO
4. Data acquisition: Techmatron
- Personal Measuring Device (PMD-1608FS)
 - 16 bit analog resolution
 - 8 analog to digital independent channels at 50 kHz scanning rate
 - Accuracy of 2.98 mV on a 5 V range
 - USB compatible
 - 2 isolated signal process control signal conditioning modules (SCM-5b38 for Dataforth Corp.)
 - $\pm 100\text{mV}$

- Accuracy of $\pm 0.08\%$ FS
- Output range of $\pm 5\text{V}$
- Full bridge input $10\text{ k}\Omega$
- Nonlinearity = $\pm 0.02\%$ FS

6 Experimental Procedures

Since the experiments conducted in connection with this research were non-routine, it was necessary to develop an experimental protocol that could be followed during each permeability test. Such a procedure was also adapted by Tidwell and Wilson (1997) in their experimental research involving the developed permeameter. As mentioned previously (section 5.1.1), a proper hydraulic seal is critical to the success of the surface permeability experiment. Calibration experiments were necessary to determine the adequate load necessary to create a hydraulic seal at the gum rubber gasket-limestone interface.

6.1 Sealing Procedure

Firstly, using the hydraulic cylinder and manually operated hand jack, a constant load (discussed in the following paragraph) was applied to the permeameter placed at a central location on the cuboidal limestone sample. Maintaining this sealing stress, water was introduced to the central cavity and the central open region of the annular region at a constant flow rate. The fluid pressure within the permeameter, monitored via the online pressure transducer, increased until it reached the steady state pressure consistent with the prescribed flow rate. Computational

methods, validated using (30), were used to calculate the permeability consistent with the applied sealing stress by inputting the appropriate boundary conditions, prescribed flow rate, steady-state pressure and temperature of the system.

The load on the gasket was then increased by 0.75 MPa and the new permeability was estimated for the increased gasket sealing load. This incremental increase in the sealing load was adopted until the estimated permeability value showed no change with a further increase in sealing load (i.e. less than 1% change). The rationale for the procedure is as follows: at low sealing pressures interface flow takes place and with a continuous increase in the sealing load, the interface flow is eliminated and flow is directed only through the Indiana Limestone block. Figure 15 shows the results of the permeability versus sealing pressure for an experiment conducted at the location A on face 1. To account for possible non-uniformity of the surface texture at various locations on the surface block, a sealing stress of 1.75 MPa was applied during all tests.

6.2 Darcy Flow in the Support Volume

The permeability has been defined to appeal to Darcy's law. Implicit in the Darcy formulation is the requirement that the reduced Bernoulli potential consists only of the datum and pressure components, with the velocity potential considered to be negligible. This requires the velocity to be small and a suitable condition to ensure low flow velocities through the pore space to verify that the Reynolds number is lower than a specified value. Zeng and Grigg (2006) have discussed the limits of applicability of Darcy flow in porous materials. The Reynolds number is a non-dimensional term defined as

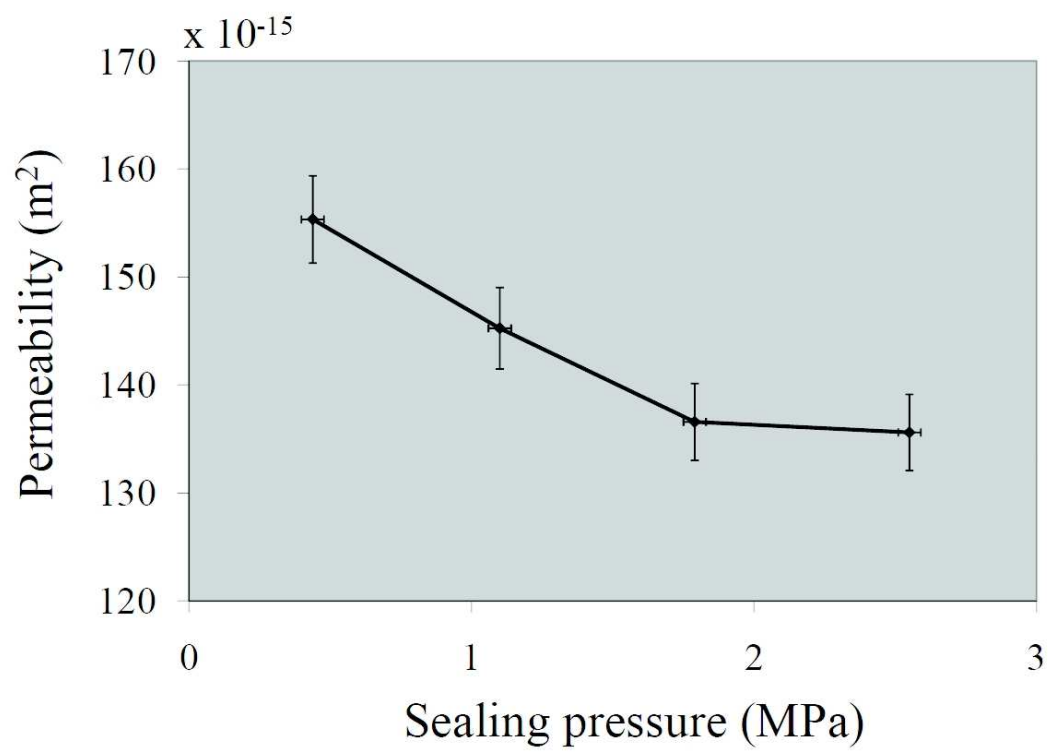


Figure 15: Determining the appropriate sealing load.

$$Re = \frac{\rho_f v d}{\mu} \quad (32)$$

where ρ_f is the fluid density (kg/m³), v is the superficial flow velocity (m/sec), d is the characteristic length (m) defined in relation to either the mean pore throat or mean pore size (Hornberger et al., 1998) and μ is the dynamic viscosity (N·sec/m²). A related non-dimensional parameter is the Forchheimer number defined by

$$Fo = \frac{k\beta\rho_f v}{\mu} \quad (33)$$

where k is the permeability at ‘zero’ velocity and β is the non-Darcy coefficient. Equation (33) is not helpful due to the fact that it requires knowledge of the permeability, which is undetermined.

According to Philips (1991), for the flow in a porous medium to be considered within the Darcy regime, $Re \ll n$, where n is the porosity. Pore throat diameter measurements are non-routine, although Wardlaw et al. (1987) have determined that the pore throat diameter (d) varies from 2×10^{-9} mm minimum to 46×10^{-9} mm maximum, with an average of 11×10^{-9} mm. These values were also confirmed by Churcher et al. (1991), who determined the pore throat diameter to be 14.8×10^{-9} mm. The velocity associated with a peak flow rate of 10 ml/min over the central opening of 25.4 mm, was found to be $v \approx 3.3 \times 10^{-4}$ m/sec. The porosity of Indiana Limestone, measured by Selvadurai and Glowacki (2008), is approximately 0.16. Comparing this to the calculated Reynolds number, $Re \approx (3 \times 10^{-9}, 5 \times 10^{-5})$, we can determine that the flow at the peak injection rate is

Darcy flow.

According to Hornberger et al. (1998), Darcy flow is considered a linear relationship while Forchheimer flow, due to the inertial effects of the fluid, is non-linear. To examine the non-linear effects that may occur at higher flow rates, an experiment was conducted where the flow rate was increased in a step-wise manner and the steady-state pressure was recorded at each step. Figure 16 shows the non-linearity that develops when the flow rate increases and the Reynolds number becomes large with respect to the porosity of the material. The enlarged portion of Figure 16 displays the low flow rate region considered to be governed by the Darcy flow regime. These results show a linear relationship, corresponding to an R^2 value equal to 0.9898, between the flow rate and steady-state pressures which is indicative of Darcy flow.

6.3 General Experimental Procedure

The goal of the surface permeability test is to determine an ‘effective’ permeability for the entire cuboidal sample. To do so, surface permeability needs to be measured over the entire block. In performing the experiments we have chosen nine locations that are ordered in regular manner. This arrangement is considered to provide for ease of recording data and their subsequent analysis. Figure 17 shows the individual test locations for one face that are used for determining the ‘effective’ permeability of the large cuboidal sample. It should be noted that each face has nine test locations; therefore in total the entire block had 54 locations with estimated permeability values. For each location a minimum of 3 permeability tests were performed; roughly 162 permeability tests were conducted on

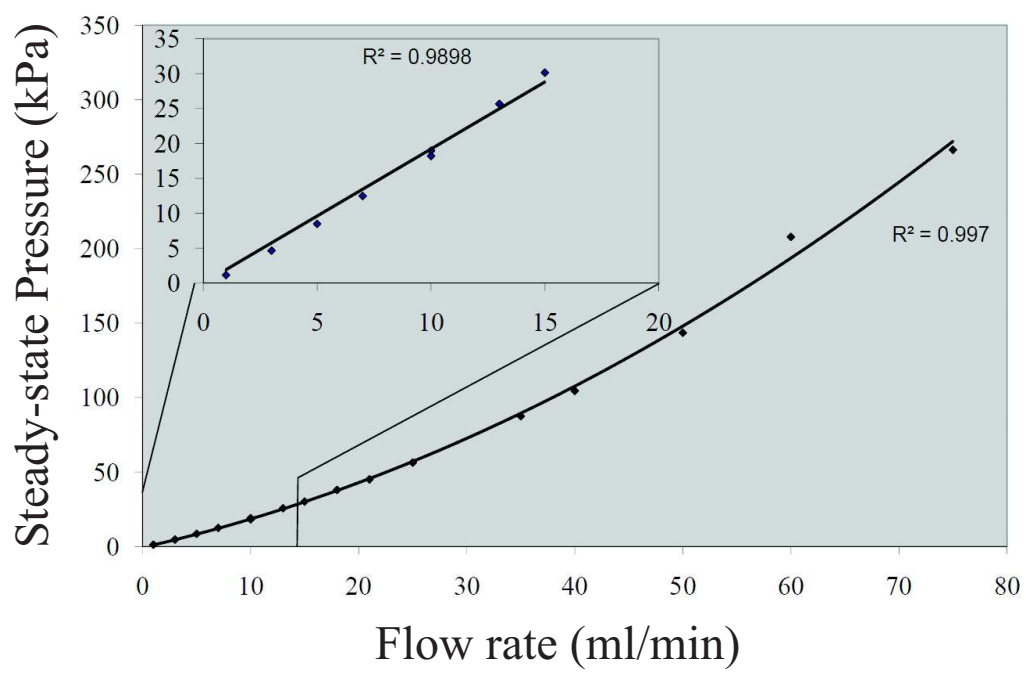


Figure 16: Steady-state pressures versus flow rate using a constant sealing pressure.

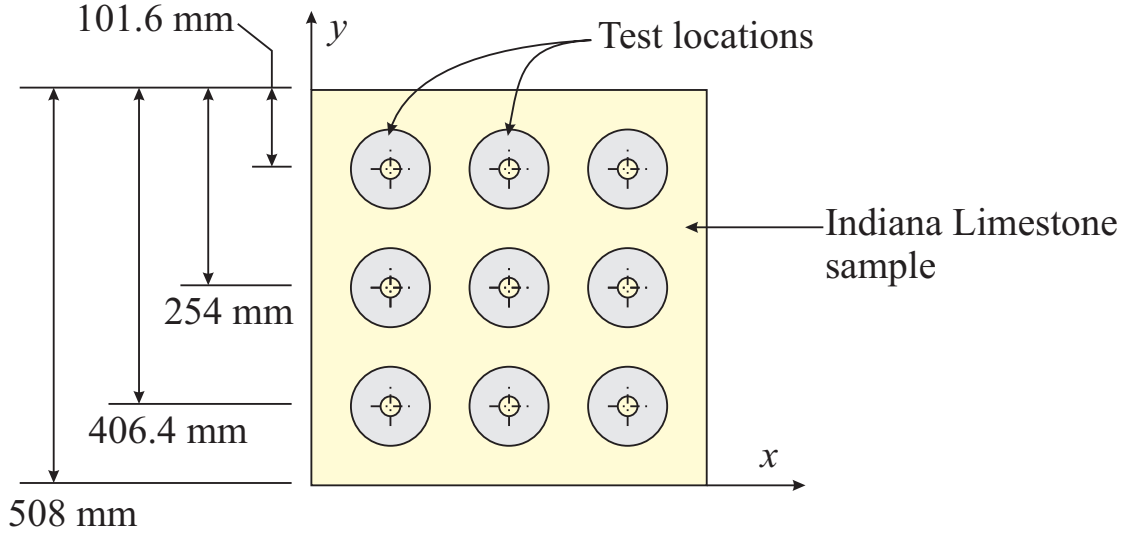


Figure 17: Plan view of the test locations (nine in total) on one surface of the cuboidal sample.

the cuboidal block. For each test, the steady-state pressure, flow rate, location and temperature of the percolating fluid, essential for determining the surface permeability of the sample, were recorded.

At each location the maximum and minimum pressures attained for a prescribed steady flow rate were recorded. The temperature of the percolating fluid was monitored to determine the dynamic viscosity, used in the permeability analysis. Extra care was taken to place the block correctly relative to the coordinate system available on the frame. Figure 18 shows the method used to locate the block at the central position using three plumb-bobs.

6.4 Influence of Boundary

According to the derivations discussed in Section 3.2, the surface permeability can be calculated using equation (30). This equation for estimating surface perme-



Figure 18: Method for centrally locating the sample with respect to the coordinate system of the reaction frame.

ability is limited to axisymmetric situations and may not be directly applied to examine the surface permeability when the permeameter is located close to the edges of the cuboid (Figure 17).

Goggin et al. (1988), provided a theoretical analysis to determine the ‘edge effect’ associated with the permeameter. A theoretical study was performed on a sample core plug, seen in Figure 19, where a is the internal tip seal radius, b is the external tip seal radius, P_i is the internal cavity pressure, P_o is the external pressure, R_{core} is the radius of the core and L_{core} is the length of the core. To determine the variation of the shape factor (G_o) with respect to these dimensions, Goggin et al. (1988) introduced the non-dimensional parameters

$$b_D = \frac{b}{a}; \quad R_D = \frac{R_{core}}{a}; \quad L_D = \frac{L_{core}}{a} \quad (34)$$

where b_D is the dimensionless tip-seal ratio, R_D is the dimensionless core-plug

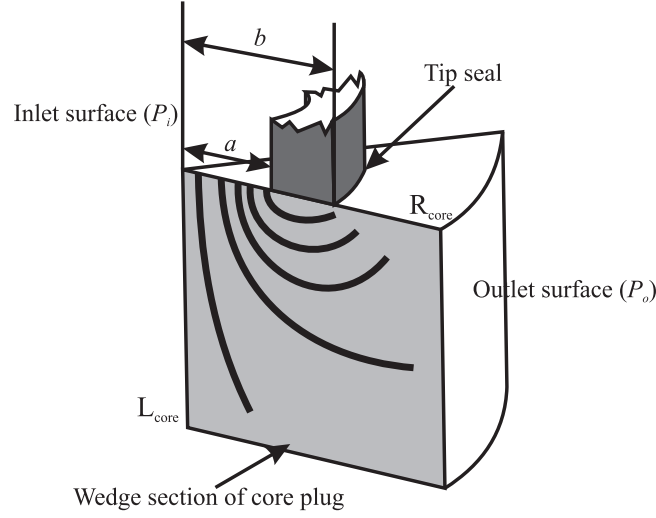


Figure 19: Sketch of the flow geometry for an unconfined core plug sample. (after Goggin et al., 1988)

radius and L_D is the dimensionless core-plug length. Using a finite difference approach to the solution of (24) a geometric factor can be developed, which accounts for all the non-dimensional parameters, i.e.

$$G_o = f(b_D, L_D, R_D) \quad (35)$$

Figures 20 and 21 show, respectively, the influence of the core sample length and core sample radius, normalized with respect to the half-space solution (i.e. $G_o = f(b_D, \infty)$).

When examining the geometries associated with corner locations of the cuboidal block of Indiana Limestone tested, we can estimate the largest plug with respect to the edge conditions (Figure 22). Using $a = 12.7$ mm, $b = 50.8$ mm, $R_{core} = 101.6$ mm and $L_{core} = 508$ mm, we can convert these values to the non-dimensional parameters and determine the edge effect, using plots in Figure 20 and 21 and

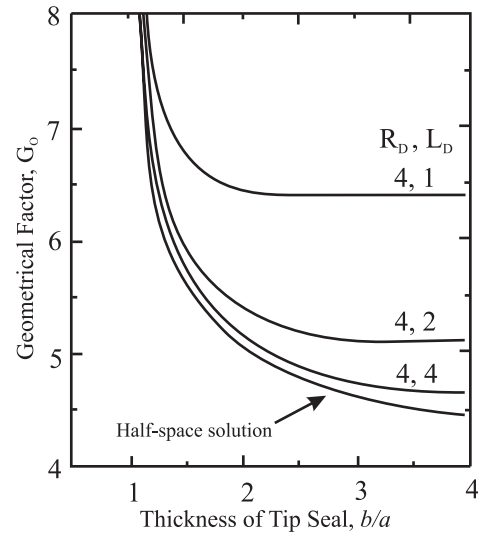


Figure 20: Plot of geometrical factor (G_o) curves showing the effect of the core sample length. (after Goggin et al., 1988)

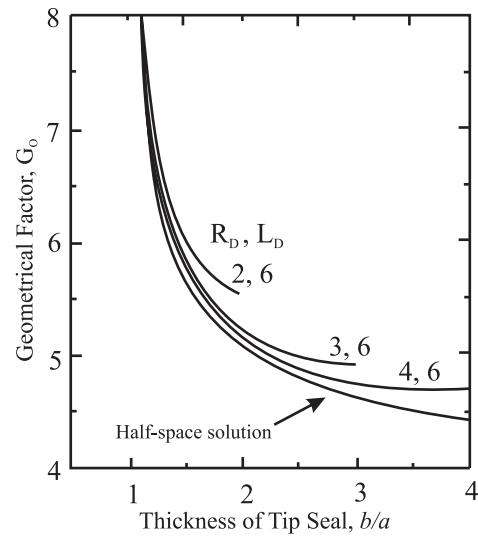


Figure 21: Plot of geometrical factor (G_o) curves showing the effect of the core sample radius. (after Goggin et al., 1988)

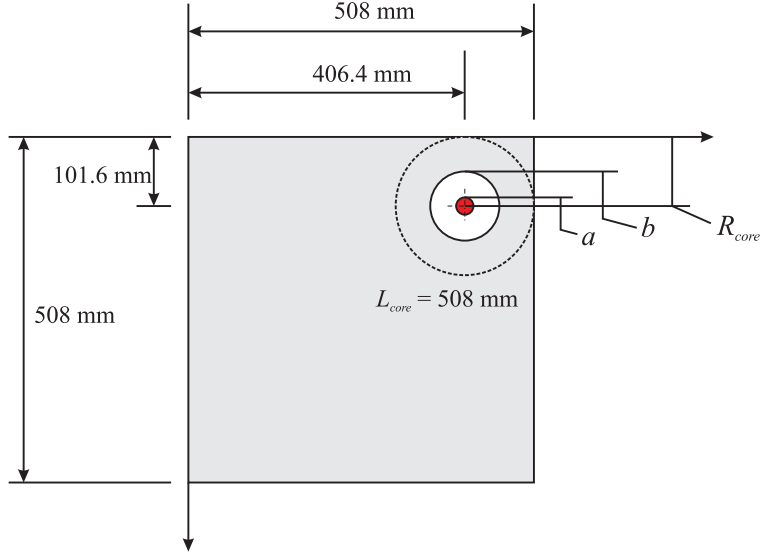


Figure 22: Plan view of estimated ‘plug’ sample for a corner location on cuboidal Indiana limestone sample (plug in dashed line).

the geometric factor in equation (10). The non-dimensional terms for b_D , R_D and L_D are 4, 8 and 40, respectively. These values demonstrate that the amount of material being tested is virtually equivalent to that encountered in the half-space region. The geometric factor, equation (10), determined from the half-space solution is valid for virtually *any test location* described in Figure 17. Figure 23 shows the theoretical core-plug applicable to the edge locations on the testing surface. The non-dimensional values of b_D , R_D and L_D are the same as for the corner core-plug.

6.5 Computational Modelling

We now confirm the findings discussed in the previous section by developing a computational model of permeameter locations relevant to the corner and edge

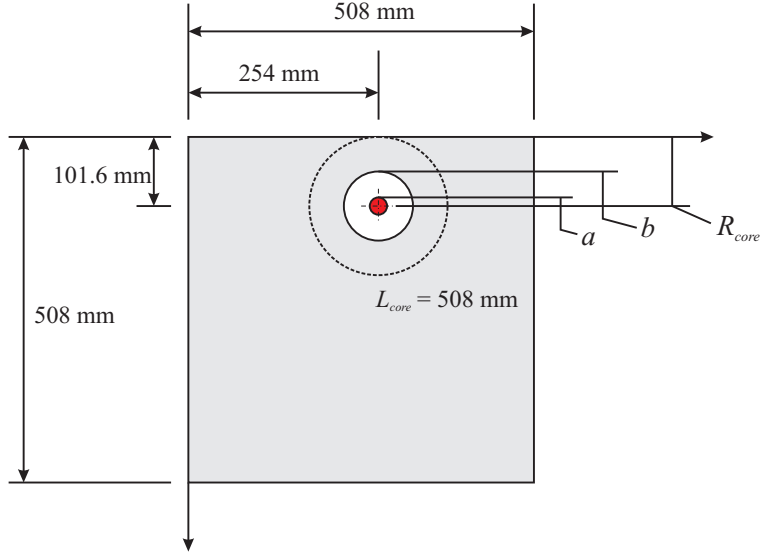


Figure 23: Plan view of estimated ‘plug’ sample for an edge location on cuboidal Indiana limestone sample (plug in dashed line).

portions shown in Figure 17. The solution (30) is rigorously valid for test locations that are sufficiently far from the edges of the block. It is also advantageous to develop a finite element approach for the solution of this problem so that the accuracy of the approaches can be further validated. This analysis was performed using a commercially available finite element code, COMSOLTM, developed for multiphysics. Further applications involving thermo-poroelastic and transversely isotropic responses using the same experimental facilities can be integrated into COMSOLTM quite easily, making the development and validation of this model applicable for future research. Table 3 shows the values that were input into COMSOLTM for validation purposes. The computational approach is based on the progressive alteration of the permeability at the specified location which is subject to the experimentally measured constant potential at the inner annular

region, until the flow rate matches the prescribed value in an experiment.

Table 3: Typical input values for COMSOLTM validation.

Variable	Value	Units	Description	Source
Φ_o	5	m	Inlet Pressure Head	Experiments
μ	9.772×10^{-4}	Pa·s	Dynamic viscosity	Experiments
ρ	9.9778×10^2	kg/m ³	Density of fluid	Experiments
K	15×10^{-15}	m ²	Permeability	Varied to match flow rate

6.5.1 Validation of the computational modelling

To establish the accuracy of the finite element approach we examine the potential problem for a semi-infinite domain where a constant potential (Φ_o) Dirchlet boundary condition is applied over the region $0 \leq r < a$ and a zero Neumann boundary condition from $a \leq r < \infty$ on the plane $z = 0$ (Figure 24). This is the limiting case where $b \rightarrow \infty$. The computational results were compared to the analytical solution developed by Selvadurai (2003), where

$$Q = a\Phi_o \left(\frac{K\gamma_w}{\mu} \right) F \quad (36)$$

and K is the permeability, γ_w is the weight of water, μ is the dynamic viscosity of the water and F is the *intake shape factor*, where $F = 4$ for the isotropic case.

The element types used in the finite element discretization were tetrahedral elements. Two types of finite element discretizations were used to assess the accuracy of the computational approach. In the first, the flow domain is modeled in

three regions of increasing mesh density, consisting of altogether 299,945 elements (Figure 25a) and in the second, the flow domain is modelled as a single zone, with a finely graded zone from $0 \leq r < a$, consisting of 252,227 elements (Figure 25b). The maximum element edge length, in the discretization shown in Figure 25b, was 1.5×10^{-4} m at the inlet. This resulted in the mesh at the inlet boundary being 1,690 times smaller than the length ($20a$) of the modeled region. This ratio should be kept if upscaling is to be used in future models. COMSOLTM used a robust solver, SPOOLES, to generate the steady state solution. The discretization 1 (Figure 25a) and discretization 2 (Figure 25b) were able to predict the permeability (given the flow rate Q and the potential Φ_0) to within 2.74 % and 2.05 % of the analytical solution given in (36), respectively. The discrepancy is mainly due to the absence of both singular elements to account for the internal boundary and the absence of infinite elements to account for the semi-infinite nature of the analytical domain.

By modifying the boundary conditions, we can model the problem with the annular sealing patch used in the experimental permeameter. This gives a new mixed boundary value problem for a semi-infinite domain that is now defined by: a constant potential (Φ_0) Dirchlet boundary condition is applied over the region $0 \leq r < a$, with a null Neumann boundary condition from $a \leq r < b$ and a zero potential Dirchlet boundary condition from $b \leq r < \infty$ on the plane $z = 0$ (Figure 26). For this validation, the mesh discretization used in Figure 25b was used. Actual block dimensions and ‘tip-seal’ ratio was used, i.e. $a = 12.7$ mm, $b = 50.8$ mm and $b/a = 4$. For computational efficiency, only a quarter of the flow domain was modelled and the symmetry of the region associated with the

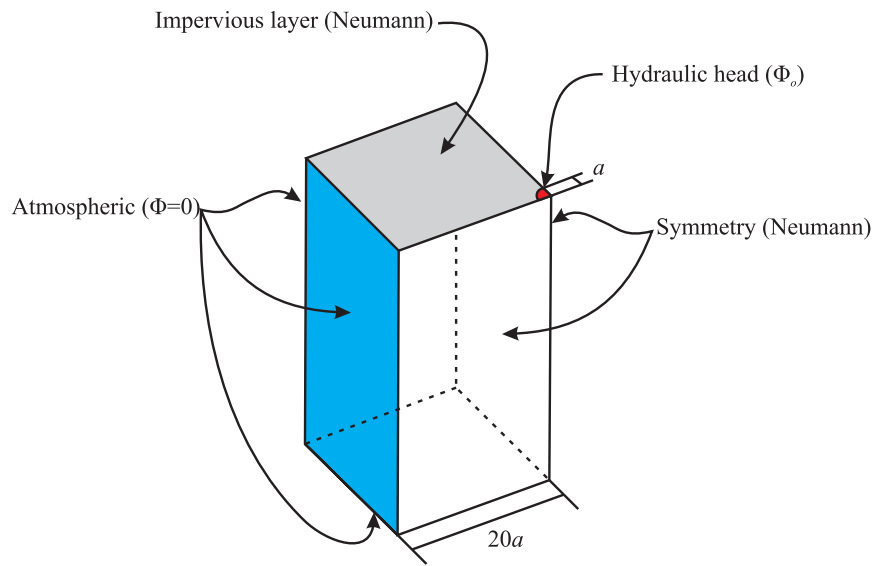


Figure 24: Computational modelling boundary conditions for validation of potential steady-state fluid flow problem.

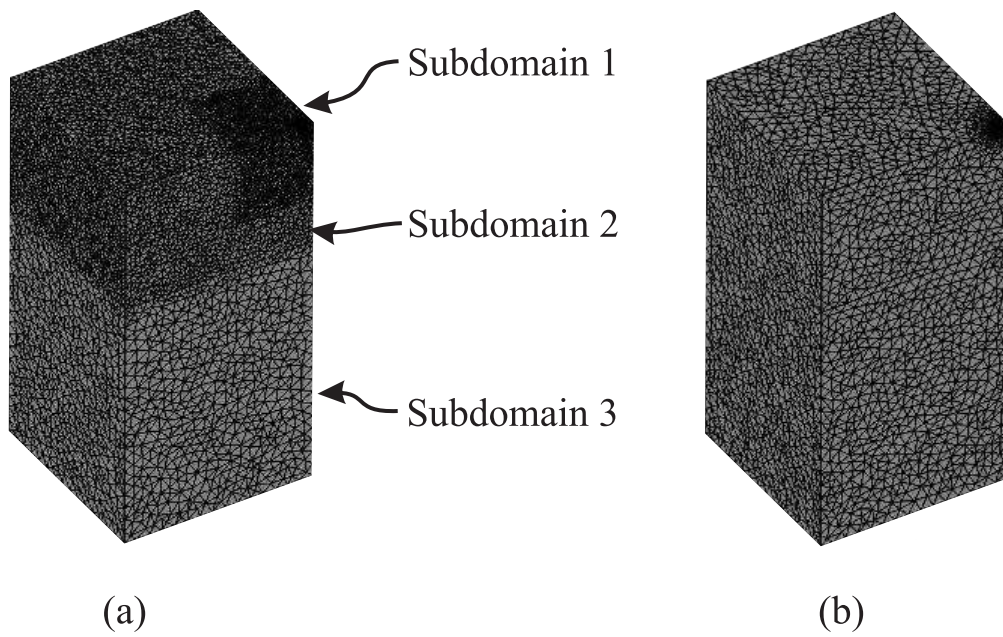


Figure 25: Finite element discretizations of the flow domain

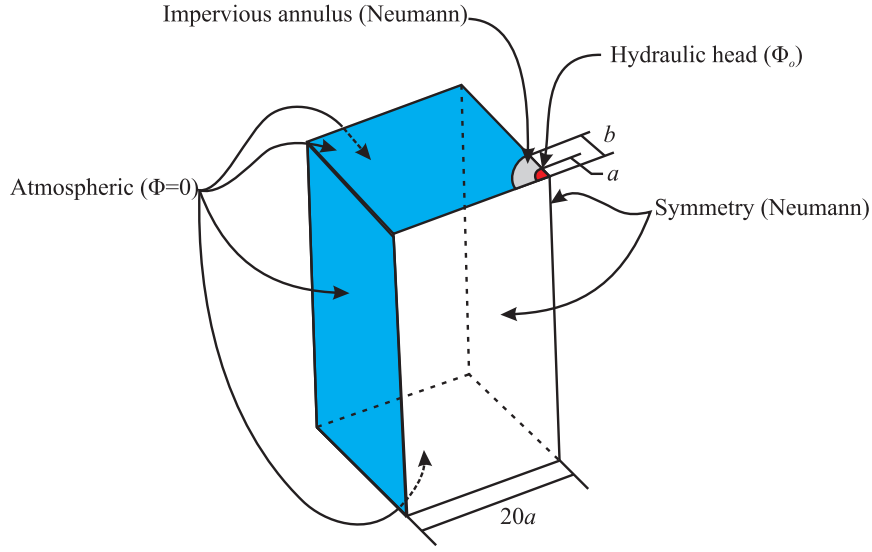


Figure 26: Annular sealing patch validation model (where a and $b = 12.7$ mm and 50.8 mm, respectively).

central test location was used. This model simulated the central test location and, according to the non-dimensional analysis discussed previously (Goggin et al., 1988), could be solved using (30). The maximum difference between the analytical and computational results was 1.95 %.

Computations were also performed to compare the results obtained for experimental configurations at the edge and corner locations. Each model employed one axis of symmetry to reduce the computing power required. The reduced domains and mesh discretizations are shown in Figure 27. Computational estimates for the edge location under-predict the analytical result given by (30) by 3.07 % and the corresponding result for the edge location under-predicts the analytical solution by 3.44 %. In summary, the validation of a permeameter, with tip-seal ratio $b/a = 4$, located at specific locations, central, edge and corner, with the

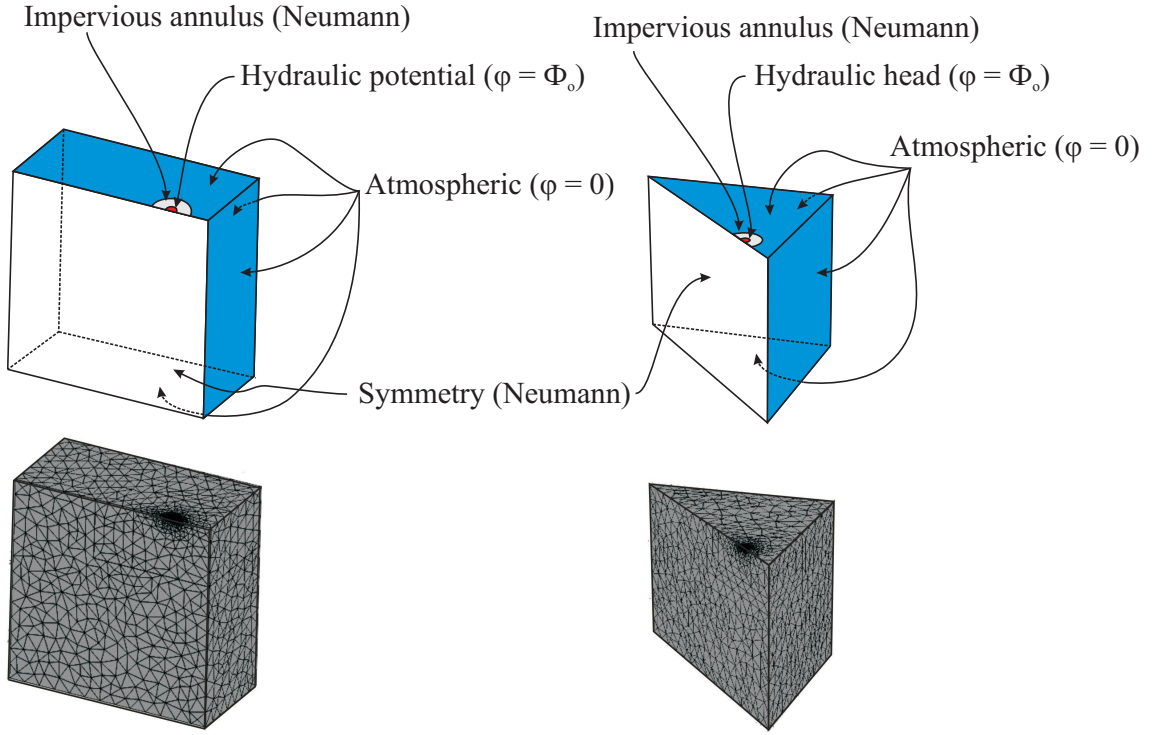


Figure 27: Computational modelling for fluid flow associated with the permeameter located either along the edge or at the corner of the cuboidal specimen

analytical solution (30) applicable to a semi-infinite domain was determined to be approximately 3.5 %.

6.5.2 Computational Validation of a sub-region

This section pertains to a basic assumption that allows us to calculate the effective permeability. The estimation of permeability from both analytical and computational approaches assumes the porous medium to exhibit both isotropy and homogeneity. The issue of isotropy cannot be addressed through the current experimental configurations. The experiments conducted at different permeame-

ter locations are, however, expected to estimate the local permeability of the cuboid region. It is therefore important to investigate how the permeability of a neighboring region can influence the estimated permeability at the test location. This can be done using several approaches; in this research, we chose to consider the sub-regions that are consistent with cube regions at the permeameters location shown in Figure 17. This approach produces a heterogeneous sample, which eliminates the isotropic assumption used to estimate the permeability. In turn, we must analyze a sub-region to ensure that the permeability chosen for a specific sub-region is relatively uninfluenced by the permeability of the neighbouring sub-regions. Firstly, it was assumed that the size of a sub-region was 127mm x 127mm x 127mm. Secondly, a similar annular patch (12.7mm internal radius and 50.8mm external radius) was applied to the center of an arbitrary face. Referring to Figure 28, the internal region of the annulus, S_0 , was given a constant Dirchlet potential, Φ_o , while the annular boundary condition, S_1 , was prescribed as null Neumann. The boundary condition associated with S_2 was null Dirchlet. To determine the effect of the surrounding media two extreme scenarios of boundary conditions were applied to S_3 and S_4 . Scenario 1 involved assuming S_3 and S_4 to be null Dirchlet and the flux over the inlet was determined from computational analysis. Scenario 2 involved applying a null Neumann boundary condition over surfaces S_3 and S_4 and, similarly, the flux was measured over the inlet. These extreme situations capture all possible intermediate values for permeability of regions neighbouring the sub-cube. These results were then compared to the flux over the inlet for the half-space solution. There were differences of only 1% and 5.43% with respect to the half-space solution for scenario 1 and 2, respectively.

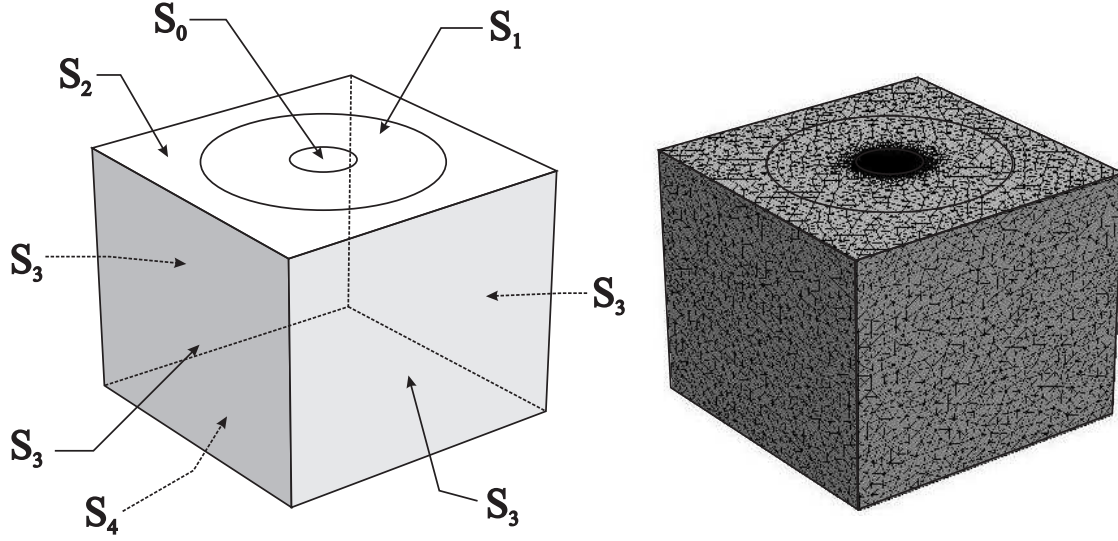


Figure 28: Modelling of flow in a sub-cube of the cuboidal region.

Therefore, the permeability of the local sub-region is virtually unaffected, within an acceptable margin of error for permeability estimations, even with extreme variations of permeability in the neighbouring sub-regions.

6.6 Experimental Results and Interpretation

Each face of the cuboid limestone sample was tested in the specific locations described in Figure 17. The nine locations on each face were tested a minimum of three times; a sample result is shown in Figure 29. The steady-state pressure stabilized approximately 30 minutes after the initial application of the steady-state flow rate. Consecutive steady-state pressures recorded during tests at individual locations varied only by 3.58 %. Previous experiments conducted by Selvadurai and Glowacki (2008) on cylindrical samples of Indiana limestone (100mm diameter by 200mm length) showed virtually no mineral dissolution that could affect the

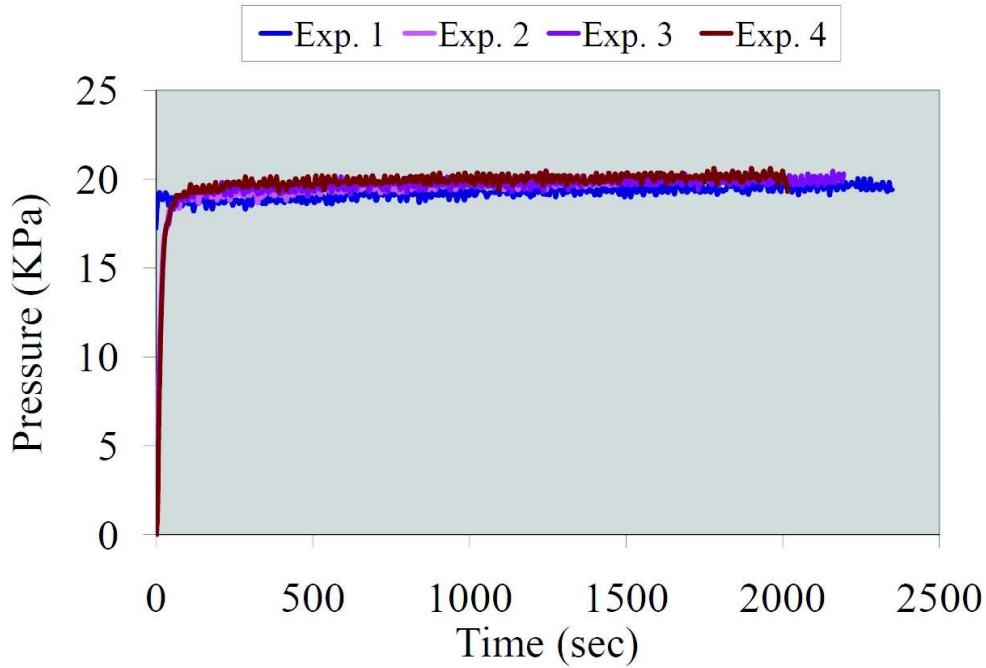


Figure 29: Sample data for steady state pressure attainment during constant flow, permeameter test (Face 1, position D).

permeability. Furthermore, subsequent tests repeated at random locations, on the Indiana limestone block over a 5 month interval indicated a variability of 2.28 % that can be explained by experimental error associated with the equipment and not due to alterations in the pore skeleton structure.

Table 4 shows the averaged 54 surface permeabilities measured on all six faces of the limestone sample, and Figure 31 provides a visual and spatial representation of the data. The preliminary permeability data in Figure 31 is represented as the outer diameter of the sealed region ($2\cdot b$) for visual convenience. A modified “Rubik-cube” was used to keep track of the locations of all the permeability data points with respect to the others. The layout of the Rubik-cube is shown in Figure

Table 4: Computational estimates of surface permeability on all six faces of a cuboidal sample of Indiana Limestone. [The Table gives the average value along with the corrections to estimate the maximum (+) and minimum (-) values]

Location	Face 1 (x 10 ⁻¹⁵ m ²)	Face 2 (x 10 ⁻¹⁵ m ²)	Face 3 (x 10 ⁻¹⁵ m ²)	Face 4 (x 10 ⁻¹⁵ m ²)	Face 5 (x 10 ⁻¹⁵ m ²)	Face 6 (x 10 ⁻¹⁵ m ²)
A	136.08 ^{+5.3} _{-12.2}	109.33 ^{+1.65} _{-1.38}	137.65 ^{+14.06} _{-6.45}	17.27 ^{+1.19} _{-0.75}	34.93 ^{+0.74} _{-0.70}	37.95 ^{+0.67} _{-0.46}
B	46.35 ^{+1.38} _{-1.70}	86.55 ^{+5.49} _{-9.17}	211.49 ^{+5.60} _{-3.08}	224.72 ^{+15.45} _{-7.55}	16.35 ^{+0.26} _{-0.22}	38.49 ^{+2.05} _{-1.94}
C	20.03 ^{+0.39} _{-0.33}	41.53 ^{+0.41} _{-0.40}	146.99 ^{+3.46} _{-3.93}	29.09 ^{+9.79} _{-2.14}	252.42 ^{+8.04} _{-18.70}	46.51 ^{+1.69} _{-1.27}
D	37.28 ^{+0.95} _{-0.43}	157.69 ^{+2.81} _{-3.39}	158.03 ^{+7.11} _{-3.91}	26.81 ^{+0.72} _{-1.26}	210.51 ^{+12.87} _{-11.31}	15.79 ^{+0.43} _{-0.33}
E	69.35 ^{+3.33} _{-2.03}	90.26 ^{+6.78} _{-13.01}	108.21 ^{+1.69} _{-1.55}	34.85 ^{+0.15} _{-0.21}	52.95 ^{+1.69} _{-1.22}	43.52 ^{+0.40} _{-0.20}
F	41.33 ^{+2.48} _{-1.22}	112.96 ^{+6.02} _{-6.72}	68.83 ^{+0.98} _{-1.56}	254.62 ^{+2.43} _{-4.43}	33.16 ^{+1.36} _{-0.67}	17.62 ^{+0.73} _{-0.76}
G	40.21 ^{+1.23} _{-0.92}	59.02 ^{+0.91} _{-0.99}	78.56 ^{+2.05} _{-1.82}	243.93 ^{+14.86} _{-20.63}	19.08 ^{+0.19} _{-0.16}	14.08 ^{+0.41} _{-0.42}
H	77.13 ^{+5.02} _{-4.14}	27.39 ^{+0.66} _{-0.54}	23.77 ^{+0.08} _{-0.27}	11.25 ^{+0.08} _{-0.04}	113.85 ^{+2.60} _{-2.33}	47.81 ^{+0.59} _{-0.39}
I	12.06 ^{+0.80} _{-0.45}	34.06 ^{+0.45} _{-1.91}	37.23 ^{+1.18} _{-0.61}	35.02 ^{+0.81} _{-0.71}	253.12 ^{+4.79} _{-1.93}	47.09 ^{+1.69} _{-1.53}

30, where the locations were also marked directly on the sample so that future tests may be performed.

6.7 Kriging

The ability to interpret the surface permeability data and to generate plausible estimations for the *internal* permeability of the cuboid sample is critical to this research project. Many statistical methods are available to determine the interior permeability based upon results obtained for a ‘cluster’ of surrounding points. ‘Kriging’ is a technique used extensively in a wide range of scientific and engineering fields such as oceanography, biosciences, neurosciences, nano-technology,

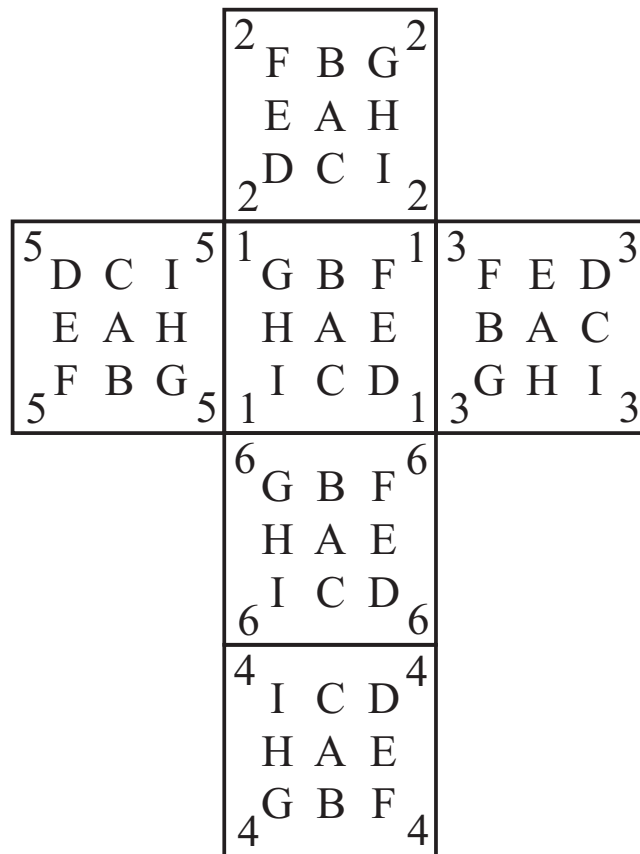


Figure 30: Locations of surface permeability with respect to Table 4. Locations are also marked on Indiana limestone sample.

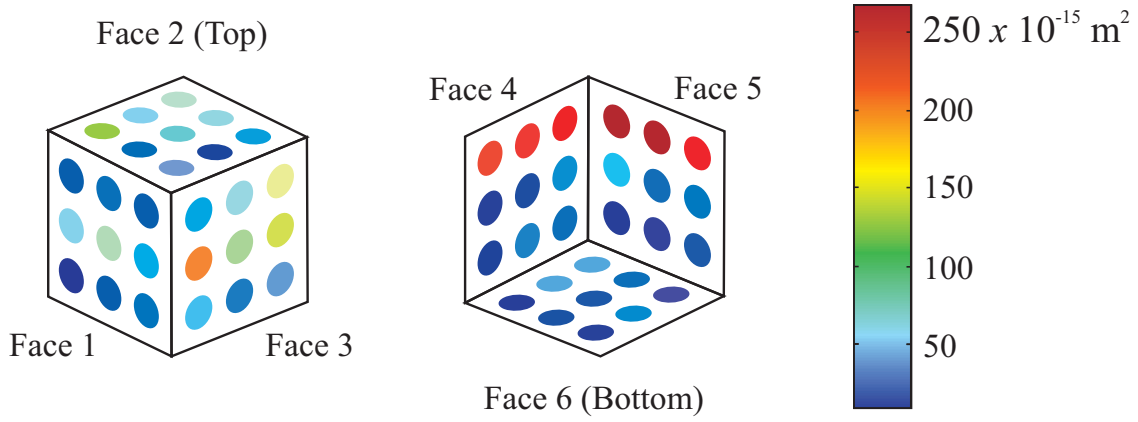


Figure 31: Preliminary distributions of permeability corresponding to the test data shown in Table 4.

mineral resources engineering and material sciences, where a collection of data is used to determine the unknown interlaying data points within an interval of statistical confidence. The mathematics associated with ‘kriging’ is well established (Journel and Huijbregts, 1978; de Marsily, 1986; Kitanidis, 1997) and detailed expositions are also presented in these references.

The MATLABTM Kriging Toolbox was chosen for this application. Easy Krig V3.0 is a well documented tool, created by Chu (2004) for the Woods Hole Oceanographic Institute. The purpose of this program is to generate variograms to express the spatial variations while reducing the error of the predicted values. The input data, i.e. the surface permeability, sampled by Easy Krig V3.0 is shown in Figure 32.

Based on the initial data, multiple variograms can be generated with varying degrees of accuracy. Easy Krig V3.0 provided a simple platform to easily vary the type of variogram while checking the values of the orthonormal residuals normalized by the sample size (Kitanidis, 1997). The orthonormal residuals, defined as

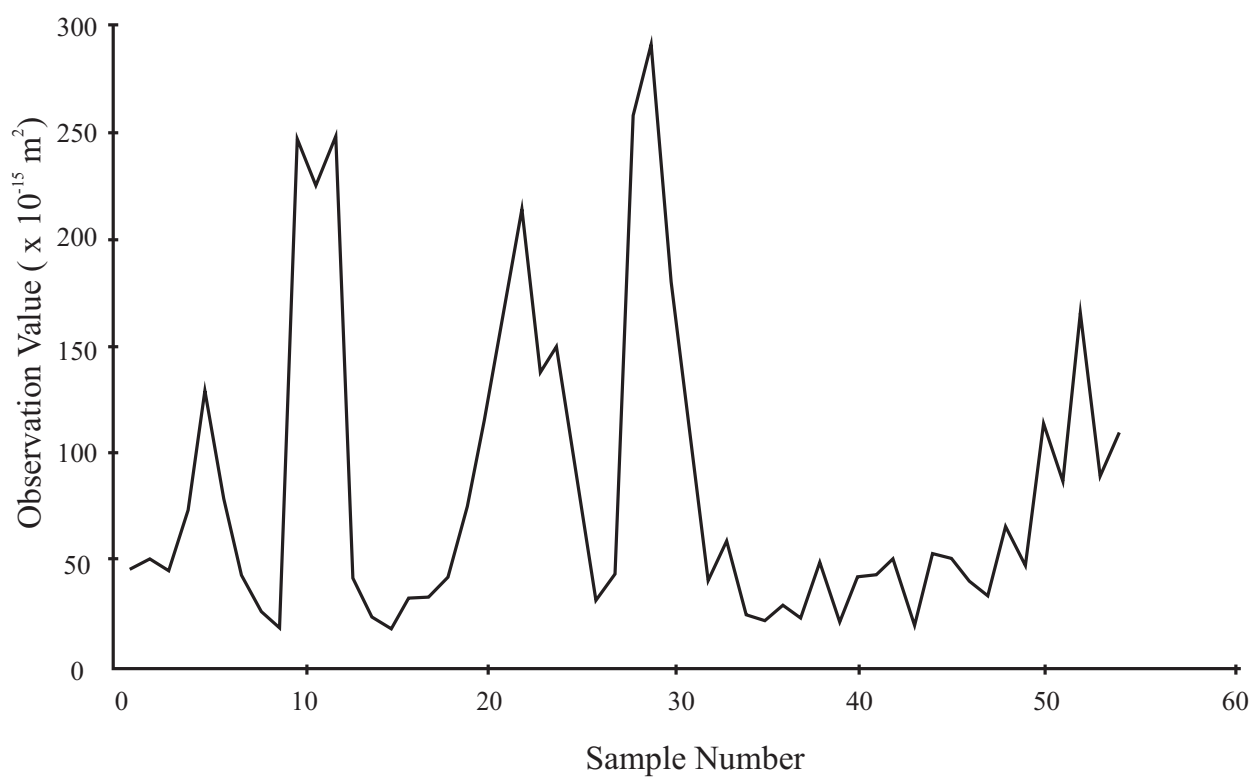


Figure 32: Initial data points (from Table 1) sampled by EasyKrig V3.0

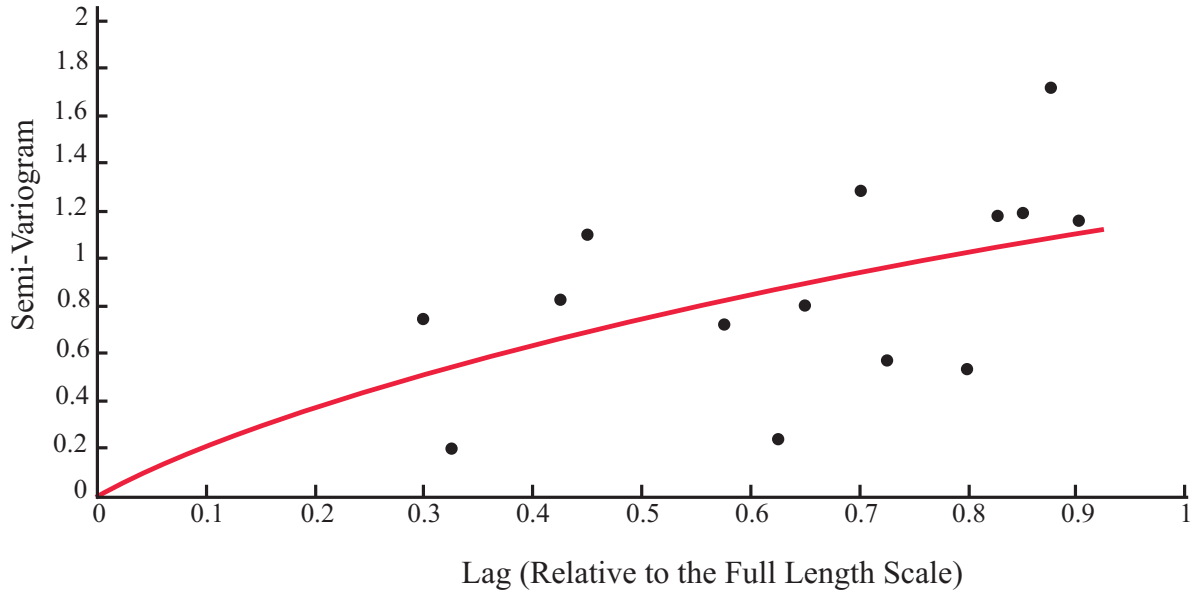


Figure 33: The exponential-Bessel theoretical semi-variogram (red) based on experimental semi-variogram (black).

Q_1 and Q_2 by Kitanidis (1997), represent the difference between the experimental surface permeabilities and the model predictions. The five tested models, in increasing order of accuracy, were *linear* ($Q_1 = -0.1535$, $Q_2 = 1.602$), *spherical* ($Q_1 = -0.1393$, $Q_2 = 1.456$), *sinc* ($Q_1 = 0.0301$, $Q_2 = 0.7873$), *Gaussian* ($Q_1 = -0.1009$, $Q_2 = 0.8983$) and *exponential-Bessel* ($Q_1 = -0.0919$, $Q_2 = 0.9865$). For this reason, the *exponential-Bessel* model was used to estimate the internal permeabilities of the Indiana limestone sample, shown in Figure 33. Satisfying the definitions of Q_1 and Q_2 (Kitanidis, 1997), a confidence interval of 95 % suggests that the correct model describing the spatial variation of the internal permeability has not been excluded.

Kriging, is also known amongst the scientific community, as a ‘smoothing’

process where the input data, i.e. the surface permeabilities, are ‘smeared’ to give plausible estimations at the unknown locations. The average change observed during the kriging procedure was $(0.01049)10^{-15} \text{ m}^2$. This error, approximately 0.01% of the actual values, was considered to be within the acceptable range of error when dealing with permeability measurements. Figure 34 shows the internal permeability distribution, generated using the *exponential-Bessel* model, from the average surface permeability measurements shown in Table 4.

6.8 Effective Permeability

6.8.1 Background

The study of subsurface flow, mainly in the fields of hydrology and petroleum engineering, is common practice. With new applications in relation to deep geological disposal of nuclear waste and carbon dioxide sequestration, computational models are being developed to enable engineers to assess the feasibility of these endeavours. The accuracy of these fluid flow models is highly dependent on the accuracy of the input variables. Improved measurements of these variables, and permeability in particular, are crucial to the reliability of the model predictions. Following this observation, we proceed, using geostatistical analysis, to determine the ‘*effective permeability*’ of the cuboid sample of Indiana Limestone and provide a more accurate definition for a permeability estimate that can be used in flow calculations.

Our experimental results indicate that the cuboid sample has heterogeneous permeability properties. Since the permeability is not an additive variable, it is

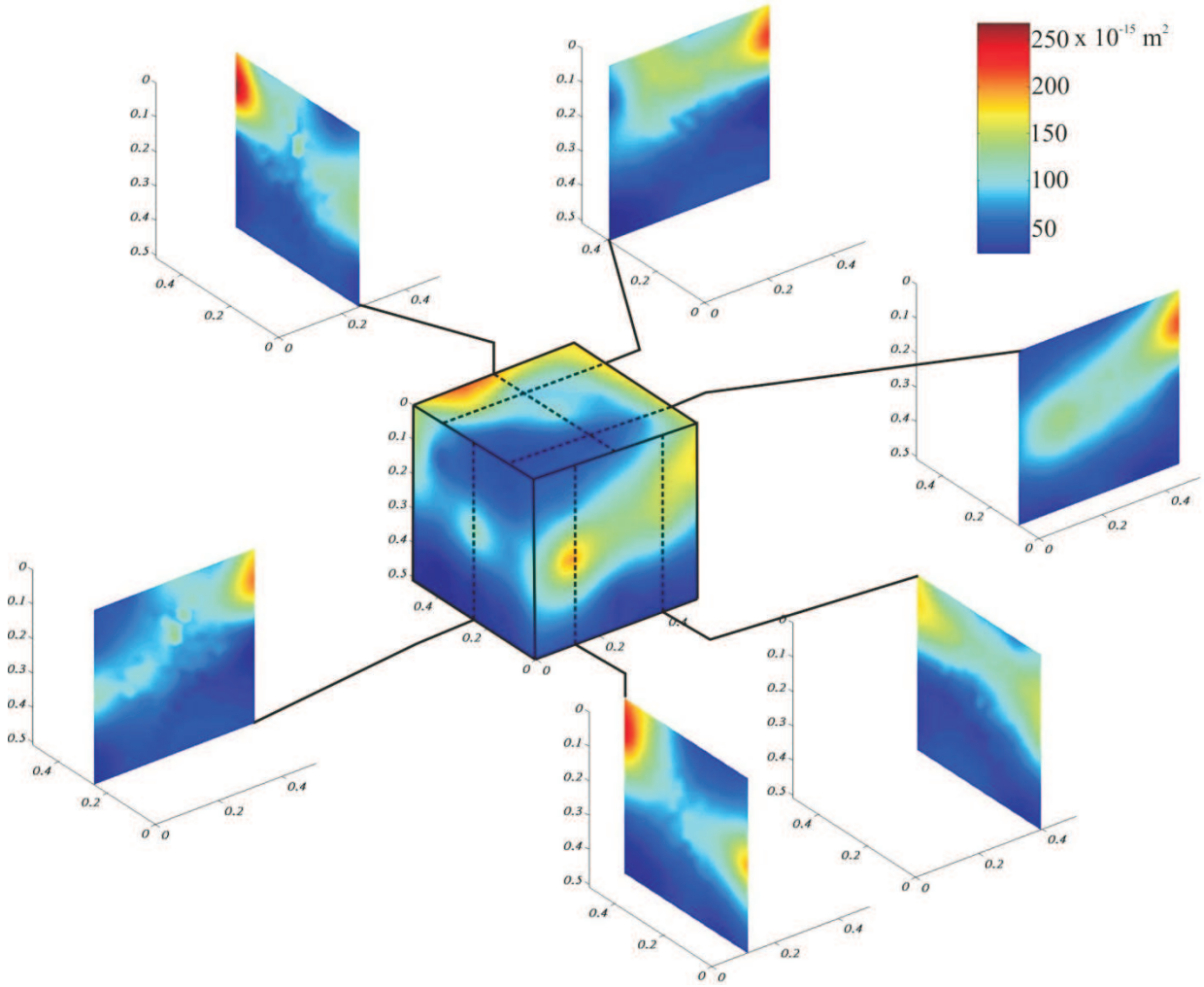


Figure 34: Distributions of permeability within the Indiana Limestone block as estimated by kriging the experimental data obtained from surface permeability measurements

not possible to determine the equivalent permeability by the use of the simple arithmetic mean (Renard and de Marsily, 1997). In the case of steady-state, uniform and single-phase flow, numerous studies have attempted to quantify the equivalent or *effective permeability* using geostatistical methods.

The ‘effective permeability’ can be expressed as the permeability determined by the flux generated when the entire region is subjected to a constant hydraulic gradient. In actual flow problems (on the scale of kilometers), the block that we have tested could be viewed as a mathematical point. The heterogeneities present in the sample at the laboratory scale become excluded. Theoretical analysis for determining the single point permeability value of a heterogeneous porous medium has been subject to extensive research (Cushman, 1986; Dagan, 1989, 1993; Noetinger, 1994; Christakos et al., 1995; Wen & Gomez-Hernandez, 1996; Renard & de Marsily, 1997; Markov & Preziosi, 2000). Multi-phase and/or transient flow scenarios have been examined in the literature but will not be used for the interpretation of our results.

In general, the concept of an effective permeability is the representation of the heterogeneity of a region by a single value that captures the variability as accurately as possible. There are two criteria that are used to describe the way in which the single homogeneous value can represent the heterogeneous distribution (Renard & de Marsily, 1997). Firstly, there must be exactly the same quantity of flow when both the inhomogeneous and the equivalent region are subjected to the same hydraulic gradient. Secondly, the energies dissipated by the viscous forces must be the same for both cases.

6.8.2 Application to the Experiment

Some of the methods used to determine the ‘effective permeability’ are quite complex and, for a heterogeneous medium, attempt to solve the *effective symmetric permeability tensor* at a point. The experimental research in this thesis is insufficiently refined to determine the complete tensor, but it is quite practical to use these techniques to determine the overall or effective permeability. These procedures are applied to estimate the effective permeability of the cuboidal block of Indiana limestone, defined as K_{eff} . An elementary approach has been adopted where the total block of Indiana Limestone was divided into 64 equally sized sub-regions of spatially appropriate permeability values determined using the kriging analysis. Each sub-region had the dimensions of 127 mm x 127 mm x 127mm. To determine the individual permeability of each sub-region, the output of the kriged permeability values were specified to coincide with the eight vertices on each sub-region. For each sub-region, the arithmetic mean was used to determine its permeability. The use of overlapping values of permeability with multiple sub-regions is justified since there is no evidence of large inclusions or inhomogeneities in the Indiana Limestone, either observed or reported in the literature. Once divided, the overall estimation of the *effective permeability* using the elementary procedures discussed in the literature can be applied.

Firstly, the Wiener (1912) bounds are used to bound the value of effective permeability K_{eff} of a porous medium with volume V_0 . The permeability distribution $K(\mathbf{x})$ is always bounded by the inequality

$$K_h \leq K_{eff} \leq K_a \quad (37)$$

where K_h and K_a are, respectively, the *harmonic mean* and the *arithmetic mean* defined by

$$K_h = \frac{\iiint_{V_0} dV}{\iiint_{V_0} [K(\mathbf{x})]^{-1} dV}; \quad K_a = \frac{\iiint_{V_0} K(\mathbf{x}) dV}{\iiint_{V_0} dV} \quad (38)$$

6.8.3 Theoretical Estimates

The following are various estimates for K_{eff} as found in the literature:

1. Matheron (1967) suggested that the effective permeability can be estimated from the weighted average of the Wiener bounds according to

$$K_{eff}^M = K_a^\alpha K_h^{(1-\alpha)} \quad (39)$$

where $\alpha \in [0, 1]$ and $\alpha = (D - 1)/D$, where D is the dimension of the space.

2. Journal et al. (1986) proposed that the effective permeability can be derived by considering the *power average* (or average of order p) with an exponent p in the interval between -1 and +1, depending on the spatial distribution of permeabilities: i.e.

$$K_{eff}^J = \left(\frac{\iiint_{V_0} [K(\mathbf{x})]^p dV}{\iiint_{V_0} dV} \right)^{1/p} \quad (40)$$

We note that $p = -1$ corresponds to the harmonic mean, $\lim_{p \rightarrow 0} K_{eff}^p$ corresponds to the geometric mean and $p = 1$ corresponds to the arithmetic mean. For a statistically homogeneous and isotropic medium, $p = 1 - (2/D)$.

3. King (1989) used the perturbation technique, which indicates that the effective permeability can be estimated from the result

$$K_{eff}^K = K_a \left\{ 1 - \frac{\sigma^2}{DK_a^2} \right\} \quad (41)$$

where σ^2 is the permeability variance for the sub-region permeability data set. Another estimate by King (1987), based on a conjecture of Landau and Lifschitz (1960) and on methods that rely on field theory, gives

$$K_{eff}^L = K_g \exp \left(\tilde{\sigma}^2 \left\{ \frac{1}{2} - \frac{1}{D} \right\} \right) \quad (42)$$

where $\tilde{\sigma}^2$ is the *variance in the logarithm of permeability* and K_g is the *geometric mean*.

4. Dagan (1993) estimated the effective permeability taking into consideration higher order terms in the variance and has the form

$$K_{eff}^D = K_g \left\{ 1 + \left(\frac{1}{2} - \frac{1}{D} \right) \sigma^2 + \frac{1}{2} \left(\frac{1}{2} - \frac{1}{D} \right)^2 (\sigma^2)^2 \right\} \quad (43)$$

where σ^2 is the variance of the permeability and D is the dimension of the space.

We further note that in order to apply Matherons formulae, the permeability variations in the experiments should conform to a lognormal distribution. Using MATLABTM, the Kolomogorov-Smirnov test was performed on the natural logarithm of the permeabilities of the 64 sub-cube regions (given in Appendix D). This set of permeabilities satisfied the lognormal distribution to within a confidence level of 95%. The code used to perform the Kolomogorov-Smirnov test and the graph of the cumulative probability distribution (CFD) is presented in Appendix E.

6.8.4 Computational Study

A computational study was performed on the subdivided block of Indiana Limestone. It would be beneficial, for future problems, to examine how the multiphysics finite element code COMSOLTM performed. Using the values of theoretical effective permeability (K_{eff}) calculated in the previous section, we can verify the accuracy of COMSOLTM. Firstly, a full cuboidal model (508 mm x 508 mm x 508 mm) was generated that consisted of 64 cuboidal sub-regions of dimensions 127 mm. Secondly, the appropriate permeabilities were prescribed to each sub-region based on its spatial position (Figure 35). The distribution of permeability within the larger cuboidal region was based on the results of the kriging procedure. All the permeability values associated with the 64 sub-regions are presented in Appendix D, where both the computational and theoretical results use the same data set.

The next step was to induce one-dimensional flow through the sample by subjecting the complete cuboid to a hydraulic gradient applied separately in the three

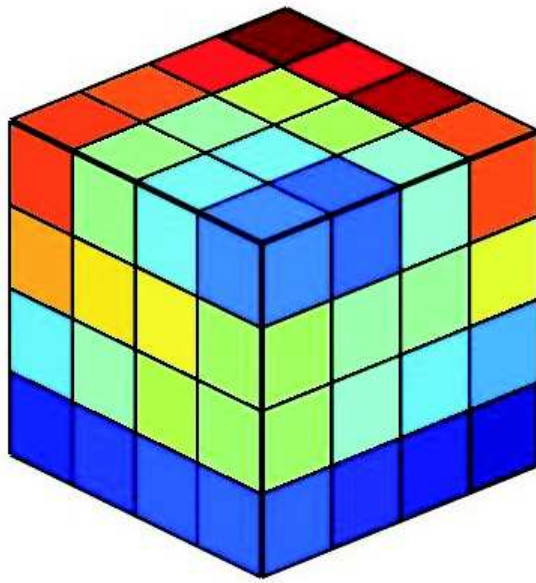


Figure 35: A sub-structured unit of the cuboidal sample of Indiana Limestone with permeabilities derived from the kriging procedure. Red is high permeability (maximum $149.54 \times 10^{-15} \text{ m}^2$) and blue is low permeability (minimum $25.18 \times 10^{-15} \text{ m}^2$).

Table 5: Input values for modelling a heterogeneous cuboidal sample of Indiana Limestone in COMSOLTM.

Variable	Value	Units	Description
Φ_i	10	m	Inlet Pressure Head
Φ_o	0	m	Outlet Pressure Head
μ	9.772×10^{-4}	Pa·s	Dynamic viscosity
ρ	9.9778×10^2	kg/m^3	Density of fluid
K	Defined by sub-regions	m^2	Permeability

orthogonal directions defined as 1, 2 and 3 [these directions are not indicative of any principal values] (Figure 36). A constant Dirchlet pressure head of 10m was applied to the inlet face and the opposite face was maintained at a zero pressure. This generated the hydraulic pressure gradient needed to generate flow through the sample. The four adjacent sides were prescribed with null Neumann boundary conditions, ensuring that although the internal flow pattern through the sample is three-dimensional the overall flow is one-dimensional. Equation (21) governs the steady-state fluid flow through a porous medium and can be applied in this situation. The input needed to solve the steady-state problem using COMSOLTM can be seen in Table 5.

The same boundary conditions were applied in each direction (i.e. hydraulic potential prescibed on the opposite faces of the cube with the four adjacent sides sealed) and the flow (Q [m^3/sec]) was measured over the entire outlet face. Using the calculated flow rates and dynamic viscosity, the directional permeability can be calculated using equation (21). The measured value of ‘*apparent one-dimensional*

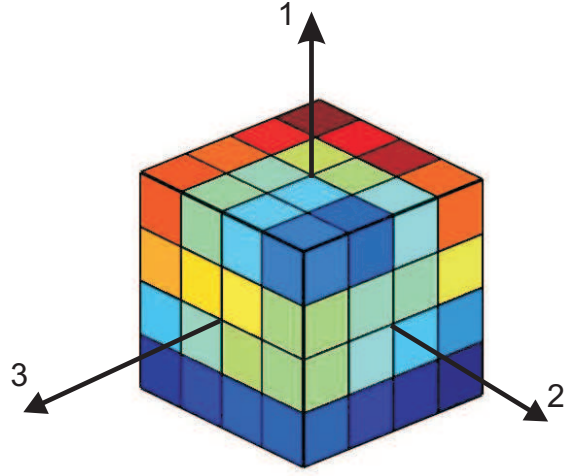


Figure 36: A sub-structured unit of the cuboidal sample of Indiana Limestone with the directions of testing denoted as 1,2 and 3.

permeabilities' of the heterogeneous cube of Indiana Limestone in orthogonal directions were:

$$K_1 = (64.76) 10^{-15} \text{ m}^2 ; \quad K_2 = (78.98) 10^{-15} \text{ m}^2 ; \quad K_3 = (78.44) 10^{-15} \text{ m}^2 ,$$

indicating a nominal measure of directional dependence. It should be noted that the ratio of orthogonal permeabilities was $1 : (1.21) : (1.22)$, which points to the near homogeneity in the overall permeability characteristics of the Indiana Limestone and the presence of a nominal transverse isotropy. A stream tube analysis in COMSOLTM confirms that there are no gross localizations in the flow patterns but there is a definite influence of the local heterogeneity of the sample as seen in Figure 37. It is proposed that the geometric mean of the '*apparent one-dimensional permeabilities*' can be regarded as the '*effective permeability*', i.e.

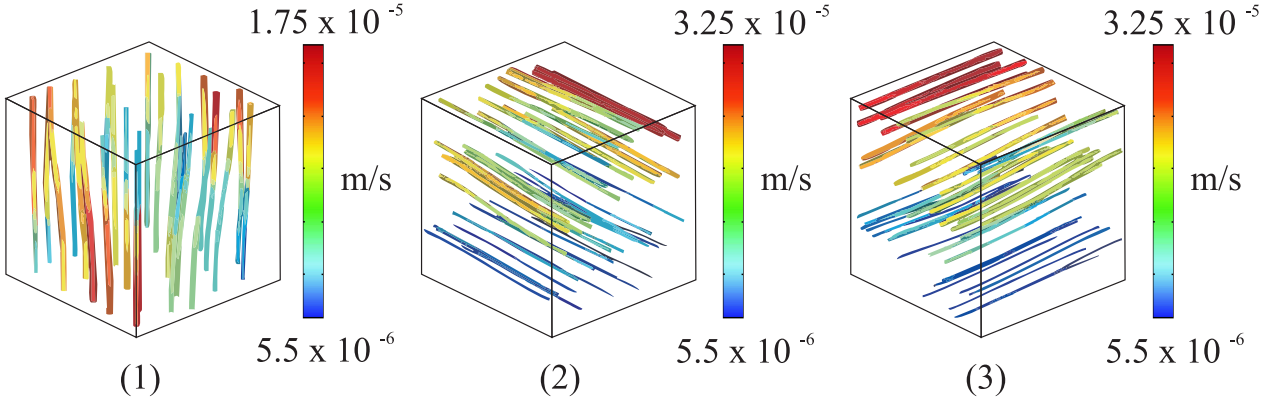


Figure 37: Stream tube patterns along three orthogonal directions

$$K_{eff}^S = \sqrt[3]{K_1 K_2 K_3} \quad (44)$$

The ‘*effective permeability*’ of the cuboidal sample of Indiana Limestone derived from research is approximately

$$K_{eff}^S = (73.75)10^{-15} \text{ m}^2$$

A comparison of the computational study with respect to the theoretical estimates derived using relationships (38) to (43) are shown in Table 6. The values generated by the computational study are very close to those found in the literature. The percentage error between the computational and the Matheron (1967) estimate is approximately 0.043% and between the computational and Journal et al. (1986) estimate is 0.442%. Furthermore, not only does the computational result seem to approximate the ‘*effective permeability*’ to within $\sim 0.45\%$ but it also takes into account the spatial variation in the permeability.

The experimental results for the permeability of the Indiana Limestone derived

Table 6: A summary of the relationships used to estimate the effective permeability of the Indiana Limestone block [$\times 10^{-15} \text{ m}^2$].

Wiener LB	King	Matheron	Landau and Lifschitz
62.164	74.049	73.786	71.649
Weiner UB	Journel et al.	Dagan	Present study computational
80.099	74.082	71.078	73.750

from the present research are comparable to those obtained in previous research using the identical Indiana Limestone. Selvadurai and Glowacki (2008) estimate the intact, unstressed, axial permeability, using equation (21), to be between (15 to 16) $\times 10^{-15} \text{ m}^2$. The studies by Churcher et al. (1991) indicate that for the three types of Indiana Limestone tested, the permeability ranged between (4 to 54) $\times 10^{-15} \text{ m}^2$. The *effective permeability* found in this study is slightly larger than previous results but is well within the range of variability ($10^{-22} < K_{eff} < 10^{-14}$) for sedimentary rocks such as limestone and dolomite (Philips, 1991).

7 Conclusions and Recommendations for Future Research

The research deals with the theoretical development necessary for interpreting local typical permeability of low permeability rocks and the associated experimental developments for conducting surface permeability tests on large cuboidal block of Indiana Limestone. It is shown that the analytical results presented by Goggin et al. (1988) and Selvadurai and Selvadurai (2010) can be effectively uti-

lized to estimate the surface distribution of permeability of a cuboidal sample of Indiana Limestone measuring 508 mm. The ‘surface permeability test’ requires the application of a constant flow rate to the central region of a sealed annular patch and measurement of the attained steady-state pressure. The results of the research shows that a permeameter can be designed and operated to fulfill these objectives. The permeameter, which accurately defined the aspect ratio of the annular sealing patch, was an integral part of the novel experimental design. Using analytical results, computational models were validated and used to extract from the experimental data, estimates of the surface permeability over the Indiana Limestone block at prescribed locations. The computational schemes developed in this research can be of benefit to future research involving experimental modelling of thermo-hydro-mechanical effects in porous media, investigating CO₂ migration in porous media and the estimation of permeability characteristics of geomaterials that display dominant direction effects in the permeability.

Using the well established kriging technique, surficial permeability measurements were then used to determine the spatial distribution of permeabilities at the interior of the block to within a 95% confidence interval. As previously discussed, these methods have been used in a wide range of scientific and engineering applications. Judicious use of statistical extrapolation/interpolation schemes such as kriging provides a valuable tool which can aid upscaling procedures for estimating bulk permeability.

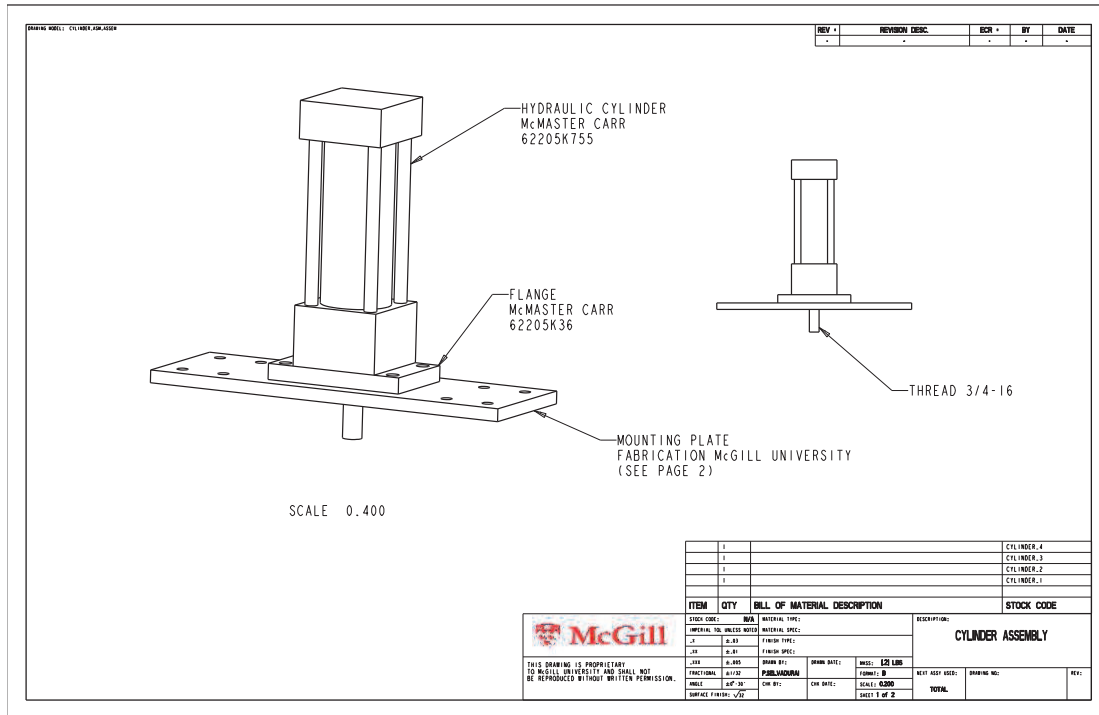
The surface values together with the interior estimates, based on kriging, were used to construct a sub-region model of the cuboidal region with spatially varying permeabilities. The sample of Indiana Limestone was then modelled as a het-

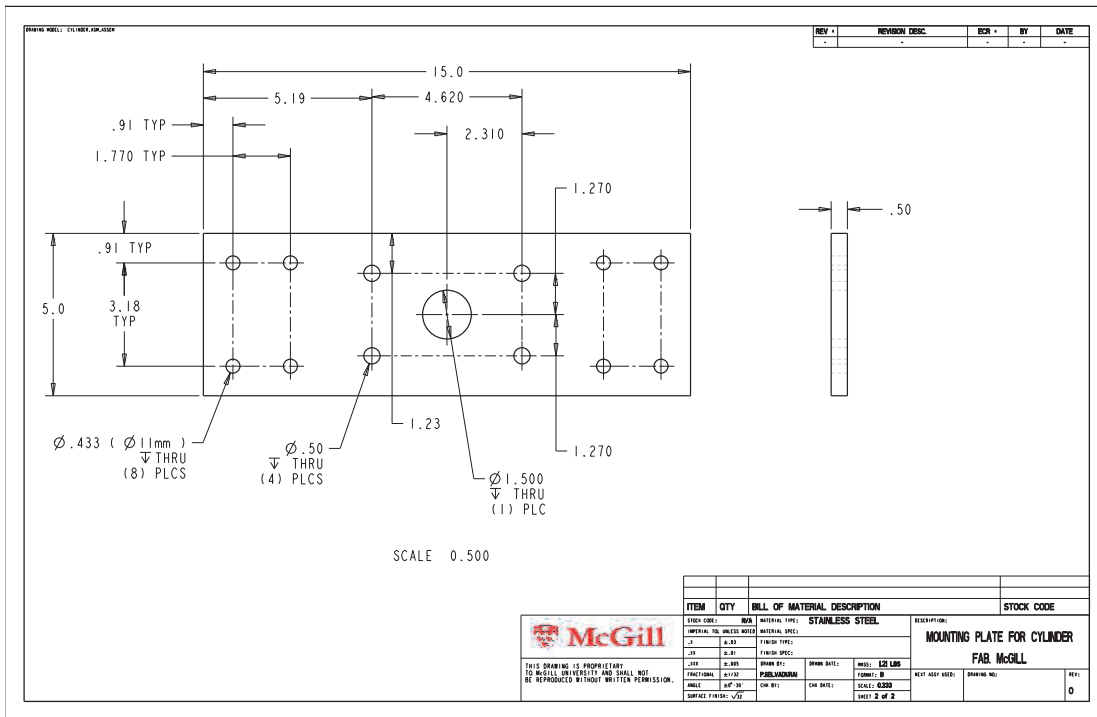
erogeneous sample. The sub-division of the sample is essential for theoretically estimating the ‘*effective permeability*’. The accuracy of the theoretical estimates for the effective permeability can be assumed by using the spatial distribution of permeability in sub-regions. The computational study of the heterogeneous block involved measuring the ‘*apparent one-dimensional permeability*’ in the three orthogonal directions. These calculations provided a result within $\sim 0.45\%$ of the theoretical estimates. Furthermore, the computational analyses provided a pictorial representation of the directional variations in the ‘*apparent one-dimensional permeability*’. The sample of Indiana Limestone used showed slight signs of transverse isotropy with regards to its permeability.

It is shown that the property of permeability of a rock can be estimated at various scales and the development of experimental methodologies that are amenable to theoretical and computational analysis can provide the necessary tools for accurately estimating not only local permeability but also the extrapolation of such data to the estimation of ‘*effective permeability*’.

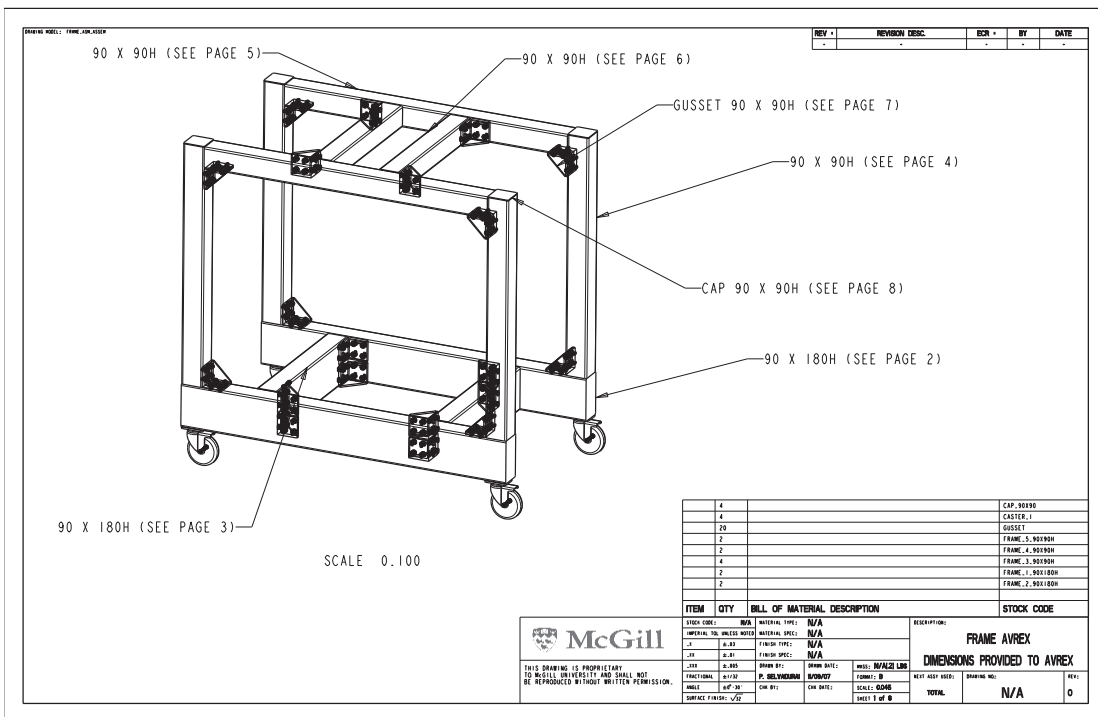
The work reported in this thesis is based on assumptions of local homogeneity of the Indiana Limestone sample at the location of measurement of the permeability. In the case of the tested block of Indiana Limestone, there were no visible manifestations that would point to the presence of anisotropy (e.g. layering or visible stratification). With certain rocks it is necessary to address this issue when conducting surface permeability tests. The experimental methodologies can be developed to examine both local inhomogeneity and local transverse isotropy of geological media. This aspect can be considered a valuable line of study for future research.

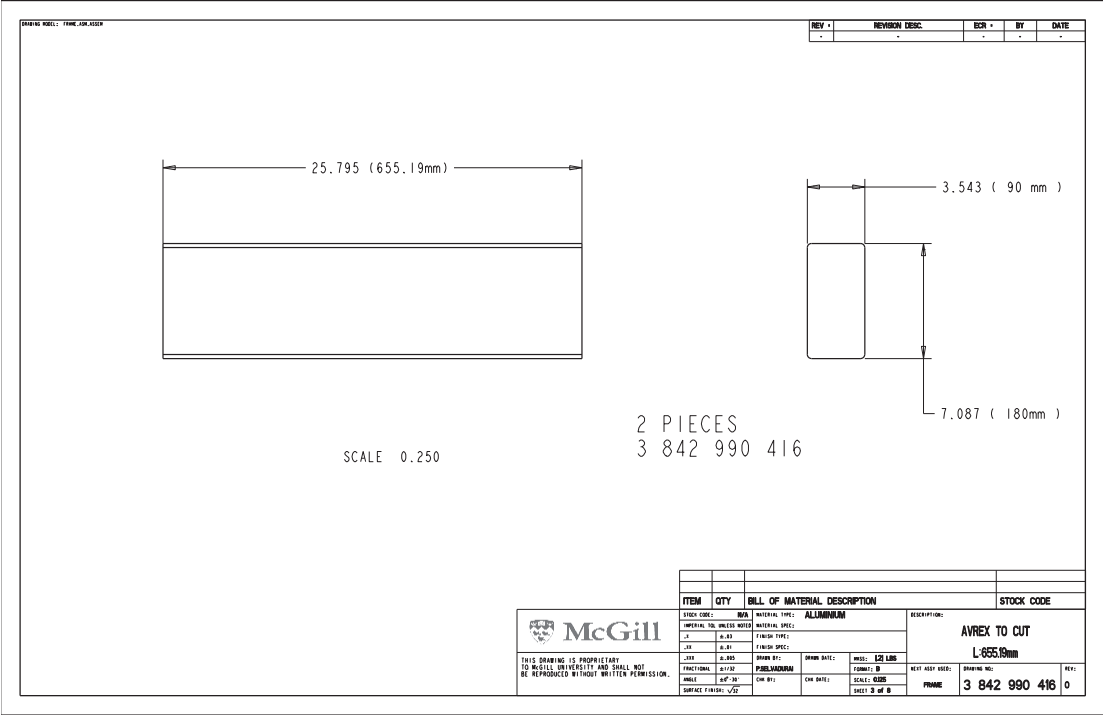
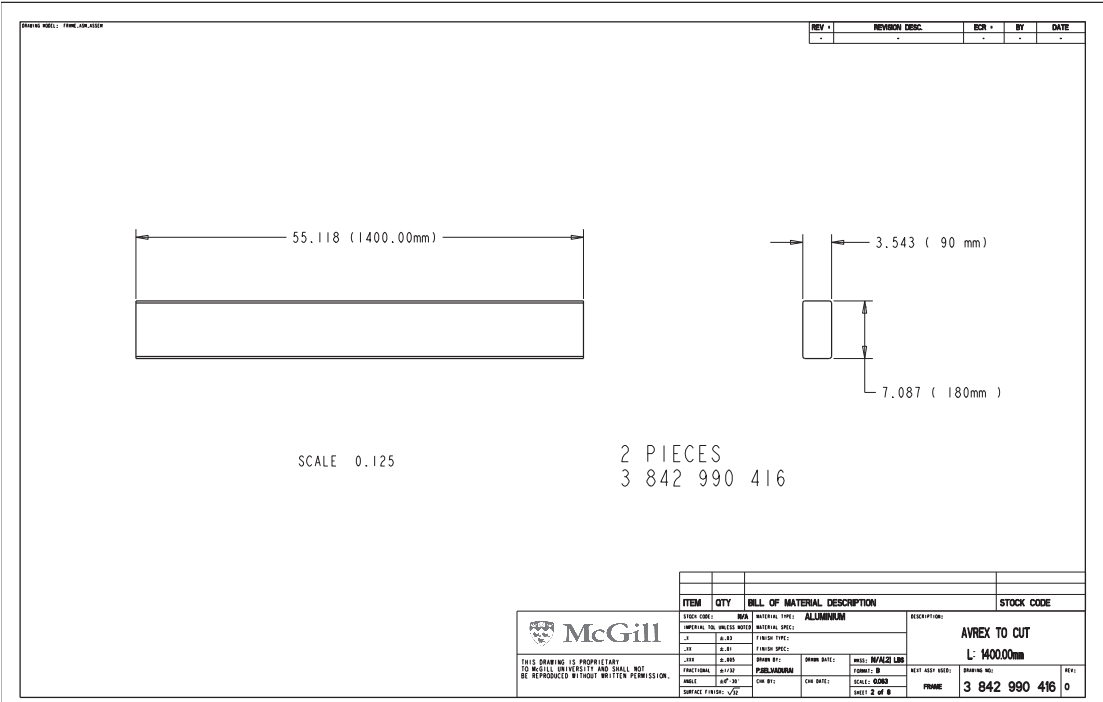
Appendix A: Details of the Hydraulic Cylinder





Appendix B: Details of the Reaction Frame





REV	REVISION DESC.	BY	DATE

39.720 (1008.89 mm)

3.543 (90mm)

SCALE 0.250

4 PIECES

3 842 990 500

ITEM		QTY	BILL OF MATERIAL DESCRIPTION		STOCK CODE
STOCK CODE: 384		MATERIAL TYPE: ALUMINUM		DESCRIPTION: CUT BY AVREX L:1008.89 mm	
IMPERIAL TOL UNLESS NOTED		MATERIAL SPEC:			
L	0.03	FINISH TYPE:			
T	0.01	FINISH SPEC:			
W	0.005	FINISH BY:			
FUNCTIONAL: 01702		PURLIN/ALUMINUM		WEIGHT: 520 LBS	NEXT STEP USED: (DRAWING NO.) 3 842 990 500
MATERIAL: 6061-T6		CUT BY:		SCALE: 0.250	
SURFACE FINISH: CP		CUT DATE:		DATE: 0-00 0	

THIS DRAWING IS PROPRIETARY TO MCGILL UNIVERSITY AND SHALL NOT BE REPRODUCED WITHOUT WRITTEN PERMISSION.

DRAWING MODEL: TAME.ARM.PIECE

REV.	REVISION DESC.	ECR.	BY	DATE
-		-	-	-

48.031 (1220.00 mm)

3.543 (90 mm)

3.543 (90mm)

SCALE 0.200

2 PIECES
3 842 990 500

ITEM	QTY	BILL OF MATERIAL DESCRIPTION	STOCK CODE
STEEL CODE:	BSN	MATERIAL TYPE: ALUMINUM	
SERIAL NO. MOULD NUMBER		MATERIAL SPEC:	
A	0.00	FINGER SPEC:	
JR	0.00	FINGER SPEC:	
JCR	0.00	FINGER SPEC:	
FUNCTIONAL PART NO.		PURCHASED BY:	
MOULD REF. NO.		CAR DATE:	
SURFACE FINISHING		CAR DATE:	

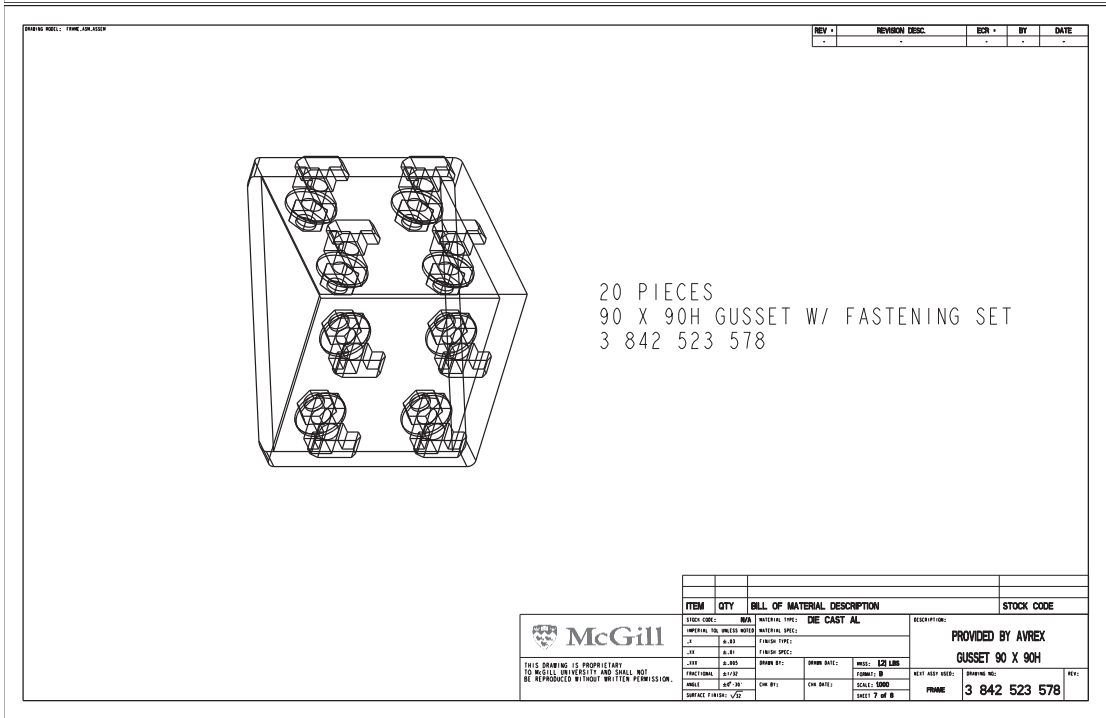
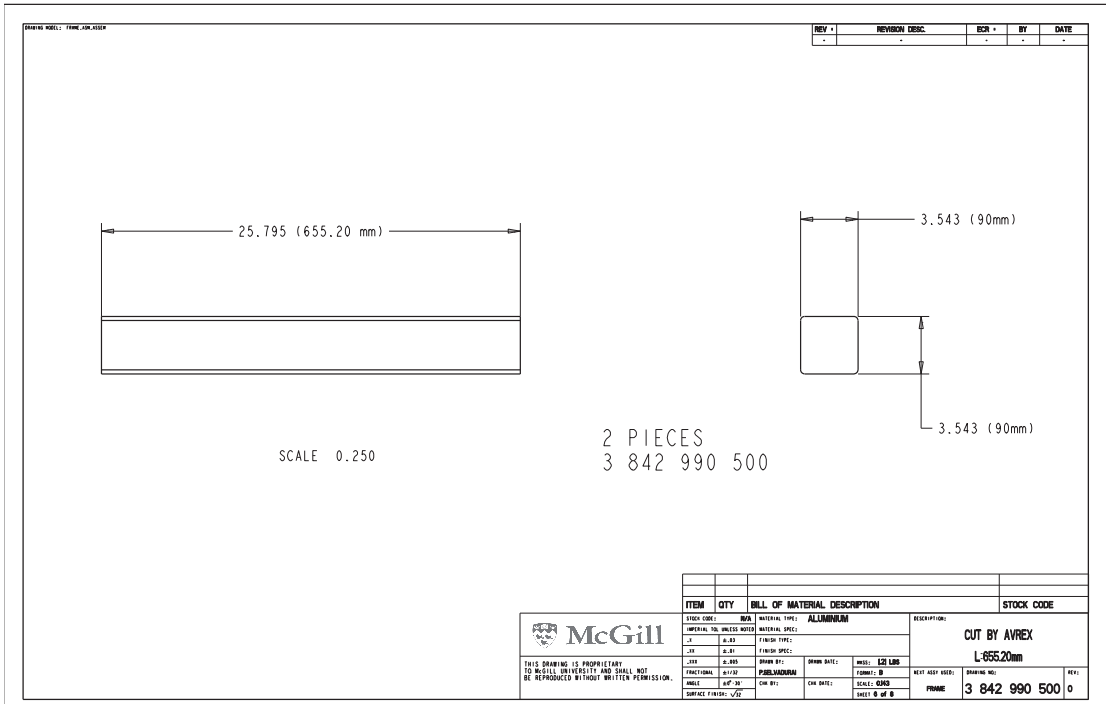
DESCRIPTION:
CUT BY AVRES
L: 1220.00mm

DRW. BY: **DAVIDE LEB**
FORMET: B
SCALA: 0.077
SHEET: 0 OF 0

NEXT STEP CODE:
PRIME
3 842 990 500 0

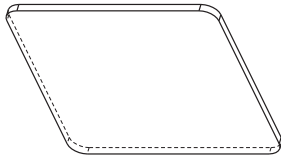
THIS DRAWING IS PROPRIETARY
OF MCGILL UNIVERSITY AND SHALL NOT
BE REPRODUCED WITHOUT WRITTEN PERMISSION.

McGill




DRAWING NO.: 3842 242 400

REV	REVISION DESC.	BY	DATE



4 PIECES
CAP FOR 90 X 90H
3 842 242 400

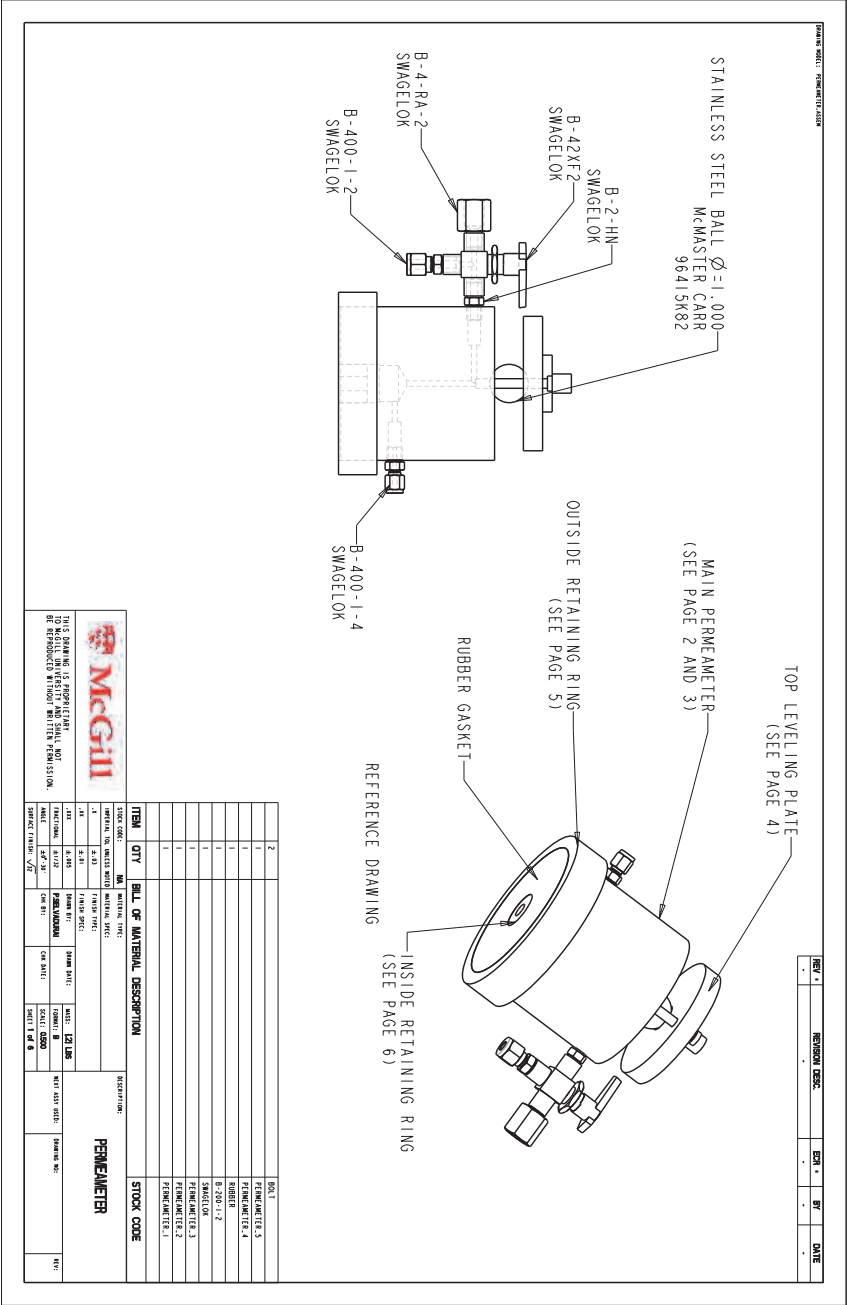


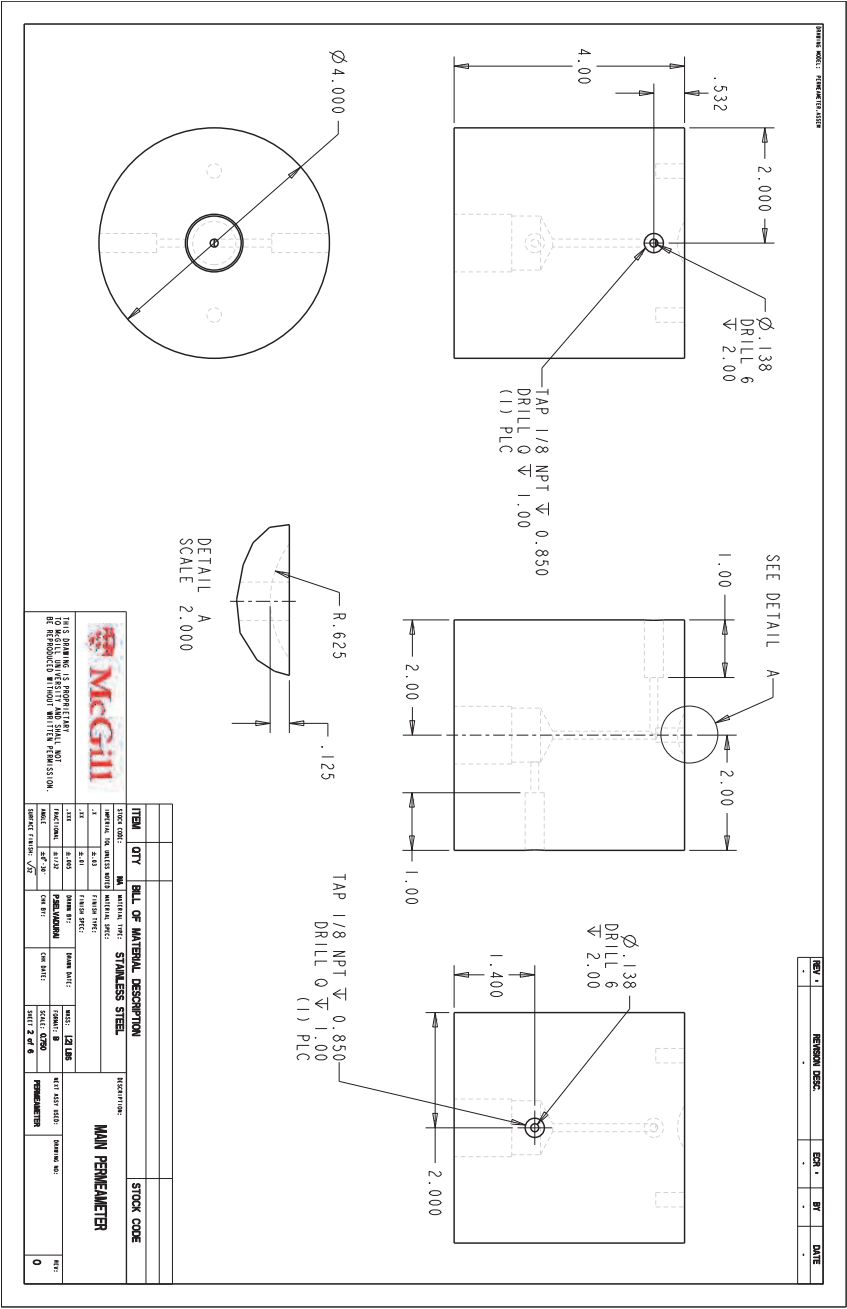
McGill

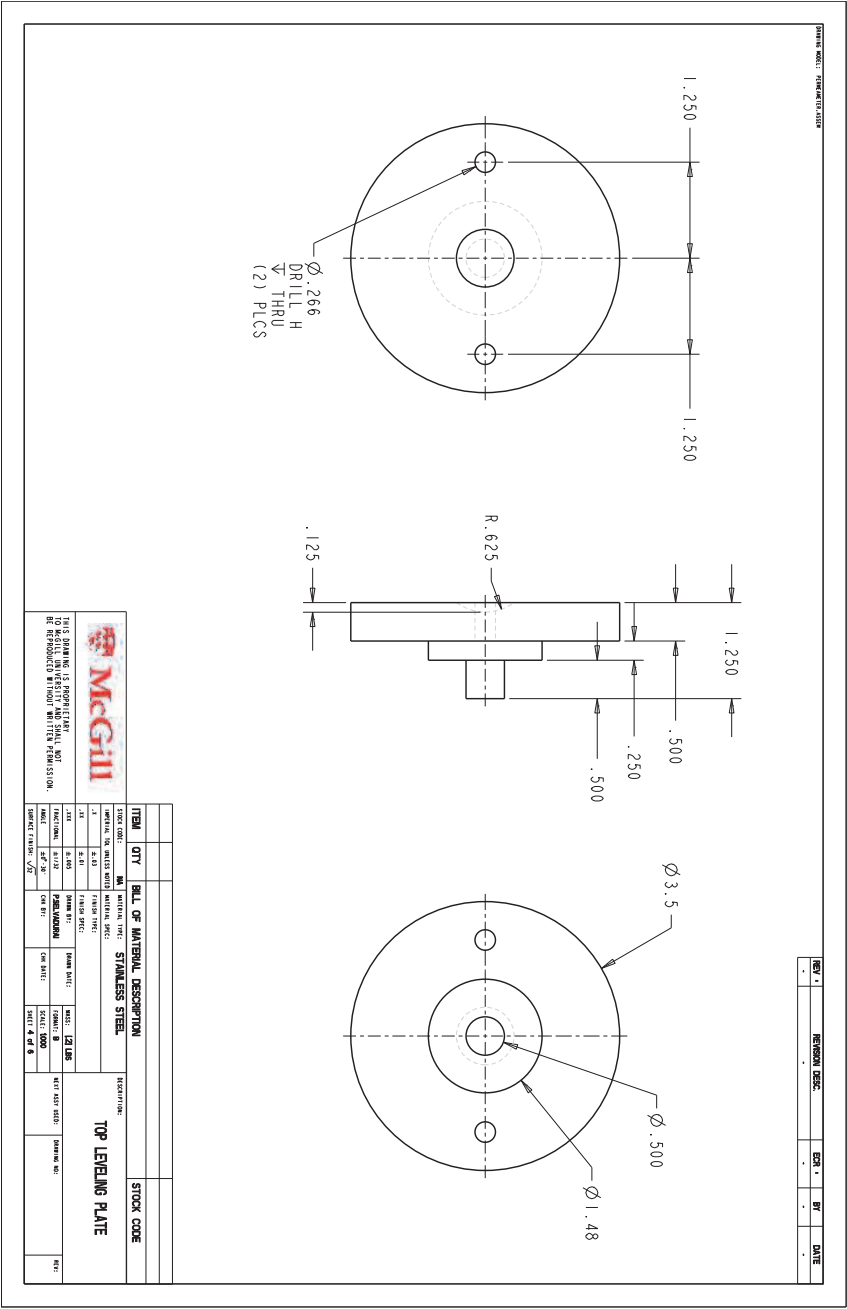
THIS DRAWING IS PROPRIETARY
TO MCGILL UNIVERSITY AND SHALL NOT
BE REPRODUCED WITHOUT WRITTEN PERMISSION.

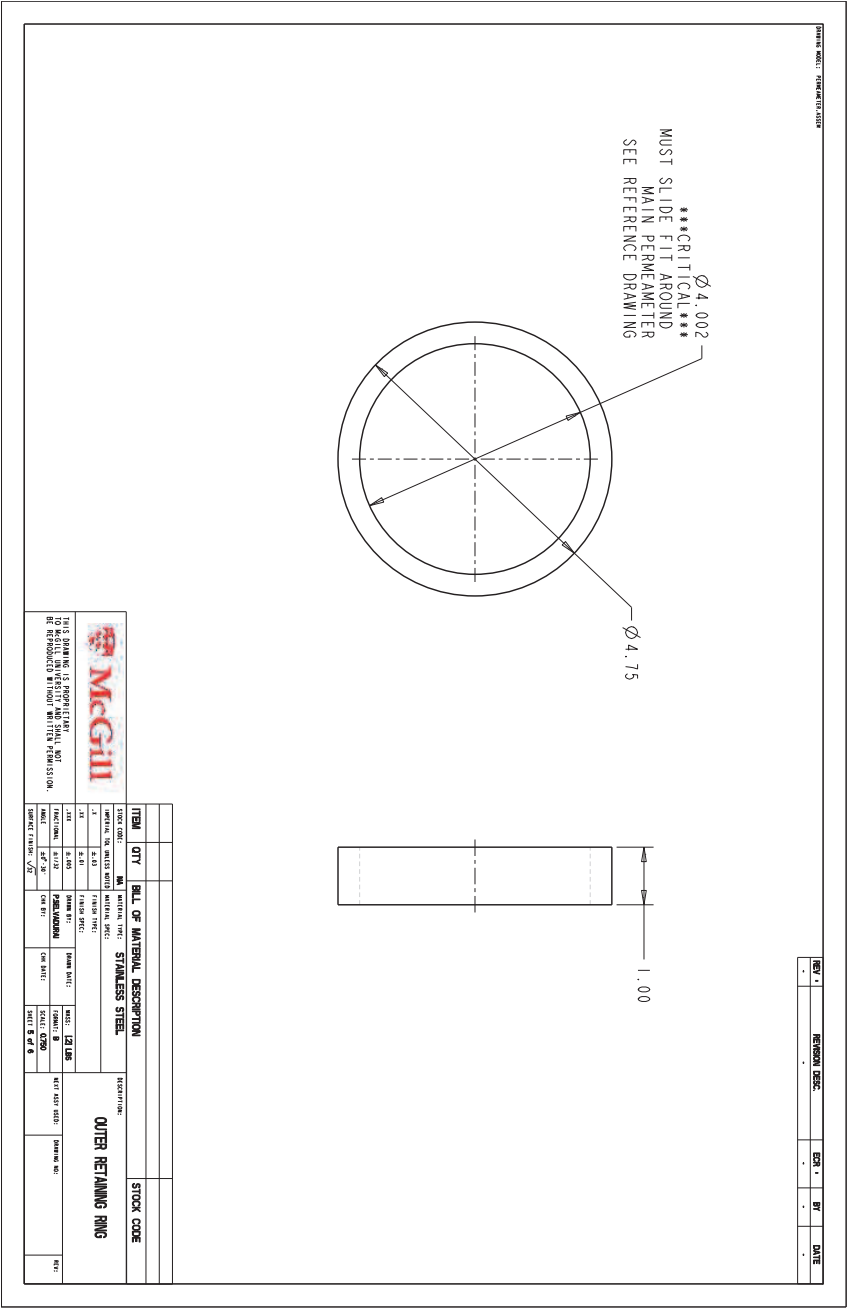
ITEM	QTY	BILL OF MATERIAL DESCRIPTION	STOCK CODE																																																																																																																																																																																																																																																																																																																																																																																																																								
<table style="width: 100%; font-size: 6px;"> <tr> <td colspan="2">STOCK CODE: 3842</td> <td colspan="2">MATERIAL TYPE: 1</td> </tr> <tr> <td colspan="2">MATERIAL TO WHICH NOTED:</td> <td colspan="2">MATERIAL SPEC:</td> </tr> <tr> <td>1</td> <td>0.00</td> <td>FINISH TYPE:</td> <td> </td> </tr> <tr> <td>2</td> <td>0.00</td> <td>FINISH SPEC:</td> <td> </td> </tr> <tr> <td>3</td> <td>0.00</td> <td>FINISH SPEC:</td> <td> </td> </tr> <tr> <td>4</td> <td>0.00</td> <td>FINISH SPEC:</td> <td> </td> </tr> <tr> <td>5</td> <td>0.00</td> <td>FINISH SPEC:</td> <td> </td> </tr> <tr> <td>6</td> <td>0.00</td> <td>FINISH SPEC:</td> <td> </td> </tr> <tr> <td>7</td> <td>0.00</td> <td>FINISH SPEC:</td> <td> </td> </tr> <tr> <td>8</td> <td>0.00</td> <td>FINISH SPEC:</td> <td> </td> </tr> <tr> <td>9</td> <td>0.00</td> <td>FINISH SPEC:</td> <td> </td> </tr> <tr> <td>10</td> <td>0.00</td> <td>FINISH SPEC:</td> <td> </td> </tr> <tr> <td>11</td> <td>0.00</td> <td>FINISH SPEC:</td> <td> </td> </tr> <tr> <td>12</td> <td>0.00</td> <td>FINISH SPEC:</td> <td> </td> </tr> <tr> <td>13</td> <td>0.00</td> <td>FINISH SPEC:</td> <td> </td> </tr> <tr> <td>14</td> <td>0.00</td> <td>FINISH SPEC:</td> <td> </td> </tr> <tr> <td>15</td> <td>0.00</td> <td>FINISH SPEC:</td> <td> </td> </tr> <tr> <td>16</td> <td>0.00</td> <td>FINISH SPEC:</td> <td> </td> </tr> <tr> <td>17</td> <td>0.00</td> <td>FINISH SPEC:</td> <td> </td> </tr> <tr> <td>18</td> <td>0.00</td> <td>FINISH SPEC:</td> <td> </td> </tr> <tr> <td>19</td> <td>0.00</td> <td>FINISH SPEC:</td> <td> </td> </tr> <tr> <td>20</td> <td>0.00</td> <td>FINISH SPEC:</td> <td> </td> </tr> <tr> <td>21</td> <td>0.00</td> <td>FINISH SPEC:</td> <td> </td> </tr> <tr> <td>22</td> <td>0.00</td> <td>FINISH SPEC:</td> <td> </td> </tr> <tr> <td>23</td> <td>0.00</td> <td>FINISH SPEC:</td> <td> </td> </tr> <tr> <td>24</td> <td>0.00</td> <td>FINISH SPEC:</td> <td> </td> </tr> <tr> <td>25</td> <td>0.00</td> <td>FINISH SPEC:</td> <td> </td> </tr> <tr> <td>26</td> <td>0.00</td> <td>FINISH SPEC:</td> <td> </td> </tr> <tr> <td>27</td> <td>0.00</td> <td>FINISH SPEC:</td> <td> </td> </tr> <tr> <td>28</td> <td>0.00</td> <td>FINISH SPEC:</td> <td> </td> </tr> <tr> <td>29</td> <td>0.00</td> <td>FINISH SPEC:</td> <td> </td> </tr> <tr> <td>30</td> <td>0.00</td> <td>FINISH SPEC:</td> <td> </td> </tr> <tr> <td>31</td> <td>0.00</td> <td>FINISH SPEC:</td> <td> </td> </tr> <tr> <td>32</td> <td>0.00</td> <td>FINISH SPEC:</td> <td> </td> </tr> <tr> <td>33</td> <td>0.00</td> <td>FINISH SPEC:</td> <td> </td> </tr> <tr> <td>34</td> <td>0.00</td> <td>FINISH SPEC:</td> <td> </td> </tr> <tr> <td>35</td> <td>0.00</td> <td>FINISH SPEC:</td> <td> </td> </tr> <tr> <td>36</td> <td>0.00</td> <td>FINISH SPEC:</td> <td> </td> </tr> <tr> <td>37</td> <td>0.00</td> <td>FINISH SPEC:</td> <td> </td> </tr> <tr> <td>38</td> <td>0.00</td> <td>FINISH SPEC:</td> <td> </td> </tr> <tr> <td>39</td> <td>0.00</td> <td>FINISH SPEC:</td> <td> </td> </tr> <tr> <td>40</td> <td>0.00</td> <td>FINISH SPEC:</td> <td> </td> </tr> <tr> <td>41</td> <td>0.00</td> <td>FINISH SPEC:</td> <td> </td> </tr> <tr> <td>42</td> <td>0.00</td> <td>FINISH SPEC:</td> <td> </td> </tr> <tr> <td>43</td> <td>0.00</td> <td>FINISH SPEC:</td> <td> </td> </tr> <tr> <td>44</td> <td>0.00</td> <td>FINISH SPEC:</td> <td> </td> </tr> <tr> <td>45</td> <td>0.00</td> <td>FINISH SPEC:</td> <td> </td> </tr> <tr> <td>46</td> <td>0.00</td> <td>FINISH SPEC:</td> <td> </td> </tr> <tr> <td>47</td> <td>0.00</td> <td>FINISH SPEC:</td> <td> </td> </tr> <tr> <td>48</td> <td>0.00</td> <td>FINISH SPEC:</td> <td> </td> </tr> <tr> <td>49</td> <td>0.00</td> <td>FINISH SPEC:</td> <td> </td> </tr> <tr> <td>50</td> <td>0.00</td> <td>FINISH SPEC:</td> <td> </td> </tr> <tr> <td>51</td> <td>0.00</td> <td>FINISH SPEC:</td> <td> </td> </tr> <tr> <td>52</td> <td>0.00</td> <td>FINISH SPEC:</td> <td> </td> </tr> <tr> <td>53</td> <td>0.00</td> <td>FINISH SPEC:</td> <td> </td> </tr> <tr> <td>54</td> <td>0.00</td> <td>FINISH SPEC:</td> <td> </td> </tr> <tr> <td>55</td> <td>0.00</td> <td>FINISH SPEC:</td> <td> </td> </tr> <tr> <td>56</td> <td>0.00</td> <td>FINISH SPEC:</td> <td> </td> </tr> <tr> <td>57</td> <td>0.00</td> <td>FINISH SPEC:</td> <td> </td> </tr> <tr> <td>58</td> <td>0.00</td> <td>FINISH SPEC:</td> <td> </td> </tr> <tr> <td>59</td> <td>0.00</td> <td>FINISH SPEC:</td> <td> </td> </tr> <tr> <td>60</td> <td>0.00</td> <td>FINISH SPEC:</td> <td> </td> </tr> <tr> <td>61</td> <td>0.00</td> <td>FINISH SPEC:</td> <td> </td> </tr> <tr> <td>62</td> <td>0.00</td> <td>FINISH SPEC:</td> <td> </td> </tr> <tr> <td>63</td> <td>0.00</td> <td>FINISH SPEC:</td> <td> </td> </tr> <tr> <td>64</td> <td>0.00</td> <td>FINISH SPEC:</td> <td> </td> </tr> <tr> <td>65</td> <td>0.00</td> <td>FINISH SPEC:</td> <td> </td> </tr> <tr> <td>66</td> <td>0.00</td> <td>FINISH SPEC:</td> <td> </td> </tr> <tr> <td>67</td> <td>0.00</td> <td>FINISH SPEC:</td> <td> </td> </tr> <tr> <td>68</td> <td>0.00</td> <td>FINISH SPEC:</td> <td> </td> </tr> <tr> <td>69</td> <td>0.00</td> <td>FINISH SPEC:</td> <td> </td> </tr> <tr> <td>70</td> <td>0.00</td> <td>FINISH SPEC:</td> <td> </td> </tr> <tr> <td>71</td> <td>0.00</td> <td>FINISH SPEC:</td> <td> </td> </tr> <tr> <td>72</td> <td>0.00</td> <td>FINISH SPEC:</td> <td> </td> </tr> <tr> <td>73</td> <td>0.00</td> <td>FINISH SPEC:</td> <td> </td> </tr> <tr> <td>74</td> <td>0.00</td> <td>FINISH SPEC:</td> <td> </td> </tr> <tr> <td>75</td> <td>0.00</td> <td>FINISH SPEC:</td> <td> </td> </tr> <tr> <td>76</td> <td>0.00</td> <td>FINISH SPEC:</td> <td> </td> </tr> <tr> <td>77</td> <td>0.00</td> <td>FINISH SPEC:</td> <td> </td> </tr> <tr> <td>78</td> <td>0.00</td> <td>FINISH SPEC:</td> <td> </td> </tr> <tr> <td>79</td> <td>0.00</td> <td>FINISH SPEC:</td> <td> </td> </tr> <tr> <td>80</td> <td>0.00</td> <td>FINISH SPEC:</td> <td> </td> </tr> <tr> <td>81</td> <td>0.00</td> <td>FINISH SPEC:</td> <td> </td> </tr> <tr> <td>82</td> <td>0.00</td> <td>FINISH SPEC:</td> <td> </td> </tr> <tr> <td>83</td> <td>0.00</td> <td>FINISH SPEC:</td> <td> </td> </tr> <tr> <td>84</td> <td>0.00</td> <td>FINISH SPEC:</td> <td> </td> </tr> <tr> <td>85</td> <td>0.00</td> <td>FINISH SPEC:</td> <td> </td> </tr> <tr> <td>86</td> <td>0.00</td> <td>FINISH SPEC:</td> <td> </td> </tr> <tr> <td>87</td> <td>0.00</td> <td>FINISH SPEC:</td> <td> </td> </tr> <tr> <td>88</td> <td>0.00</td> <td>FINISH SPEC:</td> <td> </td> </tr> <tr> <td>89</td> <td>0.00</td> <td>FINISH SPEC:</td> <td> </td> </tr> <tr> <td>90</td> <td>0.00</td> <td>FINISH SPEC:</td> <td> </td> </tr> <tr> <td>91</td> <td>0.00</td> <td>FINISH SPEC:</td> <td> </td> </tr> <tr> <td>92</td> <td>0.00</td> <td>FINISH SPEC:</td> <td> </td> </tr> <tr> <td>93</td> <td>0.00</td> <td>FINISH SPEC:</td> <td> </td> </tr> <tr> <td>94</td> <td>0.00</td> <td>FINISH SPEC:</td> <td> </td> </tr> <tr> <td>95</td> <td>0.00</td> <td>FINISH SPEC:</td> <td> </td> </tr> <tr> <td>96</td> <td>0.00</td> <td>FINISH SPEC:</td> <td> </td> </tr> <tr> <td>97</td> <td>0.00</td> <td>FINISH SPEC:</td> <td> </td> </tr> <tr> <td>98</td> <td>0.00</td> <td>FINISH SPEC:</td> <td> </td> </tr> <tr> <td>99</td> <td>0.00</td> <td>FINISH SPEC:</td> <td> </td> </tr> <tr> <td>100</td> <td>0.00</td> <td>FINISH SPEC:</td> <td> </td> </tr> </table>				STOCK CODE: 3842		MATERIAL TYPE: 1		MATERIAL TO WHICH NOTED:		MATERIAL SPEC:		1	0.00	FINISH TYPE:		2	0.00	FINISH SPEC:		3	0.00	FINISH SPEC:		4	0.00	FINISH SPEC:		5	0.00	FINISH SPEC:		6	0.00	FINISH SPEC:		7	0.00	FINISH SPEC:		8	0.00	FINISH SPEC:		9	0.00	FINISH SPEC:		10	0.00	FINISH SPEC:		11	0.00	FINISH SPEC:		12	0.00	FINISH SPEC:		13	0.00	FINISH SPEC:		14	0.00	FINISH SPEC:		15	0.00	FINISH SPEC:		16	0.00	FINISH SPEC:		17	0.00	FINISH SPEC:		18	0.00	FINISH SPEC:		19	0.00	FINISH SPEC:		20	0.00	FINISH SPEC:		21	0.00	FINISH SPEC:		22	0.00	FINISH SPEC:		23	0.00	FINISH SPEC:		24	0.00	FINISH SPEC:		25	0.00	FINISH SPEC:		26	0.00	FINISH SPEC:		27	0.00	FINISH SPEC:		28	0.00	FINISH SPEC:		29	0.00	FINISH SPEC:		30	0.00	FINISH SPEC:		31	0.00	FINISH SPEC:		32	0.00	FINISH SPEC:		33	0.00	FINISH SPEC:		34	0.00	FINISH SPEC:		35	0.00	FINISH SPEC:		36	0.00	FINISH SPEC:		37	0.00	FINISH SPEC:		38	0.00	FINISH SPEC:		39	0.00	FINISH SPEC:		40	0.00	FINISH SPEC:		41	0.00	FINISH SPEC:		42	0.00	FINISH SPEC:		43	0.00	FINISH SPEC:		44	0.00	FINISH SPEC:		45	0.00	FINISH SPEC:		46	0.00	FINISH SPEC:		47	0.00	FINISH SPEC:		48	0.00	FINISH SPEC:		49	0.00	FINISH SPEC:		50	0.00	FINISH SPEC:		51	0.00	FINISH SPEC:		52	0.00	FINISH SPEC:		53	0.00	FINISH SPEC:		54	0.00	FINISH SPEC:		55	0.00	FINISH SPEC:		56	0.00	FINISH SPEC:		57	0.00	FINISH SPEC:		58	0.00	FINISH SPEC:		59	0.00	FINISH SPEC:		60	0.00	FINISH SPEC:		61	0.00	FINISH SPEC:		62	0.00	FINISH SPEC:		63	0.00	FINISH SPEC:		64	0.00	FINISH SPEC:		65	0.00	FINISH SPEC:		66	0.00	FINISH SPEC:		67	0.00	FINISH SPEC:		68	0.00	FINISH SPEC:		69	0.00	FINISH SPEC:		70	0.00	FINISH SPEC:		71	0.00	FINISH SPEC:		72	0.00	FINISH SPEC:		73	0.00	FINISH SPEC:		74	0.00	FINISH SPEC:		75	0.00	FINISH SPEC:		76	0.00	FINISH SPEC:		77	0.00	FINISH SPEC:		78	0.00	FINISH SPEC:		79	0.00	FINISH SPEC:		80	0.00	FINISH SPEC:		81	0.00	FINISH SPEC:		82	0.00	FINISH SPEC:		83	0.00	FINISH SPEC:		84	0.00	FINISH SPEC:		85	0.00	FINISH SPEC:		86	0.00	FINISH SPEC:		87	0.00	FINISH SPEC:		88	0.00	FINISH SPEC:		89	0.00	FINISH SPEC:		90	0.00	FINISH SPEC:		91	0.00	FINISH SPEC:		92	0.00	FINISH SPEC:		93	0.00	FINISH SPEC:		94	0.00	FINISH SPEC:		95	0.00	FINISH SPEC:		96	0.00	FINISH SPEC:		97	0.00	FINISH SPEC:		98	0.00	FINISH SPEC:		99	0.00	FINISH SPEC:		100	0.00	FINISH SPEC:	
STOCK CODE: 3842		MATERIAL TYPE: 1																																																																																																																																																																																																																																																																																																																																																																																																																									
MATERIAL TO WHICH NOTED:		MATERIAL SPEC:																																																																																																																																																																																																																																																																																																																																																																																																																									
1	0.00	FINISH TYPE:																																																																																																																																																																																																																																																																																																																																																																																																																									
2	0.00	FINISH SPEC:																																																																																																																																																																																																																																																																																																																																																																																																																									
3	0.00	FINISH SPEC:																																																																																																																																																																																																																																																																																																																																																																																																																									
4	0.00	FINISH SPEC:																																																																																																																																																																																																																																																																																																																																																																																																																									
5	0.00	FINISH SPEC:																																																																																																																																																																																																																																																																																																																																																																																																																									
6	0.00	FINISH SPEC:																																																																																																																																																																																																																																																																																																																																																																																																																									
7	0.00	FINISH SPEC:																																																																																																																																																																																																																																																																																																																																																																																																																									
8	0.00	FINISH SPEC:																																																																																																																																																																																																																																																																																																																																																																																																																									
9	0.00	FINISH SPEC:																																																																																																																																																																																																																																																																																																																																																																																																																									
10	0.00	FINISH SPEC:																																																																																																																																																																																																																																																																																																																																																																																																																									
11	0.00	FINISH SPEC:																																																																																																																																																																																																																																																																																																																																																																																																																									
12	0.00	FINISH SPEC:																																																																																																																																																																																																																																																																																																																																																																																																																									
13	0.00	FINISH SPEC:																																																																																																																																																																																																																																																																																																																																																																																																																									
14	0.00	FINISH SPEC:																																																																																																																																																																																																																																																																																																																																																																																																																									
15	0.00	FINISH SPEC:																																																																																																																																																																																																																																																																																																																																																																																																																									
16	0.00	FINISH SPEC:																																																																																																																																																																																																																																																																																																																																																																																																																									
17	0.00	FINISH SPEC:																																																																																																																																																																																																																																																																																																																																																																																																																									
18	0.00	FINISH SPEC:																																																																																																																																																																																																																																																																																																																																																																																																																									
19	0.00	FINISH SPEC:																																																																																																																																																																																																																																																																																																																																																																																																																									
20	0.00	FINISH SPEC:																																																																																																																																																																																																																																																																																																																																																																																																																									
21	0.00	FINISH SPEC:																																																																																																																																																																																																																																																																																																																																																																																																																									
22	0.00	FINISH SPEC:																																																																																																																																																																																																																																																																																																																																																																																																																									
23	0.00	FINISH SPEC:																																																																																																																																																																																																																																																																																																																																																																																																																									
24	0.00	FINISH SPEC:																																																																																																																																																																																																																																																																																																																																																																																																																									
25	0.00	FINISH SPEC:																																																																																																																																																																																																																																																																																																																																																																																																																									
26	0.00	FINISH SPEC:																																																																																																																																																																																																																																																																																																																																																																																																																									
27	0.00	FINISH SPEC:																																																																																																																																																																																																																																																																																																																																																																																																																									
28	0.00	FINISH SPEC:																																																																																																																																																																																																																																																																																																																																																																																																																									
29	0.00	FINISH SPEC:																																																																																																																																																																																																																																																																																																																																																																																																																									
30	0.00	FINISH SPEC:																																																																																																																																																																																																																																																																																																																																																																																																																									
31	0.00	FINISH SPEC:																																																																																																																																																																																																																																																																																																																																																																																																																									
32	0.00	FINISH SPEC:																																																																																																																																																																																																																																																																																																																																																																																																																									
33	0.00	FINISH SPEC:																																																																																																																																																																																																																																																																																																																																																																																																																									
34	0.00	FINISH SPEC:																																																																																																																																																																																																																																																																																																																																																																																																																									
35	0.00	FINISH SPEC:																																																																																																																																																																																																																																																																																																																																																																																																																									
36	0.00	FINISH SPEC:																																																																																																																																																																																																																																																																																																																																																																																																																									
37	0.00	FINISH SPEC:																																																																																																																																																																																																																																																																																																																																																																																																																									
38	0.00	FINISH SPEC:																																																																																																																																																																																																																																																																																																																																																																																																																									
39	0.00	FINISH SPEC:																																																																																																																																																																																																																																																																																																																																																																																																																									
40	0.00	FINISH SPEC:																																																																																																																																																																																																																																																																																																																																																																																																																									
41	0.00	FINISH SPEC:																																																																																																																																																																																																																																																																																																																																																																																																																									
42	0.00	FINISH SPEC:																																																																																																																																																																																																																																																																																																																																																																																																																									
43	0.00	FINISH SPEC:																																																																																																																																																																																																																																																																																																																																																																																																																									
44	0.00	FINISH SPEC:																																																																																																																																																																																																																																																																																																																																																																																																																									
45	0.00	FINISH SPEC:																																																																																																																																																																																																																																																																																																																																																																																																																									
46	0.00	FINISH SPEC:																																																																																																																																																																																																																																																																																																																																																																																																																									
47	0.00	FINISH SPEC:																																																																																																																																																																																																																																																																																																																																																																																																																									
48	0.00	FINISH SPEC:																																																																																																																																																																																																																																																																																																																																																																																																																									
49	0.00	FINISH SPEC:																																																																																																																																																																																																																																																																																																																																																																																																																									
50	0.00	FINISH SPEC:																																																																																																																																																																																																																																																																																																																																																																																																																									
51	0.00	FINISH SPEC:																																																																																																																																																																																																																																																																																																																																																																																																																									
52	0.00	FINISH SPEC:																																																																																																																																																																																																																																																																																																																																																																																																																									
53	0.00	FINISH SPEC:																																																																																																																																																																																																																																																																																																																																																																																																																									
54	0.00	FINISH SPEC:																																																																																																																																																																																																																																																																																																																																																																																																																									
55	0.00	FINISH SPEC:																																																																																																																																																																																																																																																																																																																																																																																																																									
56	0.00	FINISH SPEC:																																																																																																																																																																																																																																																																																																																																																																																																																									
57	0.00	FINISH SPEC:																																																																																																																																																																																																																																																																																																																																																																																																																									
58	0.00	FINISH SPEC:																																																																																																																																																																																																																																																																																																																																																																																																																									
59	0.00	FINISH SPEC:																																																																																																																																																																																																																																																																																																																																																																																																																									
60	0.00	FINISH SPEC:																																																																																																																																																																																																																																																																																																																																																																																																																									
61	0.00	FINISH SPEC:																																																																																																																																																																																																																																																																																																																																																																																																																									
62	0.00	FINISH SPEC:																																																																																																																																																																																																																																																																																																																																																																																																																									
63	0.00	FINISH SPEC:																																																																																																																																																																																																																																																																																																																																																																																																																									
64	0.00	FINISH SPEC:																																																																																																																																																																																																																																																																																																																																																																																																																									
65	0.00	FINISH SPEC:																																																																																																																																																																																																																																																																																																																																																																																																																									
66	0.00	FINISH SPEC:																																																																																																																																																																																																																																																																																																																																																																																																																									
67	0.00	FINISH SPEC:																																																																																																																																																																																																																																																																																																																																																																																																																									
68	0.00	FINISH SPEC:																																																																																																																																																																																																																																																																																																																																																																																																																									
69	0.00	FINISH SPEC:																																																																																																																																																																																																																																																																																																																																																																																																																									
70	0.00	FINISH SPEC:																																																																																																																																																																																																																																																																																																																																																																																																																									
71	0.00	FINISH SPEC:																																																																																																																																																																																																																																																																																																																																																																																																																									
72	0.00	FINISH SPEC:																																																																																																																																																																																																																																																																																																																																																																																																																									
73	0.00	FINISH SPEC:																																																																																																																																																																																																																																																																																																																																																																																																																									
74	0.00	FINISH SPEC:																																																																																																																																																																																																																																																																																																																																																																																																																									
75	0.00	FINISH SPEC:																																																																																																																																																																																																																																																																																																																																																																																																																									
76	0.00	FINISH SPEC:																																																																																																																																																																																																																																																																																																																																																																																																																									
77	0.00	FINISH SPEC:																																																																																																																																																																																																																																																																																																																																																																																																																									
78	0.00	FINISH SPEC:																																																																																																																																																																																																																																																																																																																																																																																																																									
79	0.00	FINISH SPEC:																																																																																																																																																																																																																																																																																																																																																																																																																									
80	0.00	FINISH SPEC:																																																																																																																																																																																																																																																																																																																																																																																																																									
81	0.00	FINISH SPEC:																																																																																																																																																																																																																																																																																																																																																																																																																									
82	0.00	FINISH SPEC:																																																																																																																																																																																																																																																																																																																																																																																																																									
83	0.00	FINISH SPEC:																																																																																																																																																																																																																																																																																																																																																																																																																									
84	0.00	FINISH SPEC:																																																																																																																																																																																																																																																																																																																																																																																																																									
85	0.00	FINISH SPEC:																																																																																																																																																																																																																																																																																																																																																																																																																									
86	0.00	FINISH SPEC:																																																																																																																																																																																																																																																																																																																																																																																																																									
87	0.00	FINISH SPEC:																																																																																																																																																																																																																																																																																																																																																																																																																									
88	0.00	FINISH SPEC:																																																																																																																																																																																																																																																																																																																																																																																																																									
89	0.00	FINISH SPEC:																																																																																																																																																																																																																																																																																																																																																																																																																									
90	0.00	FINISH SPEC:																																																																																																																																																																																																																																																																																																																																																																																																																									
91	0.00	FINISH SPEC:																																																																																																																																																																																																																																																																																																																																																																																																																									
92	0.00	FINISH SPEC:																																																																																																																																																																																																																																																																																																																																																																																																																									
93	0.00	FINISH SPEC:																																																																																																																																																																																																																																																																																																																																																																																																																									
94	0.00	FINISH SPEC:																																																																																																																																																																																																																																																																																																																																																																																																																									
95	0.00	FINISH SPEC:																																																																																																																																																																																																																																																																																																																																																																																																																									
96	0.00	FINISH SPEC:																																																																																																																																																																																																																																																																																																																																																																																																																									
97	0.00	FINISH SPEC:																																																																																																																																																																																																																																																																																																																																																																																																																									
98	0.00	FINISH SPEC:																																																																																																																																																																																																																																																																																																																																																																																																																									
99	0.00	FINISH SPEC:																																																																																																																																																																																																																																																																																																																																																																																																																									
100	0.00	FINISH SPEC:																																																																																																																																																																																																																																																																																																																																																																																																																									

Appendix C: Details of the Permeameter







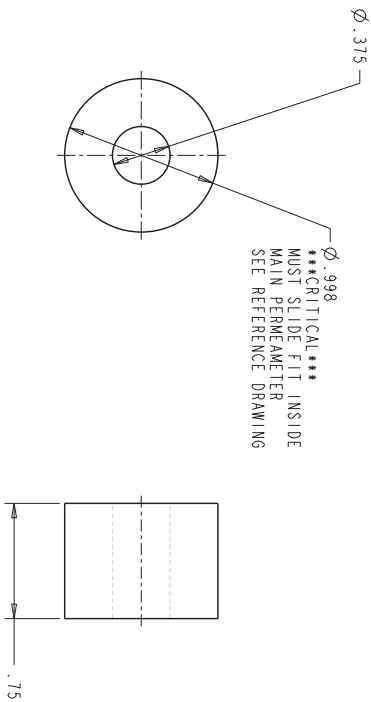


PRINTING MODEL: 7104060103 01/2019

REV. #	REVISION DESC.	DATE
1		

Ø.375

Ø.998
CRITICAL
MUST SLIDE FIT INSIDE
MAIN PERMEAMETER
SEE REFERENCE DRAWING



ITEM	QTY	BILL OF MATERIAL DESCRIPTION	STOCK CODE
1	1	INNER RETAINING RING	
MATERIAL: 304 STAINLESS STEEL			
FINISH: POLISHED			
TOLERANCES: ±0.005			
SURFACE FINISH: 32			
WEIGHT: 0.005 LBS			
PARTS LIST: 1			
DATE: 01/2019			
DRAWN BY: JET			

THIS DRAWING IS PROPERTY OF
MCGILL. IT IS TO BE USED ONLY
FOR THE PROJECT SPECIFIED.
REPRODUCTION WITHOUT PERMISSION
IS PROHIBITED.



Appendix D: Sub-region permeability values

Sub-region	Permeability ($\times 10^{-15} \text{ m}^2$)	Sub-region	Permeability ($\times 10^{-15} \text{ m}^2$)
1	57.27	33	97.23
2	71.11	34	103.20
3	92.60	35	85.77
4	141.41	36	69.32
5	52.76	37	78.83
6	71.09	38	78.00
7	87.34	39	66.68
8	138.90	40	45.01
9	77.92	41	69.86
10	100.42	42	63.98
11	106.44	43	53.59
12	149.54	44	36.63
13	139.24	45	62.47
14	166.29	46	54.94
15	155.88	47	43.75
16	171.61	48	42.01
17	98.84	49	50.91
18	117.55	50	49.97
19	120.49	51	39.96
20	129.22	52	33.34
21	86.79	53	37.42
22	92.17	54	44.80
23	95.16	55	40.45
24	107.54	56	31.93
25	89.56	57	30.67
26	94.51	58	39.06
27	92.70	59	39.89
28	102.00	60	36.40
29	112.60	61	25.18
30	126.25	62	30.80
31	112.40	63	35.85
32	113.72	64	37.10

Appendix E: Kolmogorov-Smirnov test for lognormal distribution

MATLABTM coding and output: Input:

1. Input the natural logarithm of the 64 sub-cube permeabilities:

```
>> x=[-30.49099947, -30.27454842, -30.01048725, ..., -30.92515943]
```

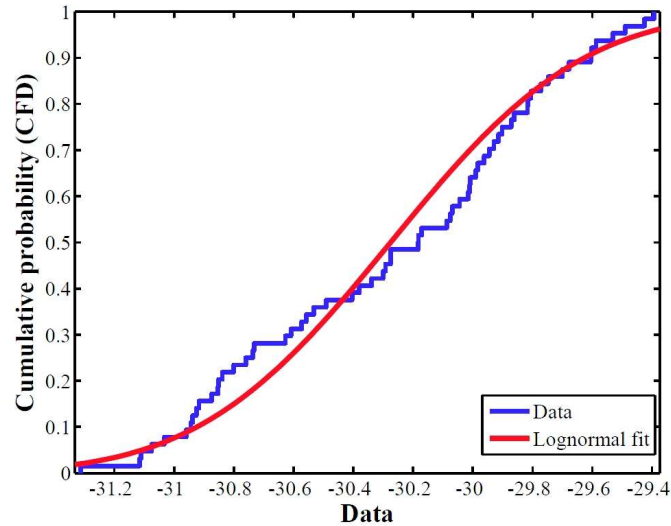
2. Calculate the CDF (Cumulative probability Density Function):

```
>> CDFx=normcdf(x,mean(x),std(x,1))
```

3. Apply the Kolmogorov-Smirnov test:

```
>> [H,P,KSSTAT,CV] = kstest(x,[x,CDFx],0.05)
```

Output: H = 0, P = 0.3423, KSSTAT = 0.1147, CV = 0.1669



References

- Ahmed, U., Crary, S. F. and R., C. G. (1991), ‘Permeability estimation: The various sources and their interrelationships’, *J. Pet. Technol.* **43**(5), 578–587.
- Apps, J.A. & Tsang, C.-F. (1996), *Deep Injection Disposal of Hazardous Wastes*, Academic Press, San Diego.
- Barenblatt, G. I., Entov, V. M. and Ryzhik, V. M. (1990), *Theory of Fluid Flows Through Natural Rocks*, Kluwer Academic Publishers, Dordrecht, The Netherlands.
- Bear, J. (1972), *Dynamics of Fluids in Porous Media*, Dover Publications, New York.
- Bencsik, M. and Ramanathan, C. (2001), ‘Method for measuring local hydraulic permeability using magnetic resonance imaging’, *Phys. Rev. E: Stat. Phys. Plasmas Fluids Relat. Interdisciplin. Top.* **63**, 65302–65303.
- Bernabe, Y. (1987), ‘The effective pressure law for permeability during pore and confining pressure cycling of several crystalline rocks’, *J. Geophys. Res.* **92**(B1), 649657.
- Bernabé, Y., Brace, W. F. and Evans, B. (1982), ‘Permeability, porosity and pore geometry of hot-pressed Calcite’, *Mech. Mater.* **1**, 173–183.
- Brace, W. F. (1977), ‘Permeability from resistivity and pore shape’, *J. Geophys. Res.* **82**, 3343–3349.

- Brace, W. F., Walsh, J. B. and Frangos, W. T. (1968), ‘Permeability of Granite under high pressure’, *J. Geophys. Res.* **73**, 2225–2236.
- Butler Jr., J. (1998), *The Design, Performance and Analysis of Slug Tests*, Lewis Publishers, Boca Raton, FL.
- Carnaffan, P. (1994), An experimental technique for determining the permeability of rock, concrete and cement grout, M. Eng. Thesis, Carleton University.
- Chandler, M. A., Kocurek, G., Goggin, D. J. and Lake, L. W. (1989), ‘Effects of stratigraphic heterogeneity on permeability in Eolian Sandstone sequence’, *AAPG Bull.* **73**(5), 658–668.
- Chapman, N. A. and McKinley, I. (1987), *The Geological Disposal of Nuclear Waste*, John Wiley and Sons, New York.
- Cheif, K., Ferre, T. and Nijssen, B. (2006), ‘Field testing of a soil corer air permeameter (SCAP) in desert soils’, *Vadose Zone J.* **5**, 12571263.
- Christakos, G., Hristopulos, D. and Miller, C. (1995), ‘Stochastic diagrammatic analysis of groundwater flow in heterogeneous porous media’, *Water Resour. Res.* **31**, 1687–1703.
- Chu, D. (2004), *The GLOBEC Kriging Software Package*, 3rd edn, Woods Hole Oceanographic Institution.
- Churcher, P., French, P., Shaw, J. and Schramm, L. (1991), Rock properties of Berea Sandstone, Baker Dolomite, and Indiana Limestone, Technical report, SPE, DOI:10.2118/21044-MS.

- Cooper, H., Bredehoeft, J. and Papadopoulos, I. (1967), ‘Response of a finite diameter well to an instantaneous charge of water’, *Water Resour. Res.* **3**, 263–269.
- Cushman, J. (1986), ‘On measurement, scale, and scaling’, *Water Resour. Res.* **22**, 129–134.
- Dagan, G. (1989), *Flow and Transport in Porous Formations*, Springer-Verlag, Berlin.
- Dagan, G. (1993), ‘Higher-order correction of effective permeability of heterogeneous isotropic formations of lognormal conductivity distributions’, *Transp. Porous Media* **12**, 279–290.
- Darcy, H. (1856), *Les fontaines publiques de la ville de Dijon*, Paris, France.
- Davis, J. M., Lohmann, R. C., Phillips, F. M., Wilson, J. L. and Love, D. W. (1993), ‘Architecture of the Sierra Ladrones formation, central New Mexico: Depositional controls on the permeability correlation structure’, *Geol. Soc. Am. Bull.* **105**(8), 998–1007.
- Daw, G. (1971), ‘A modified Hoek-Franklin triaxial cell for rock permeability measurements’, *Geotech.* **21**, 89–91.
- de Marsily, G. (1986), *Quantitative Hydrogeology. Groundwater Hydrology for Engineers*, Academic Press, San Diego.
- Dreyer, T., Scheie, A. and Walderhaug, O. (1990), ‘Minipermeameter-based study of permeability trends in channel sand bodies’, *AAPG Bull.* **74**(4), 359–374.

- Dykstra, H. and Parsons, R. (1950), *The prediction of oil recovery by waterflood*, Secondary Recovery of Oil in the United States.
- Eijpe, R. and Weber, K. J. (1971), ‘Mini-permeameters for consolidated rock and unconsolidated sand’, *AAPG Bull.* **55**(2), 307–309.
- Franklin, I. A. and Dusseault, M. B. (1989), *Rock Engineering*, McGraw-Hill.
- Fuller, C. M. and Sharp Jr., J. M. (1992), ‘Permeability and fracture patterns in extrusive volcanic rocks: Implication from the welded Santana tuff’, *Geol. Soc. Am. Bull.* **104**, 1485–1496.
- Glowacki, A. (2007), Permeability hysteresis of Indiana Limestone subjected to isotropic compression, M. eng., McGill University.
- Gnirk, P. (1993), OECD/NEA International STRIPA project overview, *in* ‘Natural Barriers’, Stockholm, Sweden: SKB.
- Goggin, D., Thrasher, R. and Lake, L. (1988), ‘A theoretical and experimental analysis of minipermeameter response including gas slippage and high velocity flow effects’, *In Situ* **12**, 79–116.
- Haimson, B. C. (1975), ‘Deep in-situ stress measurements by hydrofracturing’, *Tectonophysics* **29**, 41–47.
- Harr, M. E. (1962), *Groundwater Seepage*, Dover Publications.
- Heidland, J. (2003), ‘Laboratory testing of coupled hydro-mechanical processes during rock deformation’, *Hydrogeol. J.* **11**, 122–141.

- Herrmann, L. R. (1965), ‘Elasticity equations for incompressible and nearly incompressible materials by a variational theorem (variational theorem that is equivalent to elastic field equations for incompressible and nearly incompressible materials)’, *AIAA J.* **3**, 1896–1900.
- Heystee, R. and Roegiers, J. C. (1981), ‘The effect of stress on primary permeability- a facet of hydraulic fracturing’, *Can. Geotech. J.* **18**, 195–204.
- Hoek, E. and Franklin, J. A. (1967), *A Simple Triaxial Cell for Field or Laboratory Testing of Rock*, Imperial College of Science and Technology, University of London.
- Hornberger, G., Raffensperger, J. P., Wiberg, P. L. and Eshleman, K. N. (1998), *Elements of Physical Hydrology*, JHU Publications Press, Baltimore.
- Hsieh, P. A., Tracy, J., Neuzil, C., Bredehoeft, J. and Silliman, S. (1981), ‘A transient laboratory method for determining the hydraulic properties of ‘tight’ rocks - I. theory’, *Int. J. Rock Mech. and Min. Sci. and Geomech. Abs.* **18**(3), 245–252.
- ILIA (1998), *Indiana Limestone Handbook*, Indiana Limestone Institute of America Inc, Bedford, IN.
- Jalbert, M. and Dane, H. (2003), ‘A handheld device for intrusive and nonintrusive field measurements of air permeability’, *Vadose Zone J.* **2**, 611–617.
- Journel, A., Deutsch, C. and Desbrats, A. (1986), Power averaging for block effective permeability, Technical report, DOI: 10.2118/15128-MS.
- Journel, A. and Huijbregts, C. J. (1978), *Mining Geostatistics*, Academic Press, San Diego.

- King, P. (1988), *Effective values in averaging, In*, Mathematics in Oil Production, Oxford University Press, Oxford.
- King, P. (1989), ‘The use of renormalization for calculating effective permeability’, *Transp. Porous Media* **4**, 37–58.
- Kitanidis, P. (1997), *Introduction to Geostatistics: Applications to Hydrogeology*, Cambridge University Press, Cambridge.
- Kittridge, M. G., Lake, L. W., Lucia, F. J. and Fogg, G. E. (1990), ‘Outcrop/subsurface comparisons of heterogeneity in the San Andres formation’, *SPE Form. Eval.* **5**(3), 233–240.
- Klinkenberg, L. J. (1941), ‘The permeability of porous media to liquids and gases’, *Drilling and Production Practices Am. Pet. Inst.*, 200213.
- Knutson, C. F. and Bohor, B. F. (1963), Reservoir rock behaviour under moderate confining pressure, *in* ‘Fifth Symposium on Rock Mechanics, Pergamon Press, New York’, pp. 627–659.
- Landau, L. and Lifshitz, E. (1960), *Electrodynamics of Continuous Media*, Pergamon Press, Oxford.
- Laughton, A. S., Roberts, L., Wilkinson, D. and Gray, D. (1986), The disposal of long-lived and highly radioactive wastes, *in* ‘Proceedings of a Royal Society Discussion Meeting’, London: Royal Society, London.
- Liang, Y., Price, D., Wark, D. and Watson, E. (2001), ‘Nonlinear pressure diffusion in a porous medium: Approximate solutions with applications to per-

- meability measurements using transient pulse decay method’, *J. Geophys. Res.* **106**(B1), 529535.
- Markov, K. and Preziosi, L. (2000), *Heterogeneous Media. Micromechanics, Modelling, Methods and Simulations*, Birkhauser-Verlag, Boston.
- Matheron, G. (1967), *Eléments pour une Théorie des Milieux Poreux*, Masson, Paris.
- Mattar, P. (2009), Permeability determination of intact and fractured Indiana Limestone, Master’s thesis, McGill University.
- Morrow, C., Lockner, D., Moore, D. and Byerlee, J. (1981), ‘Permeability of Granite in a temperature gradient’, *J. Geophys. Res.* **86**, 3002–3008.
- Noetinger, B. (1994), ‘The effective permeability of a heterogeneous porous medium’, *Transp. Porous Media* **15**, 99–127.
- Papadopoulos, I., Bredehoeft, J. and Cooper, H. (1973), ‘On the analysis of “slug test” data’, *Water Resour. Res.* **9**, 1087–1089.
- Philips, O. (1991), *Flow and Reactions in Permeable Rocks*, Cambridge University Press, Cambridge.
- Renard, P. and de Marsily, G. (1997), ‘Calculating equivalent permeability: A review’, *Adv. Water Resour.* **29**, 253–278.
- Rutquist, J. (1995), ‘Determination of hydraulic normal stiffness of fractures in hard rock from well testing’, *Int. J. Rock Mech. and Min. Sci. and Geomech. Abs.* **32**, 513–523.

- Selvadurai, A. P. S. (2000), *Partial Differential Equations in Mechanics. Vol.1. Fundamentals, Laplace's Equation, Diffusion Equation, Wave Equation*, Springer-Verlag, Berlin.
- Selvadurai, A. P. S. (2002), Some remarks on the elastic drive equation, *in* L. Vulliet, L. Laloui and B. Schrefler, eds, 'Environmental Geomechanics, Proceedings of the International Workshop on Environmental Geomechanics', Monte Verita, Ascona, EPFL Press, Lausanne, pp. 253–258.
- Selvadurai, A. P. S. (2003), 'Intake shape factors for entry points in porous media with transversely isotropic hydraulic conductivity', *Int. J. Geomech.* **3**, 152–159.
- Selvadurai, A. P. S. (2004), 'Fluid intake cavities in stratified porous media', *J. Porous Media* **7**(3), 1–17.
- Selvadurai, A. P. S. (2006), 'Gravity-driven advective transport during deep geological disposal of contaminants', *Geophys. Res. Lett.* **33**(8), L08408.
- Selvadurai, A. P. S. (2007), 'The analytical method in geomechanics', *Appl. Mech. Rev.* **60**, 87–106.
- Selvadurai, A. P. S. (2009), 'Influence of residual hydraulic gradients on decay curves for one-dimensional hydraulic pulse tests', *Geophys. J. Int.* **177**, 1357–1365.
- Selvadurai, A. P. S. and Armand, G. (2003), Simulation of the FEBEX experiment as a test case for Decovalex III, Technical report, Canadian Nuclear Safety Commission, Ottawa, Canada.

- Selvadurai, A. P. S., Boulon, M. and Nguyen, T. (2005), ‘The permeability of an intact Granite’, *Pure Appl. Geophys.* **162**(2), 373–407.
- Selvadurai, A. P. S. and Carnaffan, P. (1997), ‘A transient pressure pulse method for the measurement of permeability of a cement grout’, *Can. J. Civil Eng.* **24**(3), 489–502.
- Selvadurai, A. P. S. and Glowacki, A. (2008), ‘Permeability hysteresis of limestone during isotropic compression’, *Ground Water* **46**(1), 113–119.
- Selvadurai, A. P. S., Letendre, A. and Hekimi, B. (2010), Axial flow hydraulic pulse testing of an Argillaceous Limestone. (in preparation)
- Selvadurai, A. P. S. and Nguyen, T. (1997), ‘Scoping analysis of the coupled thermal-hydrological-mechanical behaviour of the rock mass around a nuclear fuel waste repository’, *Eng. Geol.* **47**(4), 379–400.
- Selvadurai, A. P. S. and Selvadurai, P. A. (2010), ‘Surface permeability tests: Experiments and modelling for estimating effective permeability’, *Proc. R. Soc. London, Ser. A* **Under Review**, RSPA–2009–0475.R2.
- Selvadurai, P. A. and Selvadurai, A. P. S. (2007), ‘On cavity flow permeability testing of a sandstone’, *Ground Water* **45**(1), 93–97.
- Shmonov, V. M., Vitiovtova, V. M., Zharikov, A. V. and Grafchikov, A. A. (2003), ‘Permeability of the continental crust: implications of experimental data’, *J. Geochem. Explor.* **78-79**, 697 – 699.
- Shmonov, V. M., Vitovtova, V. M. and Zarubina, I. V. (1994), *Permeability of Rocks at Elevated Temperatures and Pressures*, Chapman and Hall, London,

chapter Fluids in the Crust; Equilibrium and Transport Properties, pp. 285–313.

Sneddon, I. (1966), *Mixed Boundary Value Problems in Potential Theory*, North-Holland Publ. Co, Amsterdam, The Netherlands.

Summers, R., Winkler, K. and Byerlee, J. (1978), ‘Permeability changes during the flow of water through Westerly Granite at temperatures of 100°-400°c’, *J. Geophys. Res.* **83**, 339–343.

Suri, P., Azeemuddin, M., Zaman, M., Kukreti, A. and Roegiers, J.-C. (1997), ‘Stress-dependent permeability measurement using the oscillating pulse technique’, *J. Pet. Sci. and Eng.* **17**, 247–264.

Tartakovsky, D. M., Moulton, J. D. and Zlotnik, V. (2000), ‘Kinematic structure of mini-permeameter flow’, *Water Resour. Res.* **36**(9), 2433–2442.

Terzaghi, K. and Peck, R. B. (1967), *Soil Mechanics in Engineering Practice*, 2 edn, John Wiley and Sons, New York.

Tidwell, V. C. and Wilson, J. (1997), ‘Laboratory method for investigating permeability upscaling’, *Water Resour. Res.* **33**(7), 1607–1616.

Tokunaga, T. and Kameya, H. (2003), ‘Determination of specific storage of a porous material from flow pump experiments: theoretical analysis and experimental evaluation’, *Int. J. Rock Mech. Min. Sci.* **40**(5), 739–745.

Trimmer, D., Bonner, B., Heard, H. and Duba, A. (1980), ‘Effect of pressure and stress on water transport in intact and fractured Gabbro and Granite’, *J. Geophys. Res.* **85**, 7059–7071.

- Vitovtova, V. M. and Shmonov, V. M. (1982), 'Permeability of rocks at pressures to 2000 kg/cm² and temperatures to 600°C', *Dokl. Akad. Nauk. SSR* **266**, 1244–1248.
- Wang, H. F. and Hart, D. J. (1993), 'Experimental error for permeability and specific storage from pulse decay measurements', *International Journal of Rock Mechanics and Mining Science & Geomechanics Abstracts* **30**(7), 1173–1176.
- Wardlaw, N. C., Li, Y. and Forbes, D. (1987), 'Pore-throat size correlation from capillary pressure curves', *Trans. Porous Med* **2**, 597–614.
- Wen, X.-H. and Gómez-Hernández, J. (1996), 'Upscaling hydraulic conductivities in heterogeneous media: An overview', *J. Hydrology* **183**, 9–32.
- Wiener, O. (1912), 'Die Theorie des Mischkörpers für das Feld des stationären Strömung. Erste Abhandlung die Mittelswertesätze für Kraft, Polarisierung und Energie', *Abh. Math.-Physischen Klasse Königl. Sächsl. Gesell. Wissen* **32**, 509–604.
- Wu, Y. S. and Pruess, K. (2000), 'Integral solutions for transient fluid flow through a porous medium with pressure-dependent permeability', *Int. J. Rock Mech. and Min. Sci. and Geomech. Abs.* **37**, 51–61.
- Zeng, Z. and Grigg, R. (2006), 'A criterion for non-darcy flow in porous media', *Transp. Porous Media* **63**, 57–69.
- Zoback, M. and Byerlee, J. (1975), 'The effect of micro-crack dilatancy on the permeability of westerly granite', *J. Geophys. Res.* **80**, 752–755.

Zonov, S. V., Zaisky, G. P. and Balashov, V. N. (1989), 'The effect of thermal decompaction on permeability of Granites with lithostatic pressures being slightly in excess of fluid pressure', *Dokl. Akad. Nauk. SSR* **307**, 191–195.